



Master Thesis

Derivatization-NMR Techniques in the Analysis of Lignocellulosics

carried out for the purpose of obtaining the degree of Master of Science (MSc),

under the supervision of

Univ.Prof. Dipl.-Chem. Dr.rer.nat. DDr.h.c Thomas Rosenau

Institute of Renewable Resources, H77400 (BOKU)

Univ.Prof. Dipl.Ing. Dr.techn. Anton Friedl

Institute of Chemical, Environmental and Bioscience Engineering, E166-06 (TU Wien)

submitted at the Technische Universität Wien

Faculty of Technical Chemistry

by

Johanna Zieher, BSc

*“All truths are easy to understand
once they are discovered -
the point is to discover them.”*

- Galileo Galilei

ACKNOWLEDGMENTS

A challenging and intense time lies behind me, but I am incredibly grateful for what I have learned and experienced during my master thesis. I would like to show my gratitude to all the people who have supported and helped me during this time.

First of all, I would like to thank Univ. Prof. **Thomas Rosenau** for the supervision of my master thesis and the opportunity to work on this interesting project. Thanks for the helpful expert inputs.

I would like to thank Univ. Prof. **Anton Friedl** for the supervision and the great support on behalf of the TU Wien.

I want to thank Univ. Prof. **Antje Potthast**, who was always very helpful and made it possible for me to conduct my thesis in this great research group. It has been a pleasure for me to be part of the NAWARO group.

I would like to say a special thanks to Dr. **Markus Bacher**, who supervised and supported me throughout my master thesis. I am very grateful for all the experience, especially concerning NMR spectroscopy, that he passed on to me and for everything, he taught me. I would like to thank him for his helpfulness all the time, especially for the time-consuming corrections of all my evaluations and for the nice conversations, we had in between. Working with Markus has been a great pleasure and enrichment for me.

I would like to express my thanks to Dr. **Martina Opietnik** from the Lenzing Group, who introduced me to this research group and made it possible for me to conduct my master thesis in this research group.

Thanks to the entire **NAWARO research group**. I have rarely experienced such a great willingness to help as in this group, every single person was very supportive and helpful. Thank you for the enjoyable conversations during the breaks and the many delicious cakes that were offered each day.

Finally, I would like to thank the people who are always there for me and support me in every situation. I am so grateful to my family, who always has an open ear for me, and encourages me with motivating words. Without the support of my parents and my siblings, I would not have made it to where I am now in my life.

Thanks to all my friends who are always there for me and give me the necessary balance and joy of life in challenging times.

My greatest support is my boyfriend, to who I am infinitely grateful. I am very thankful for the many encouraging words, the support, and the patience, he gave me during this time.

ABBREVIATIONS

amu	atomic mass unit
BMIM	1-Butyl-3-methylimidazoliumbromid
br. s	broad singlet (NMR)
COSY	correlation spectroscopy
d	doublet (NMR)
dd	doublet of doublets (NMR)
ddd	doublet of doublets of doublets (NMR)
ddt	doublet of doublets of triplets (NMR)
D1	relaxation delay (NMR)
DHAP	dihydroxyacetophenone
DHBQ	dihydroxybenzoquinone
DHNQ	dihydroxynaphthoquinone
dm	doublet of multiplets
DMAc	dimethylacetamide
DMSO	dimethyl sulfoxide
dt	doublet of triplets (NMR)
em	exponential multiplication (NMR)
EMIM	1-Ethyl-3-methylimidazolium chloride
FTIR	fourier transformation IR spectroscopy
GB	gaussian maximal position
gm	Lorentzian to gaussian transformation (NMR)
HMBC	heteronuclear multiple bond correlation (2D NMR)
HOSE	hierarchically ordered spherical environment
HSQC	heteronuclear single quantum coherence (2D NMR)
Hz	hertz
J	coupling constant
jmod	j-modulated spin echo
LB	line broadening
LCC	lignin-carbohydrate complex
m	multiplet (NMR)
MHz	megahertz
ml	milliliter

NMMO	<i>N</i> -methylmorpholine- <i>N</i> -oxide
NMR	nuclear magnetic resonance spectroscopy
O1	transmitter frequency offset (NMR)
P1	90° pulse width (NMR)
PLW	power level in watt (NMR)
ppm	parts per million
PyICl	pyridinium iodochloride
pyr-d₅	deuterated pyridine
q	quartet (NMR)
rpm	rounds per minute
r.t.	room temperature
s	seconds
s	singlet (NMR)
SF	spectrometer frequency (NMR)
SI	size of real spectrum (NMR)
SM	starting material
SW	spectral width (NMR)
t	triplet (NMR)
TD	size of fid
tm	tripletic multiplet (NMR)
TMDP	2-chloro-4,4,5,5-tetramethyl-1,3,2-dioxaphospholane
TMS	trimethyl silane
TOCSY	total correlation spectroscopy (NMR)
W	watt
WDW	window function (NMR)
zg30	pulse program using a 30° flip angle
δ	NMR chemical shift in ppm
μl	microliter
μs	microsecond

ABSTRACT

Lignocellulosic biomass, composed of cellulose, hemicellulose, and lignin, is the most abundant renewable carbon-containing resource on earth. While nowadays the focus lies more on efficiently converting (hemi)cellulose only to valuable biobased products, technical lignin is typically still regarded as a waste product and therefore mainly used for energy production. Lignin is the most underutilized high energy resource that is available in massive quantities and would provide great potential for a wide range of applications. However, to achieve the valorization of technical lignins, their chemical behavior and characterization need to be further investigated.

The main objective of this master thesis is, therefore, to better analyze the reactivity and chemical behavior of technical lignins using derivatization reactions. Given their extremely complex and changeable composition, lignins are rather difficult to characterize directly and for this reason lignin model compounds are employed. The selected model compounds, for the first part of the thesis, share structural features of native lignin and can therefore serve as good reference objects. Subsequently, for the second approach, model compounds associated with the pretreatment of biomass, which may appear as traces in isolated lignin, are investigated.

In the first course of this work, derivatization reactions with an iodination reagent (PyI₂) are performed with the model compounds. With the targeted iodination of hydroxylated aromatic model compounds and the subsequent analysis of the iodinated derivatives applying different NMR-techniques being the aim of this approach. The results obtained with the model compounds provide valuable information for lignin research.

The second part includes the derivatization of several model substances by a phosphitylation reagent (TMDP) and the obtained results are analyzed using also ³¹P-NMR. The aim is to investigate the reaction behaviour and to determine also the exact ³¹P-NMR chemical shifts of these components which could serve as valuable and informative spectral data in characterizing lignins and lignocellulose-based compounds.

Five of the 14 selected model compounds (isoeugenol, vanillin, vanillyl alcohol, *p*-cresol, and coniferyl alcohol) were successfully iodinated by the derivatization method with PyI₂. The respective iodinated quaternary ¹³C atoms exhibit a characteristic chemical shift in the range of about 80-90 ppm. Through the phosphitylation reactions with TMDP, the ³¹P chemistry shifts of several biomass-related components (DHBQ, DHNQ, 2,5-DHAP, 2,6-DHAP, morpholine, ellagic acid, gallic acid, and propyl gallate) were successfully identified in the range of approximately 140 ppm.

KURZFASSUNG

Lignocellulose Biomasse, bestehend aus Cellulose, Hemicellulose und Lignin, ist die am häufigsten vorkommende, erneuerbare, kohlenstoffhaltige Ressource der Erde. Während heutzutage der Schwerpunkt eher auf der effizienten Umwandlung von (Hemi-)Cellulose in wertvolle biobasierte Produkte liegt, wird technisches Lignin in der Regel immer noch als Abfallprodukt betrachtet und daher hauptsächlich energetisch genutzt. Lignin ist die am wenigsten genutzte energiereiche Ressource, die in großen Mengen vorhanden ist und großes Potenzial für eine Vielzahl von Anwendungen aufweisen würde. Um jedoch die technischen Lignine wertvoller zu verwerten, müssen das chemische Verhalten und die Charakterisierung noch weiter untersucht werden.

Das Hauptziel dieser Masterarbeit ist es daher, die Reaktivität und das chemische Verhalten von technischen Ligninen durch Derivatisierungsreaktionen besser zu analysieren. Da Lignine aufgrund ihrer äußerst komplexen und veränderlichen Zusammensetzung nur schwer direkt charakterisierbar sind, werden Lignin-Modellverbindungen für die Untersuchungen herangezogen. Die im ersten Teil der Arbeit ausgewählten Modellverbindungen weisen strukturelle Merkmale von nativem Lignin auf und können daher als gute Referenzobjekte dienen. Zusätzlich werden im zweiten Teil Modellverbindungen ausgewählt, die mit der Vorbehandlung von Biomasse in Verbindung stehen und als Spuren im isolierten Lignin auftreten können.

Im ersten Abschnitt dieser Arbeit werden mit den Modellverbindungen Derivatisierungsreaktionen mit einem Iodierungsreagenz (PyICl) durchgeführt. Ziel dieses Ansatzes ist die gezielte Iodierung von hydroxylierten aromatischen Modellverbindungen und die anschließende Analyse der iodinierten Derivate mittels NMR-Technik. Die mit den Modellverbindungen erzielten Ergebnisse liefern in weiterer Folge wertvolle Informationen für die Ligninforschung.

Der zweite Teil umfasst die Derivatisierung mehrerer Modellsubstanzen mit einem Phosphitylierungsreagenz (TMDP) und die anschließende Analyse der erhaltenen Ergebnisse mittels ^{31}P -NMR Spektroskopie. Ziel ist es, die genauen chemischen Verschiebungen der ^{31}P -NMR Signale dieser Komponenten herauszufinden, um womögliche Fehlinterpretationen der Signale zu vermeiden. Die ^{31}P -NMR Signale könnten als wertvolle und informative Spektraldaten bei der Charakterisierung von Ligninen und Verbindungen auf Lignocellulosebasis dienen.

Fünf der 14 ausgewählten Modellverbindungen (Isoeugenol, Vanillin, Vanillylalkohol, *p*-Cresol und Coniferylalkohol) wurden erfolgreich durch die Derivatisierungsmethode mit PyICl iodiniert. Die jeweiligen iodinierten quaternären ^{13}C -Atome weisen charakteristische chemische Verschiebung im Bereich von etwa 80-90 ppm auf. Durch die Phosphitylierungsreaktionen mit TMDP wurden erfolgreich

die ^{31}P chemischen Verschiebungen mehrerer biomassebezogener Komponenten (DHBQ, DHNQ, 2,5-DHAP, 2,6-DHAP, Morpholin, Ellagsäure, Gallussäure und Propylgallat) im Bereich von etwa 140 ppm identifiziert.

MODEL COMPOUNDS – IODINATION

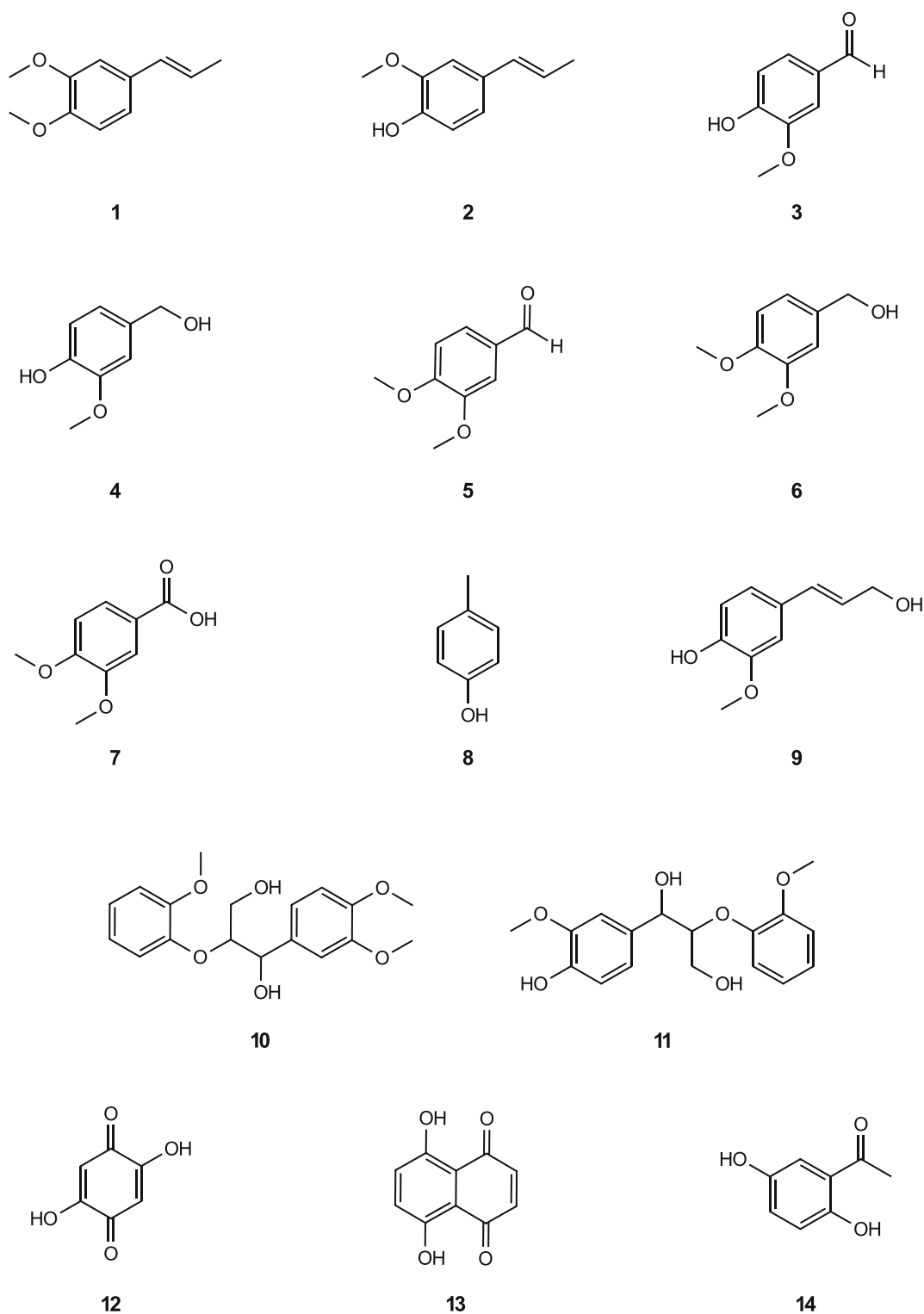
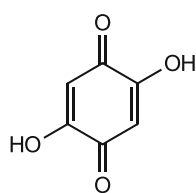


Figure 1: Structures and the corresponding numbers of the model compounds used for derivatization method I – iodination. **1:** methyl isoeugenol; **2:** isoeugenol; **3:** vanillin; **4:** vanillyl alcohol; **5:** veratraldehyde; **6:** veratryl alcohol; **7:** veratric acid; **8:** p-cresol; **9:** coniferyl alcohol; **10:** veratrylglycerol- β -guaiacyl ether; **11:** guaiacylglycerol- β -guaiacyl ether; **12:** 2,5-Dihydroxy-1,4-benzoquinone; **13:** 5,8-Dihydroxy-1,4-naphthoquinone; **14:** 2,5-Dihydroxyacetophenone.

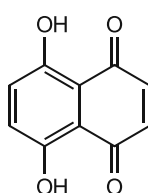
Table 1: Model compounds selected for derivatization method I - iodination with corresponding number, IUPAC name and molecular formula.

	<u>Model compound</u>	<u>IUPAC-Name</u>	<u>Molecular formula</u>
1	Methyl isoeugenol	1,2-Dimethoxy-2-propenylbenzol	C ₁₁ H ₁₄ O ₂
2	Isoeugenol	2-Methoxy-4-propenylphenol	C ₁₀ H ₁₂ O ₂
3	Vanillin	4-Hydroxy-3-methoxybenzaldehyde	C ₈ H ₈ O ₃
4	Vanillyl alcohol	4-Hydroxy-3-methoxybenzyl alcohol	C ₈ H ₁₀ O ₃
5	Veratraldehyde	3,4-Dimethoxybenzaldehyde	C ₉ H ₁₀ O ₃
6	Veratryl alcohol	3,4-Dimethoxybenzyl alcohol	C ₉ H ₁₂ O ₃
7	Veratric acid	3,4-Dimethoxybenzoic acid	C ₉ H ₁₀ O ₄
8	<i>p</i> -Cresol	4-Methylphenol	C ₇ H ₈ O
9	Coniferyl alcohol	4-3-Hydroxy-1-propenyl-2-methoxyphenol	C ₁₀ H ₁₂ O ₃
10	Veratrylglycerol-β-guaiacyl ether	1-(3,4-Dimethoxyphenyl)-2-(2-methoxyphenoxy)propane-1,3-diol	C ₁₈ H ₂₂ O ₆
11	Guaiacylglycerol-β-guaiacyl ether	1-(4-Hydroxy-3-methoxyphenyl)-2-(2-methoxyphenoxy)-1,3-propanediol	C ₁₇ H ₂₀ O ₆
12	2,5-Dihydroxy-1,4-benzoquinone	2,5-Dihydroxycyclohexa-2,5-diene-1,4-dione	C ₆ H ₆ O ₄
13	5,8-Dihydroxy-1,4-naphthoquinone	5,8-Dihydroxynaphthalene-1,4-dione	C ₁₀ H ₆ O ₄
14	2,5-Dihydroxyacetophenone	1-(2,5-Dihydroxyphenyl)ethanone	C ₈ H ₈ O ₃

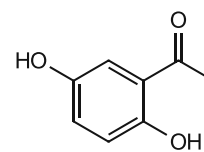
MODEL COMPOUNDS – PHOSPHITYLATION



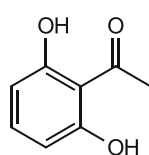
12



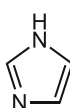
13



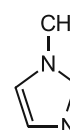
14



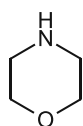
15



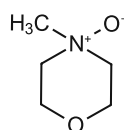
16



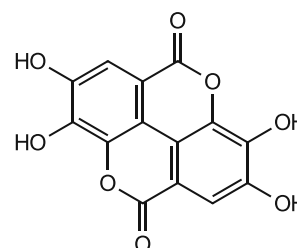
17



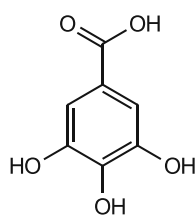
18



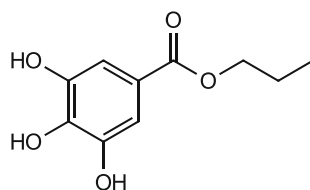
19



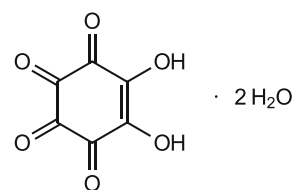
20



21



22



23

Figure 2: Structures and the corresponding numbers of the model compounds used for derivatization method II-phosphitylation. **12**: 2,5-Dihydroxy-1,4-benzoquinone; **13**: 5,8-Dihydroxy-1,4-naphthoquinone; **14**: 2,5-Dihydroxyacetophenone; **15**: 2,6-Dihydroxyacetophenone; **16**: imidazole; **17**: 1-methyl imidazole; **18**: morpholine; **19**: N-methylmorpholine N-oxide; **20**: ellagic acid; **21**: gallic acid; **22**: propyl gallate; **23**: rhodizonic acid dihydrate.

Table 2: Model compounds selected for derivatization method II - phosphitylation with the corresponding number, IUPAC name, and molecular formula.

	<u>Model compound</u>	<u>IUPAC-Name</u>	<u>Molecular formula</u>
12	2,5-Dihydroxy-1,4-benzoquinone	2,5-Dihydroxycyclohexa-2,5-diene-1,4-dione	C ₆ H ₆ O ₄
13	5,8-Dihydroxy-1,4-naphthoquinone	5,8-Dihydroxynaphthalene-1,4-dione	C ₁₀ H ₆ O ₄
14	2,5-Dihydroxyacetophenone	1-(2,5-Dihydroxyphenyl)ethanone	C ₈ H ₈ O ₃
15	2,6-Dihydroxyacetophenone	1-(2,6-Dihydroxyphenyl)ethanone	C ₈ H ₈ O ₃
16	Imidazole	1,3-Diaza-2,4-cyclopentadiene	C ₃ H ₄ N ₂
17	1-Methyl imidazole	1-Methyl-1H-imidazole	C ₄ H ₆ N ₂
18	Morpholine	1-Oxa-4-azacyclohexane	C ₄ H ₉ NO
19	<i>N</i> -Methylmorpholine <i>N</i> -oxide	4-Methyl-4-oxidomorpholin-4-ium	C ₅ H ₁₁ NO ₂
20	Ellagic acid	2,3,7,8-Tetrahydroxy[1]benzopyrano[5,4,3- <i>cde</i>][1]benzopyran-5,10-dione	C ₁₄ H ₆ O ₈
21	Gallic acid	3,4,5-Trihydroxybenzoic acid	C ₇ H ₆ O ₅
22	Propyl gallate	Propyl 3,4,5-trihydroxybenzoate	C ₁₀ H ₁₂ O ₅
23	Rhodizonic acid dihydrate	5,6-Dihydroxycyclohex-5-ene-1,2,3,4-tetrone dihydrate	C ₆ H ₂ O ₆ ·2H ₂ O

TABLE OF CONTENT

Acknowledgments.....	I
Abbreviations.....	II
Abstract	IV
Kurzfassung.....	V
Model compounds – Iodination.....	VII
Model compounds – Phosphitylation.....	IX
1 Introduction.....	1
1.1 Aim of the thesis	2
1.2 Lignin.....	2
1.2.1 Technical lignins	6
1.3 Derivatization methods.....	8
1.3.1 Iodination with pyridinium iodochloride.....	8
1.3.2 Phosphitylation with phospholane.....	11
1.4 NMR-spectroscopy.....	14
1.4.1 Principle.....	14
1.4.2 ³¹ P-NMR.....	15
1.4.3 Lignin elucidation by NMR.....	16
1.5 Model compounds.....	19
1.5.1 Methyl isoeugenol and Isoeugenol	19
1.5.2 Vanillin.....	19
1.5.3 Vanillyl alcohol.....	20
1.5.4 Veratraldehyde and veratric acid	20
1.5.5 Veratryl alcohol	20
1.5.6 <i>p</i> -Cresol.....	20
1.5.7 Coniferyl alcohol.....	20
1.5.8 Guaiacylglycerol- β -guaiacyl ether	21
1.5.9 Veratrylglycerol- β -guaiacyl ether	21
1.5.10 Chromophoric compounds.....	21
1.5.11 <i>N</i> -Methylmorpholine- <i>N</i> -oxide monohydrate.....	22
1.5.12 Morpholine.....	23
1.5.13 Imidazole and 1-Methyl imidazole	23
1.5.14 Rhodizonic acid dihydrate	23
1.5.15 Gallic acid.....	23

1.5.16	Ellagic acid	23
1.5.17	Propyl gallate	24
2	Experimental part	25
2.1	Materials and Methods	25
2.1.1	Reagents and solvents	25
2.1.2	Lignins	25
2.1.3	NMR analysis	25
2.2	Derivatization method I – Iodination	27
2.2.1	Solvent selection	27
2.2.2	Sample preparation	28
2.2.3	Workup	28
2.2.4	Lignin purification	28
2.3	Derivatization method II – Phosphitylation	29
2.3.1	Solvent selection	29
2.3.2	Sample preparation	29
3	Results and discussion	30
3.1	NMR analysis of the pure model compounds	30
3.1.1	Methyl isoeugenol	30
3.1.2	Isoeugenol	31
3.1.3	Vanillin	32
3.1.4	Vanillyl alcohol	32
3.1.5	Veratraldehyde	33
3.1.6	Veratryl alcohol	34
3.1.7	Veratric acid	35
3.1.8	<i>p</i> -Cresol	35
3.1.9	Coniferyl alcohol	36
3.1.10	Veratrylglycerol- β -guaiacyl ether	37
3.1.11	Guaiacylglycerol- β -guaiacyl ether	38
3.1.12	2,5-Dihydroxy-1,4-benzoquinone	39
3.1.13	5,8-Dihydroxy-1,4-naphtoquinone	39
3.1.14	2,5-Dihydroxyacetophenone	40
3.1.15	2,6-Dihydroxyacetophenone	40
3.1.16	Imidazole	41
3.1.17	1-Methyl imidazole	41
3.1.18	Morpholine	42
3.1.19	<i>N</i> -Methylmorpholine- <i>N</i> -oxide	42

3.1.20	Ellagic acid	43
3.1.21	Gallic acid.....	43
3.1.22	Propyl gallate.....	44
3.2	Derivatization method I – Iodination	45
3.2.1	Methyl isoeugenol.....	45
3.2.2	Isoeugenol	55
3.2.3	Vanillin	63
3.2.4	Vanillyl alcohol.....	69
3.2.5	Veratraldehyde.....	72
3.2.6	Veratryl alcohol	74
3.2.7	Veratric acid.....	74
3.2.8	<i>p-Cresol</i>	75
3.2.9	Coniferyl alcohol.....	77
3.2.10	Veratrylglycerol- β -guaiacyl ether	78
3.2.11	Guaiacylglycerol- β -guaiacyl ether	79
3.2.12	2,5-Dihydroxy-1,4-benzoquinone.....	80
3.2.13	5,8-Dihydroxy-1,4-naphtoquinone.....	81
3.2.14	2,5-Dihydroxyacetophenone.....	82
3.2.15	Native lignins	84
3.3	Mass spectrometry.....	88
3.3.1	Methyl isoeugenol.....	88
3.3.2	Isoeugenol	90
3.3.3	Vanillin	94
3.3.4	Vanillyl alcohol.....	95
3.4	NMR-Measurements - Iodination	96
3.4.1	Methyl isoeugenol.....	96
3.4.2	Isoeugenol	97
3.4.3	Vanillin	99
3.4.4	Vanillyl alcohol.....	100
3.4.5	Veratraldehyde.....	100
3.4.6	<i>p-Cresol</i>	101
3.4.7	Coniferyl alcohol.....	101
3.5	Derivatization Method II – Phosphitylation.....	102
3.5.1	In deuterated chloroform/deuterated pyridine (CDCl ₃ : C ₅ D ₅ N = 1: 1.6).....	102
3.5.2	In deuterated pyridine (C ₅ D ₅ N).....	104
3.6	NMR-Measurements - Phosphitylation	141

3.6.1	2,5-Dihydroxyacetophenone.....	141
3.6.2	2,6-Dihydroxyacetophenone.....	142
3.6.3	Morpholine.....	143
3.6.4	Gallic acid.....	144
3.6.5	Propyl gallate.....	145
3.6.6	4,4,5,5-Tetramethyl-1,3,2λ ⁵ -dioxaphospholan-2-one.....	145
4	Conclusion and Outlook	146
4.1	Derivatization Method I – Iodination.....	146
4.2	Derivatization Method II – Phosphitylation.....	149
5	Bibliography.....	151
6	Appendix.....	154

1 INTRODUCTION

Nowadays, society is based on geologically extracted raw materials such as petroleum, coal, and natural gas. Those materials are critical to the functioning of our society, but the strong dependence on fossil resources is responsible for several global problems, including anthropogenic greenhouse gas emissions, which, among other things, lead to global warming and eventual oil depletion. The great need for alternative, sustainable resources is now recognized, as global petroleum resources continue to decline while energy demand increases and climate problems are becoming more serious.

In recent years, biomass has been recognized as an extremely attractive and promising renewable source of chemicals, materials, and fuels. Biomass is a collective term for plant material (e.g., trees, grasses, and algae) that is produced at a high rate. Lignocellulosic biomass (40/25/25 cellulose/hemicellulose/lignin on average [1]) is the most abundant renewable material in the world, which has a high potential to replace fossil raw materials. The renewable resource can be used as a platform to produce bio-based materials in a wide range of areas.

Lignin for instance is the most underutilized high energy resource that is available to a large extent. Although lignin's structure is of more complexity compared to the polysaccharide fraction, as well as its higher carbon and lower oxygen content, it is an attractive feedstock to produce biofuels and chemicals. In particular, the highly functionalized and aromatic nature of lignin offers the potential for direct production of aromatic chemicals, overcoming the need for complete defunctionalization to "BTX" (benzene, toluene, and xylene) and subsequent re-functionalization to desired platform chemicals [2].

However, to operate the biorefinery concept on an economically lucrative scale, feedstock processing strategies need to be reconsidered. Furthermore, new technologies that not only focus on generating one of the lignocellulose components in high quality and yield but also fractionate the other parts of the raw material to streams that can be valorized, need to be developed [1]. The lignocellulose biorefinery concept, based on the chemical separation of the major components (cellulose, hemicellulose, and lignin) and their further individual processing is a promising approach for the valorization of the final products.

1.1 Aim of the thesis

The focus of the first part of this work is to better explore and understand the chemical behavior and reactivity of lignin. Derivatization reactions on suitable model compounds are intended to achieve these goals. Targeted iodination at the *ortho*-position on hydroxylated aromatic model compounds by using the iodination reagent pyridinium iodochloride (PyI₂) would be aimful. Given the structural resemblances between model compounds and lignins, the results obtained by this method should also be applicable to lignins and thus contribute to an even better characterization of the macromolecule. The pretreatment of lignocellulosic biomass, accompanied by a significant deconstruction of the cell wall, usually generates by-products and/or impurities from solvents and decomposition products during the process [3]. The next approach of this project, therefore, includes biomass-related model substances that may still be present as traces in lignin after its isolation from the lignocellulose complex. By converting these model components into phosphitylated derivatives (*via* TMDP-phosphitylation), their ³¹P-NMR chemical shifts can be identified. This information would provide a valuable contribution to and greatly facilitate lignin analysis.

The overall objective of this thesis is to provide a constructive contribution to the valorization of this still underestimated but abundant renewable resource through the investigations and results obtained.

1.2 Lignin

Lignin is by far the most abundant aromatic-based substance in nature and is the largest contributor to soil organic matter [4], [5]. Together with cellulose and hemicellulose, lignin is one of the most plentiful natural polymers, which are major sources of non-fossil carbon and thus make a particularly important contribution to the carbon cycle [6]. Native lignin is one of the main components of the secondary cell walls of plants and contributes to the maintenance of the cellulose/hemicellulose/pectin matrix and provides rigidity to the plant. In addition, it ensures the internal transport of nutrients in plants and protects them from attack by microorganisms. During paper-producing processes, the native lignins are modified and obtained as a by-product referred as technical lignins [7], [8].

Lignin is not considered to be a constitutionally defined compound, but rather a physically and chemically heterogeneous substance. It shows an intrinsic molecular complexity and a diverse structural composition, depending on its origin. The structural diversity of lignin arises mainly from the combination of three phenylpropane derivatives, called monolignols, of which almost all lignin species occurring in nature are composed [9]. These monolignols are commonly known as *p*-coumaryl alcohol

(H), coniferyl alcohol (G), and sinapyl alcohol (S). As shown below in Figure 3 each monolignol produces in the polymer the respective residues (*p*-hydroxyphenyl (H), guaiacyl (G), and syringyl (S) residues) [8].

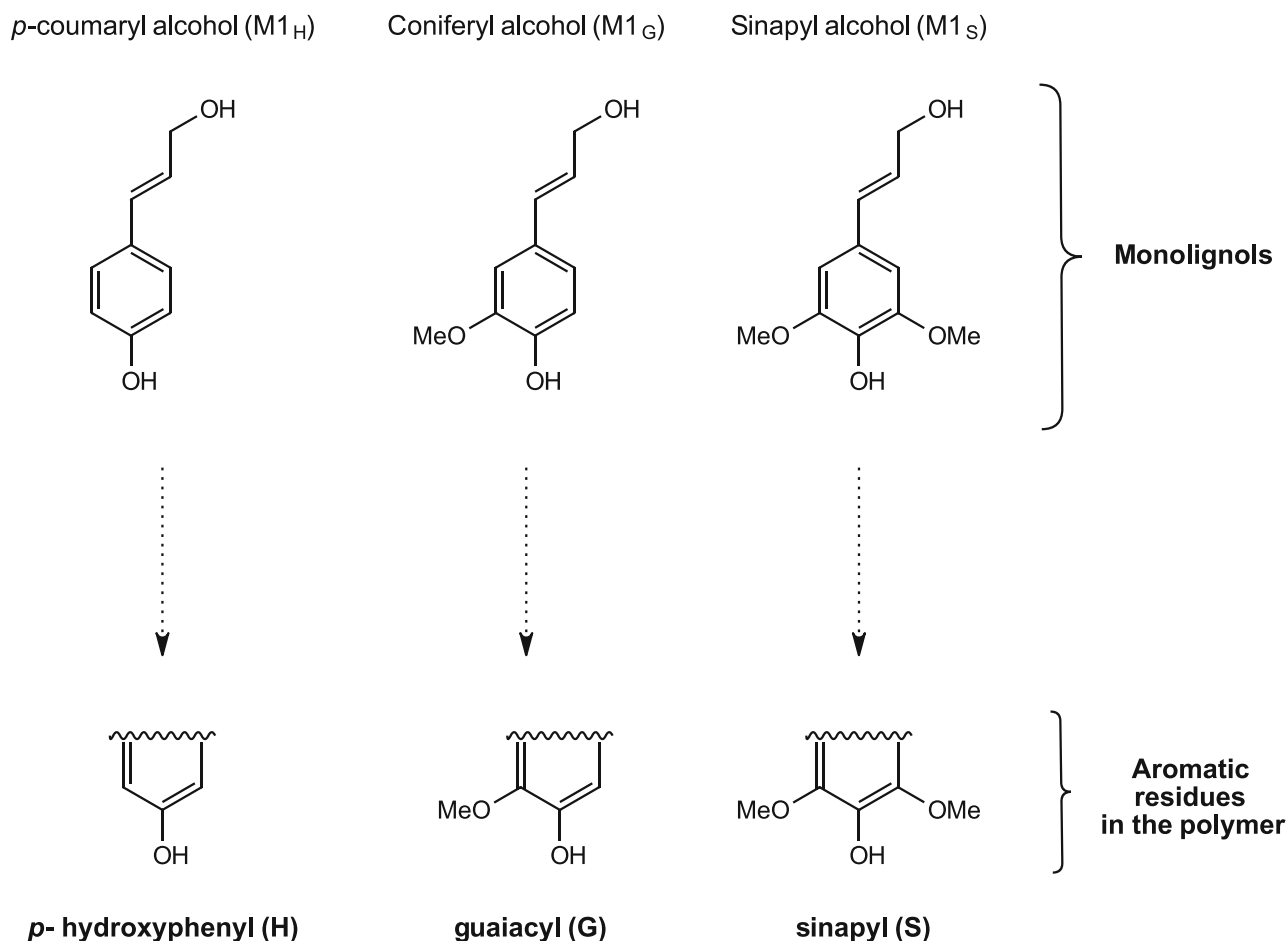


Figure 3: Three monolignols, which share the phenylpropane unit (M1) and differ in the phenyl functionalization (upper part) inclusive of the respective residues in lignin (lower part).

The proportions of monolignols differ significantly in each plant depending on the botanical species or geographic location for instance [10]. For example, softwood lignin consists mainly of coniferyl alcohol units (type-G), while lignin from hardwood is composed of coniferyl and sinapyl alcohol units (type-G-S). Monocotyledons like grasses, cereals, or maize produce all three types: guaiacyl, syringyl, and hydroxyphenyl structural units (type-H-G-S). In general, the amount of lignin in lignocellulosic biomass is 27-33% in softwood, 18-25% in hardwood, and 17-24% in grass [11].

According to the abundance of the basic phenol units *p*-hydroxyphenyl (H), guaiacyl (G), and syringyl (S) in the polymer, four main lignin group types can be classified: type-G, type-G-S, type-H-G-S, and type-H-G.

The biosynthesis of lignin takes place by peroxidase-mediated dehydrogenation of monolignol units, resulting in a heterogeneous structure. By oxidizing the monolignols through the abstraction of their phenolic hydrogens, the corresponding phenolic radicals are formed. The dehydrogenation of monolignols to radicals is attributed to different classes of proteins, with peroxidases and laccases being most involved. Peroxidases use hydrogen peroxide (H_2O_2) and laccases use oxygen to oxidize their substrates. After dehydrogenation of the monolignol, the phenolic radicals are coupled. The radicals are relatively stable owing to the delocalization of electrons, having various sites of enhanced single-electron density in the molecule. The radical cross-coupling with a monolignol radical or with a phenolic radical derived from another growing polymer chain is the most important reaction to extend the complex three-dimensional lignin network [12], [13]. The mutual coupling of monolignols and the cross-coupling with the growing polymer lead not only to the characteristic H, G, and S units but also to various interunit linkage types [8]. The enormous variation in the primary structure of the polymer is attributed to combinatorial linkage synthesis, the random generation of new optical centers each time a monolignol is coupled via its side chain, and the inclusion of monomers other than monolignols [12].

The complex macromolecular structure is formed by basic units linked by C-C-bonds and aryl-ether linkages with aryl-glycerol and β -aryl ether [10]. The process of forming phenylpropanoid macromolecules (termed lignin) is called lignification [8]. Since lignin is considered a polydisperse polymer that does not contain extended sequences of regularly repeating units, its composition is generally characterized by the relative abundance of H/G/S units and by the distribution of interunit linkages in the polymer.

Various C-C and C-O intermonomeric bonds exist between the monolignols and some of the common and most familiar linkages found in lignin (softwood) are depicted in Figure 4 [10], [11].

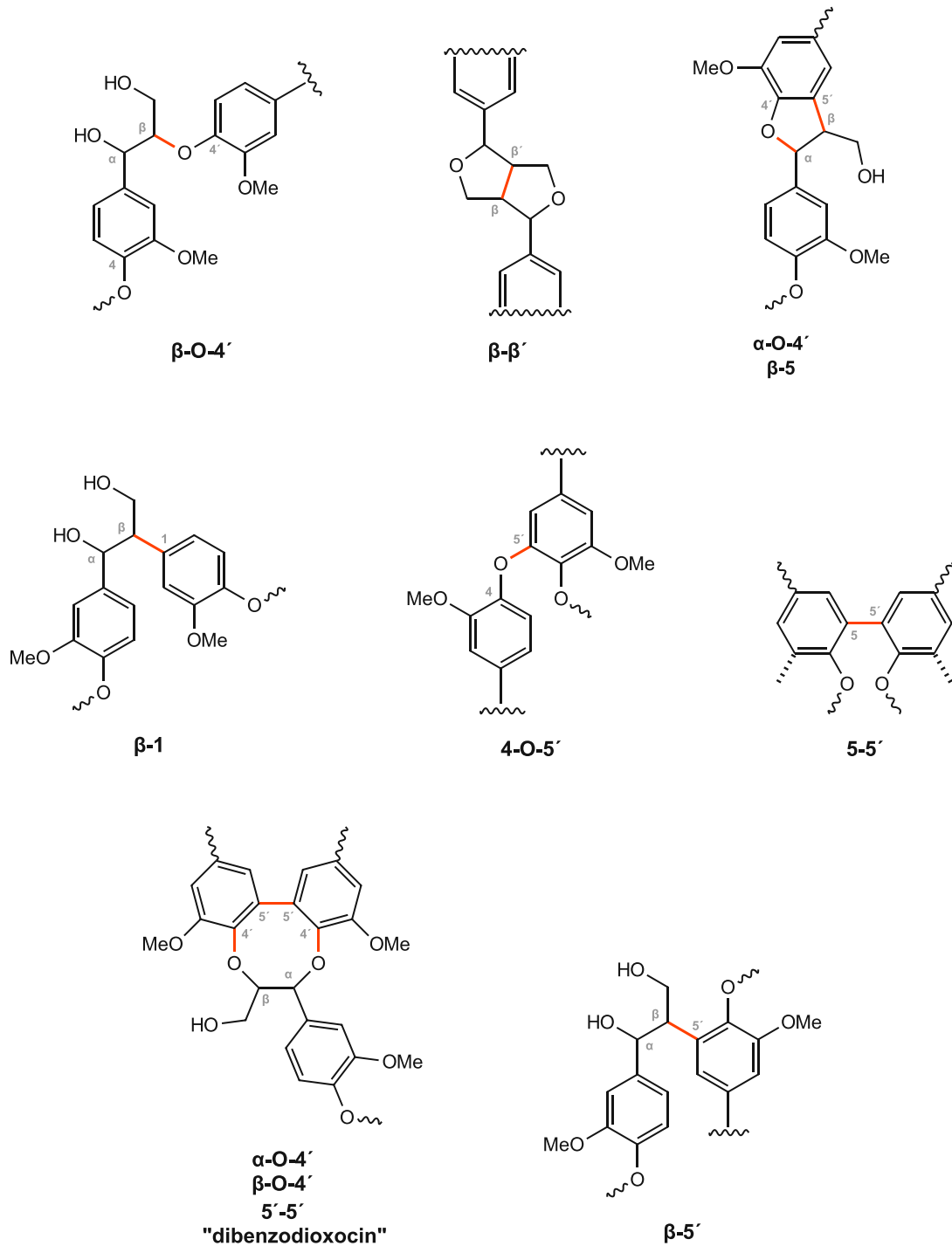


Figure 4: Primary inter-unit linkages (red) found in softwood lignin.

The relative percentage of linkages occurring in lignin depends on the biomass sources and varies depending on the technique used to isolate lignin. However, it has been shown that the β -O-4' -linkage is the most abundant among all other bonds, and in most plant species it turns out to be more than 50% [10], [14].

In addition, the lignin polymer in plants is covalently bonded to carbohydrates *via* various bonds, which are believed to be phenyl glycoside bonds, esters, and benzyl ethers. These bindings create a complex

structure, which is known as lignin-carbohydrate complexes (LCC) [10]. Therefore, the isolation of lignin from plant biomass through pulping processes is still a difficult task, since the cleavage of the covalent lignin-carbohydrate bonds and the depolymerization of lignin needs to be considered.

In pulping and pretreatment processes for biomass, depolymerization largely occurs through the cleavage of β -O-4'-linkages, because these are the weakest, most unstable bonds. In lignin, however, the amount of β -O-4'-bonds depends on the proportion of S-, G-, and H-units and is therefore variable. The formation of β -5', 5'-5', or dibenzodioxocin-linkages is prevented by the methoxy groups at the third and fifth position of the aromatic ring in the S-unit and thus, the ratio of the units (S/G/H) directly affects the percentage of β -O-4'-bonds in the lignin polymer. Consequently, the degradability of lignin depends not only on its isolation process but also on its source [10], [15].

1.2.1 Technical lignins

Lignins as by-products of the pulp and paper industry are called technical lignins or industrial lignins, exhibiting a considerable difference in their properties compared to native lignins found in plants. Technical lignin is obtained as a result of lignocellulosic biomass processing, currently mainly by conventional pulp mills. Most of the commercially available types of technical lignin produced during wood preparation are lignosulfonates and kraft lignin [16]. The reason for the significant difference between technical lignins and the corresponding native lignins lies in the fact that they result from a combination of several reactions. These reactions include among others catalyzed hydrolysis of biomass, condensation of lignin fragments, elimination of native lignin functional groups, formation of new functional groups. They are in terms of their chemical structure and molecular mass significantly more heterogeneous than native lignins. Further, technical lignins show a large variety of structural moieties that are present in rather small quantities [17].

The global annual production of technical lignin as a by-product of the pulp and paper industry amounts to approximately 50 million tons, of which up to 99% is incinerated for the production of energy and steam [18]. These lignins offer great potential as an energy source, as owing to their very high fuel content they can be burned to produce "green" electricity, power, fuel, steam, or syngas. All of those energy forms are already being used to power industrial facilities where technical lignins are by-products [14].

Currently, specific uses for technical lignin by-products in the pulp industries are as already stated above the use as a fuel feedstock in the kraft pulp industry, while the sulfite industry uses the lignin to produce lignosulfonates, after a minor chemical treatment [18]. With the majority of technical lignins

being used to meet internal energy demands by combustion, lignins are substantially underutilized in the current biorefinery systems.

The reason for classifying biorefinery lignins often as low-value products of approximately fuel value or low-cost chemical feedstock value is mainly the low lignin purity in the crude material [16]. Also, the complex structure of lignin, its low reactivity, and solubility are the main factors limiting its large-scale use in biorefinery so far. Unlike other biorefinery products (ethanol, butanol, etc.), technical lignins do not possess a clearly defined structure, complicating their handling significantly. The heterogeneous chemical structure of lignin and its high polydispersity, which can lead to undesirable properties, pose further obstacles to its application for new products. There is a wide variety of products called “lignin”, but these lignins are different in chemical composition, molecular structure, and hence physical properties. Therefore, it is not surprising that the behavior of these lignins varies in different applications, posing an additional challenge [16].

For applications of lignins in high-quality products, several techniques need to be further developed, and certain processes adapted and improved. Above all, lignin as a macromolecule, including its properties and reactivities, must be better researched.

However, the possibilities and opportunities arising from using the pulp and paper industry as a lignin biorefinery are very large and promising and could make a major contribution to a more sustainable future. Fortunately, a lot of research is being done in this area and there have already been recent achievements concerning the valorization of lignin. The three major areas of lignin valorization, defined by the Department of Energy (DOE), are the following: 1. Heating fuel and energy through combustion (short term); 2. Application of lignin as macromolecule (middle term); 3. Lignin as a source of aromatic monomers and oligomers (long term) [16], [19].

1.3 Derivatization methods

1.3.1 Iodination with pyridinium iodochloride

Pyridinium iodochloride (PyICl), shown in Figure 5, serves as an efficient reagent for the iodination of hydroxylated aromatic compounds with no hazardous effects. Scheme 1 shows the general reaction of hydroxy-substituted aromatic substrates with pyridinium iodochloride. According to a study [20], the resulting isolated product indicated regioselective iodination at the electron-rich *ortho*- or *para*-position. In the case of a blocked *ortho*-position iodination could only be observed at the *para*-position.

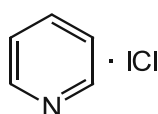
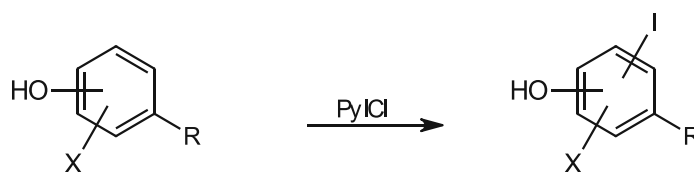


Figure 5: Structure of pyridinium iodochloride.

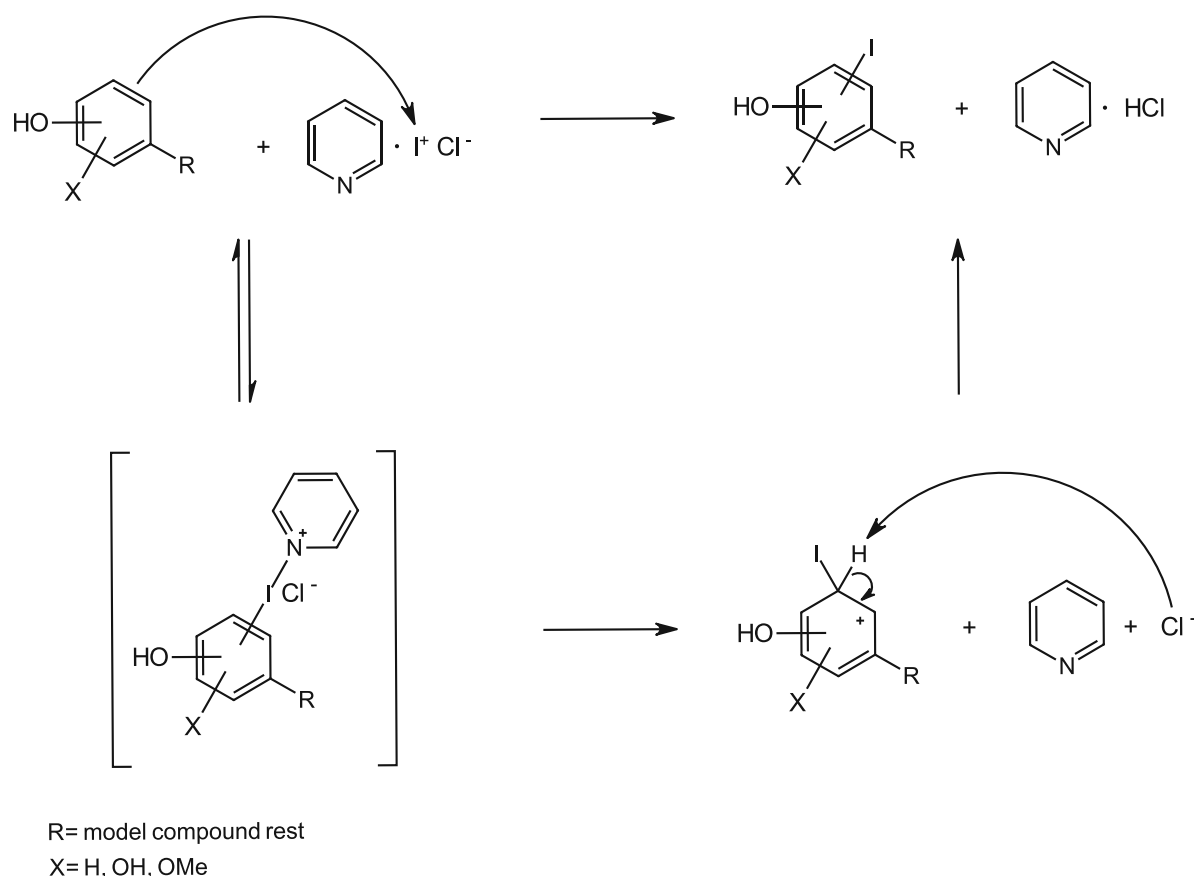


R= model compound rest

X= H, OH, OMe

Scheme 1: Iodination of hydroxy-substituted aromatic substrates using pyridinium iodochloride as a reagent.

The iodination reaction with PyICl can be classified as an electrophilic aromatic substitution. In this type of reaction, an electrophile (in this case iodine from PyICl) attacks the electron-rich aromatic system and substitutes a proton. The hydroxy group exhibits a positive mesomeric effect, which increases the electron density in the π -system and enhances the attack of electrophilic reagents. The hydroxy group (+ M-effect, - I-effect) has a directing effect on the attacked position of the electrophile resulting predominantly in *ortho*- and *para*-substituted products. The reaction mechanism of an electrophilic aromatic substitution is depicted below in Scheme 2 in a generalized form for hydroxylated aromatic compounds, with iodine serving as the electrophile.



Scheme 2: Reaction mechanism of an electrophilic aromatic substitution in generalized form for hydroxylated aromatic compounds, with iodine serving as the electrophile.

1.3.1.1 Potential application of the method

Determination of degree of branching

The type of linkages (*c.f.* Figure 4) in a lignin macromolecule depends on the respective monolignol moieties (*c.f.* Figure 3) occurring in the polymer. In turn, the different types of linkages define the degree of branching of the macromolecule. The determination of branching in lignin is traditionally very cumbersome, but the derivatization method with PyI₂ offers the potential to subsequently infer the degree of branching in lignins. In biosynthesis, phenolic hydroxy groups in lignins are the “active” or “growing” end of lignin molecules and are therefore molecular end-groups in lignins [13]. It is known that the terminal groups in lignins mainly consist of free G-unit monolignol moieties (coniferyl alcohol). As shown in Figure 3, the aromatic guaiacyl-residue is hydroxy- and methoxy-substituted and as described above, PyI₂ as an iodinating reagent could be applied for the iodination. This derivatization method consequently could allow the identification of the chain ends in the macromolecule by successfully iodinating them (in the case of G-unit monolignols).

All unsubstituted *ortho*-positions of the G-units in the polymer could be identified accordingly and "labeled" with an iodine atom. This information could then be used to deduce the degree of branching of the macromolecule.

Targeted property modification

The valorization of lignin and its targeted use for specific applications could be achieved through its modification. Corresponding to the desired application, attaching different (functional) chemical groups to the molecule could be an option to achieve the required properties of the substance. Phenolic end groups on lignin molecules are important sites for the molecular properties of lignin, and their potential for derivatization to produce new lignin materials [13].

Targeted iodination at a specific position on the aromatic ring ("I-tagging") directed by specific substituents, can be achieved, for instance, by iodination with PyI₂. Since iodine acts as a very good leaving group, aromatic iodides are considered versatile intermediates in organic synthesis that can be converted into a variety of functional groups. Thus, the attached iodine can be easily substituted by other functional groups selected according to the desired application to be achieved with the modified lignin.

Since the position of the attached iodine is known (*ortho*-position to the aromatic hydroxy group), the position of the new attached group would consequently also be precisely known. Due to the structural complexity of lignin, this would be a major step towards targeted property modification. However, this application is limited assuming that only the terminal groups consist of free G-unit monolignols carrying a phenolic hydroxy group where iodination at the *ortho*-position could occur.

1.3.2 Phosphitylation with phospholane

2-chloro-4,4,5,5-tetramethyl-1,3,2-dioxaphospholane (TMDP or “phospholane”) as a phosphitylation reagent, depicted in Figure 6, shows great potential and has already proven to be able to provide quantitative structural information for lignins. The phosphitylation reagent is used to derivatize labile protons of biomass-based compounds which can then be analyzed and quantified using ^{31}P -NMR spectroscopy [21]. Therefore the phosphitylation reagent TMDP has seen wide applicability and is now considered as the most commonly employed phosphitylating reagent for hydroxy group analysis of biorefinery resources [22].

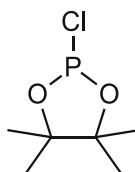


Figure 6: Structure of TMDP.

1.3.2.1 ^{31}P -NMR protocol with TMDP

Nowadays, the quantitative ^{31}P -NMR technique is widely used to characterize and quantify the hydroxy groups of biorefinery resources. According to studies, it was found that the values of hydroxy groups in lignins determined by ^{31}P -NMR are in good agreement with those obtained by other independent techniques, such as FTIR/pyrolysis, conductometric titration, and ^1H - and ^{13}C -NMR spectroscopy [22], [23]. Due to its high signal resolution, the ^{31}P -NMR method allows the discrimination of phenolic hydroxy groups attached to syringyl, guaiacyl, and *p*-hydroxyphenyl units instead of simply determining the total aromatic hydroxy groups [22]. ^{31}P -NMR also serves as a powerful technique for the analysis of phosphitylated labile protons in characterizing different types of functional groups such as aliphatic alcohols and phenols (OHs), aliphatic and aromatic acids (COOH), amines (NH), and thiols (SH) [24].

In the typical ^{31}P -NMR protocol, the hydroxy or amine groups of the substrate are phosphitylated with an appropriate phosphitylation reagent (e.g., TMDP), followed by the quantitative analysis using ^{31}P -NMR-spectroscopy and finally calculating the amounts of different hydroxy groups contained in the molecule. The decisive factor for the quantification of the hydroxy groups is the use of an internal standard.

1.3.2.2 Application of the method

Identification of bioprocess derived and involved residues in lignin

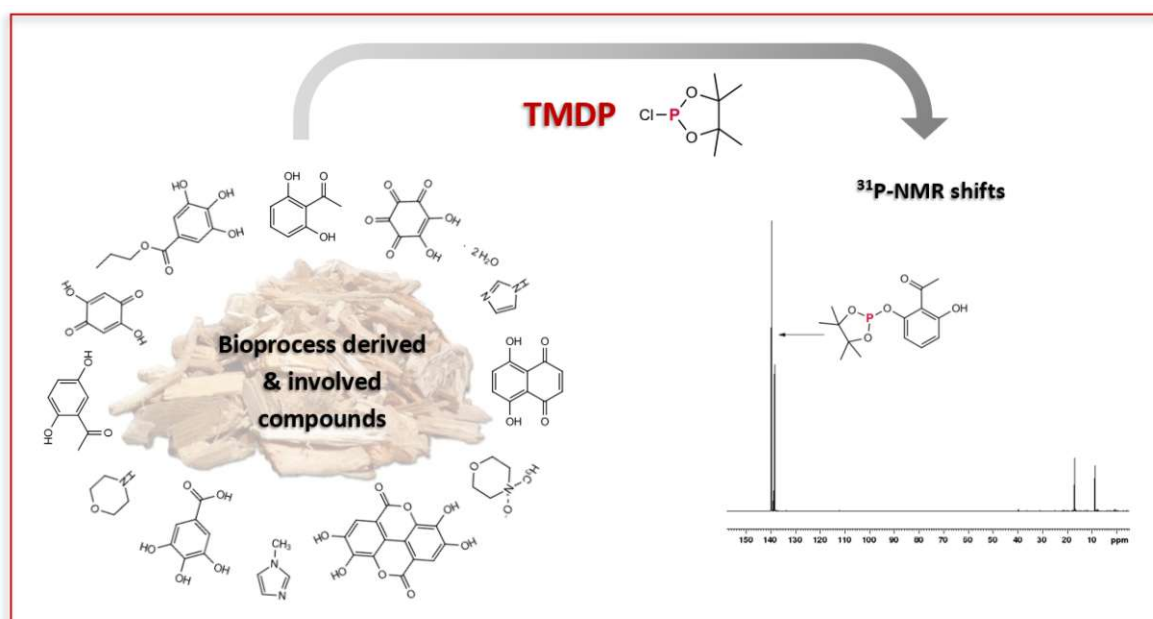
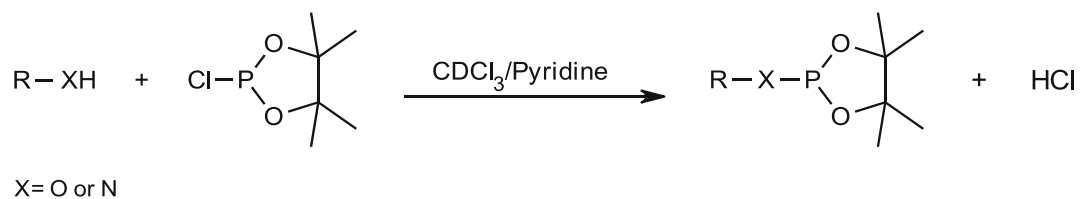


Figure 7: Illustration of the purpose of the derivatization method with TMDP. Biomass-related model compounds or chemicals typically used or generated in biomass pretreatment are phosphitylated with TMDP, allowing their chemical shifts to be identified using ^{31}P -NMR spectroscopy.

Within this study, the focus lies on the derivatization of labile protons from hydroxy groups and amine groups of lignocellulose-related compounds, or chemicals typically used or generated in biomass pretreatment and the subsequent analysis of the derivatization products by ^{31}P -NMR spectroscopy. Since the quantification of the hydroxy groups is not part of this work, no internal standard is included in the protocol. Phosphitylation of the different biomass-, and residual- or degraded compounds allows accurate determination of their ^{31}P -chemical shifts, which are of great importance in the qualitative analysis of lignin. Therefore, misinterpretation of these signals is avoided resulting in a more proper NMR analysis of lignin since such compounds can occur as undesirable impurities (degradation products, solvent residues, etc.) in lignins.

Scheme 3 represents the phosphitylation with TMDP of the labile proton from a hydroxy or an amine group in general form, where “R” should represent the selected biomass-related model compound or pretreatment residues/by-products.



Scheme 3: Phosphitylation of the labile proton from a hydroxy (OH) or amine (NH) group from the selected biomass-related model compounds (R) with TMDP.

1.4 NMR-spectroscopy

1.4.1 Principle

Nuclear magnetic resonance (NMR) is a spectroscopic method applied for the observation of the electronic environment of individual atoms and their interactions with neighbor atoms.

The method is based on a resonant interaction between the magnetic moment of the atomic nuclei and a strong, static magnetic field. The NMR signal is generated by exciting the atomic nuclei of the sample with radiofrequency waves.

The prerequisite for analyzing a nucleus with NMR spectroscopy is the existence of a magnetic moment. All nuclei possessing a spin, and accordingly do not have an even number of neutrons and protons at the same time, fulfill this requirement. The magnetic moment μ thus results according to (1) from the Planck's quantum of action h and the nuclear spin I . The proportionality factor γ , called the gyromagnetic ratio, is a specific constant for each NMR-active nucleus.

$$\mu = \frac{\gamma h}{2\pi} \cdot \sqrt{I(I + 1)} \quad (1)$$

When an external magnetic field with magnetic flux density B_0 is applied, alignment of the magnetic moments occurs. The different spins of the observed nuclei then distribute to $2I + 1$ energetic state, called Zeeman levels, and their energy difference is given by (2).

$$\Delta E = \frac{\gamma h}{2\pi} \cdot B_0 \quad (2)$$

One of the two (in the case of a nucleus with $I = \frac{1}{2}$) energy states is energetically more favorable and is called the ground state N_0 , while the energetically higher state N_1 has a lower population owing to the higher energy demand. This population difference is the basic requirement for recording NMR spectra and can be increased, for instance, by amplifying the B_0 field.

By irradiation with a resonance frequency ν_0 , spins are raised from the ground state to the excited state, and spins occupying the excited state are lowered to the ground state. Given the stronger population of the ground state, absorption predominates and at the end of the excitation, pulse saturation occurs, implying the equal occupation of both energy states. This is reflected in a transverse magnetization in the x,y-plane, which precedes around the z-axis, the direction of the static magnetic

field. The frequency of the precession is detected as a time-dependent signal and after Fourier transformation, the frequency-dependent NMR spectrum is obtained. During the relaxation of the spins, the transverse magnetization slowly dissipates and equilibrium with population difference according to Boltzmann distribution is restored. The resonance frequency ν_0 required for excitation depends on the gyromagnetic ratio γ of the observed nucleus, as shown in equation (3).

$$\nu_0 = \frac{\gamma}{2\pi} \cdot B_0 \quad (3)$$

A lower resonance frequency results in poorer resolution and sensitivity, as this reduces the population difference. In addition, the sensitivity is affected by the natural abundance of the observed nucleus. Protons, for instance, show a natural abundance of 99.98 %, while the abundance of ^{13}C -atoms is much lower, amounting to only 1.11 % [25].

1.4.2 ^{31}P -NMR

Phosphorus-31 has a natural abundance of 100%, showing a lower NMR sensitivity compared to ^1H -NMR but higher than ^{13}C -NMR. The most common reference substance is 85% aqueous phosphoric acid (H_3PO_4) as the external standard. Since it must be applied externally, it is not an ideal reference substance, but it is still the best option since many phosphorus compounds are very reactive and spectra of both organic and inorganic compounds should be able to be recorded. Other possibilities for compounds that could serve as secondary references are triphenyl phosphite ($\text{C}_{18}\text{H}_{15}\text{O}_3\text{P}$) (+ 127 ppm) and phosphorus tribromide (PBr_3) (+ 227 ppm). Considering phosphorus' nuclear spin quantum number ($I = \frac{1}{2}$) and its high relative sensitivity compared to other nuclei, the recording of ^{31}P -NMR spectra does not present major experimental difficulties apart from the large spectral widths. The range of chemical shifts for phosphorus compounds is nearly 4000 ppm. The coupling of a ^{31}P -nucleus to a directly bonded atom X, $J(\text{P}, \text{X})$, can be as large as 17 kHz. However, if X is a non-metallic element, the range is usually from 50 to 1500 Hz. The relaxation times of ^{31}P -nuclei are typically between 1 and 50 seconds, which means that the linewidths in high-resolution spectra are usually less than 0.5 Hz [26].

To label functional groups in lignins for NMR analyses, a few requirements are placed on the NMR-active nuclei: the sensitivity of the nuclei in an NMR experiment, the availability of suitable derivatization reagents, the ease of quantitative derivatization under mild conditions, and the stability of the reaction products. All these conditions are fulfilled by the ^{31}P -nucleus [24].

The characterization of lignins and biomass-related components employing the ^{31}P -NMR method involves the derivatization of the components with an appropriate derivatization reagent (e.g., TMDP). The reaction of the derivatization reagent with the labile protons of the substance to be characterized results in a phosphite ester, in which a phosphorus atom is surrounded by three oxygen atoms (in the case of hydroxy groups). This fact is of considerable importance from the NMR point of view because it ensures that the ^{31}P -NMR signals of such derivatives are observed as singlets that do not contain any coupling information leading to simpler spectra [24].

1.4.3 Lignin elucidation by NMR

The advent of sophisticated nuclear magnetic resonance (NMR) technology has greatly improved the study of complex lignin macromolecules. Due to its versatility in revealing structural features and structural changes of lignin polymers, this method has been established as the most widely used technique for the structural characterization of lignin. In particular, the application of multidimensional NMR technology shows great potential in elucidating the complex arrangement of lignin subunits and types of linkages. Compared to conventional 1D NMR spectra, by adding another spectral dimension, the chemical shift space is considerably extended, benefitting the evaluation. Currently, the most widely used experiment for lignin research is the 2D-HSQC (heteronuclear single-quantum coherence), in which ^{13}C and ^1H nuclei are correlated by developing and transferring single-quantum coherence *via* one-bond C-H coupling ($^1J_{\text{CH}}$). The HSQC-spectrum represents a 2D spectrum in which one dimension corresponds to the ^1H chemical shifts and the other dimension to the ^{13}C chemical shifts, with a cross-peak in the two dimensions then representing the one-bond C-H relationships [27]. To illustrate the evaluation of NMR spectra of lignins in general, both the aromatic (*c.f.* Figure 8) and the aliphatic range (*c.f.* Figure 9) of softwood lignin and hardwood lignin are shown as examples. In the aromatic region, cross-peaks, characteristic for the respective monolignol units in lignin, appear. The cross-peaks in the aliphatic region represent the side chains and the respective linkage types occurring therein.

Aromatic regions

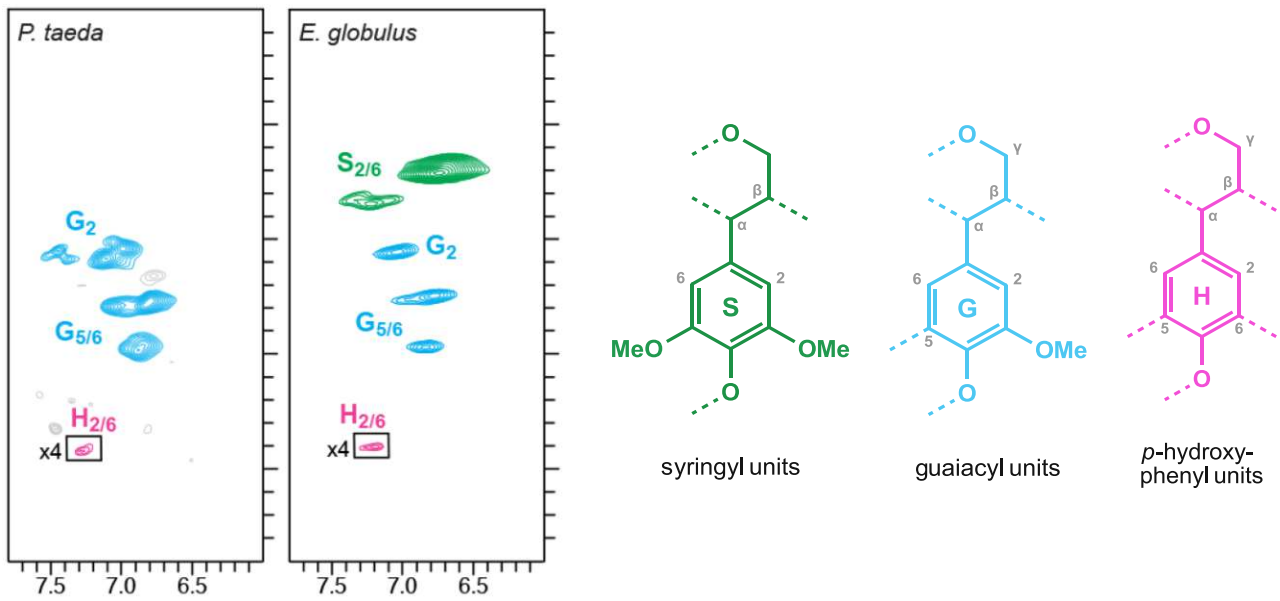


Figure 8: Aromatic regions of 2D $^1\text{H}/^{13}\text{C}$ -HSQC spectra of whole-cell-wall samples from an exemplary softwood (*Pinus taeda*) on the left and an exemplary hardwood (*Eucalyptus globulus*) on the right, adopted from [27]. In addition, the structures of the monolignol units S (syringyl-unit) in green, G (guaiacyl-unit) in blue, and H (*p*-hydroxyphenyl-unit) in pink are shown. In softwood lignin, mainly guaiacyl-units occur, whereas in hardwood a mixture guaiacyl- and syringyl- units are present [11].

Aliphatic regions

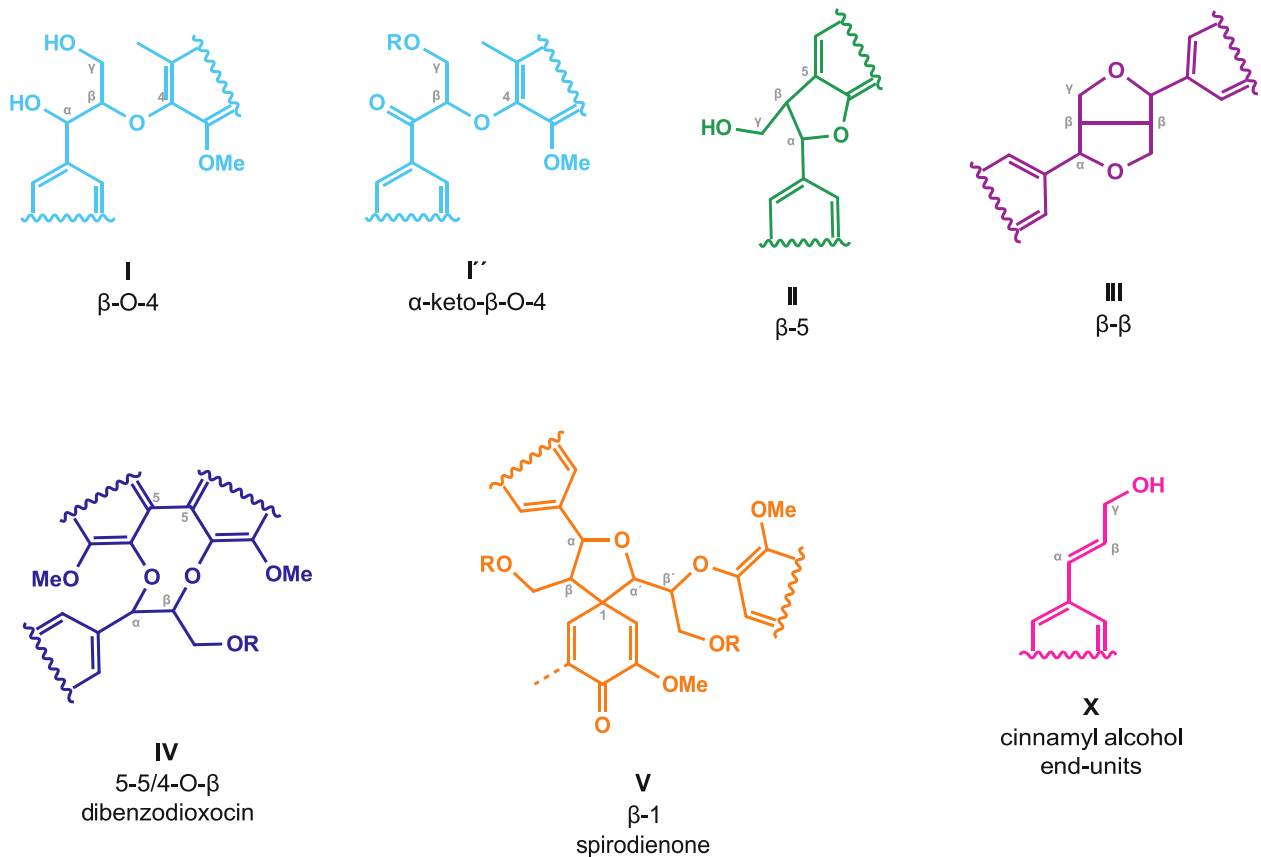
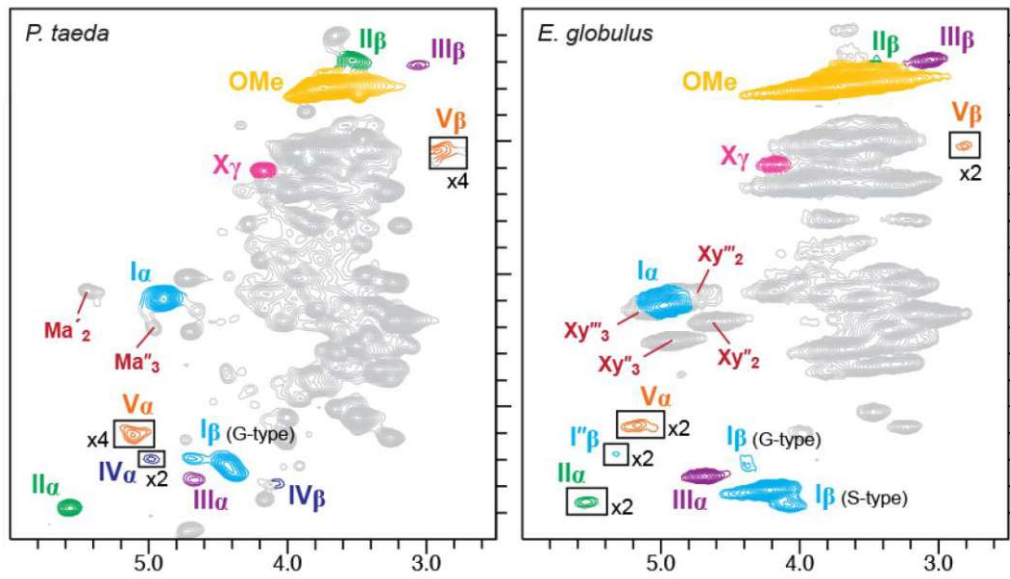


Figure 9: Aliphatic regions of 2D $^1\text{H}/^{13}\text{C}$ -HSQC spectra of whole-cell-wall samples from an exemplary softwood (*Pinus taeda*) on the left and hardwood (*Eucalyptus globulus*) on the right, adopted from [27]. The linkage types I-V and X, which occur in these two lignins are shown and are color-coded to match the cross-peaks that represent them. The gray, abundant cross-peaks originate from non-associated polysaccharides, solvents, etc. As indicated in the spectrum, the yellow cross-peaks represent methoxyl groups (OMe). The following abbreviations indicate: Ma' : 2-O-Ac mannan, Ma'' : 3-O-Ac mannan, $\text{X}\gamma'$: 3-O-Ac xylan, $\text{X}\gamma''$: 2,3-di-O-Ac xylan.

1.5 Model compounds

Due to lignin's heterogeneous structure and varying composition, it is difficult to predict its reactivity and to characterize the polymer's behavior, and therefore it is of great advantage using model compounds, bearing similar linkages and functionalities of native lignin. A large part of lignin derivatives is made up of aromatic rings and substituent groups such as phenolic hydroxy groups, methoxy groups, alcoholic hydroxy groups, and aldehyde groups. Lignin model compounds play an important role in studying reaction patterns and predicting the chemical behavior of the polymer.

The model compounds selected for iodination (*c.f.* Figure 1) feature similar structures to native lignin, while the model compounds selected for phosphitylation (*c.f.* Figure 2) include biomass-derived compounds (by-products, solvent residues, decomposition products, etc.).

The model compounds investigated in this master thesis are briefly explained below.

1.5.1 Methyl isoeugenol and Isoeugenol

Lignin can be regarded as a higher molecular weight derivative of phenylpropane, and since these two substances, methyl isoeugenol, and isoeugenol, belong to the group of phenylpropanoids, they serve as suitable model compounds. The lignin-related phenylpropanoid isoeugenol is also one of the most abundant phenolic compounds formed by depolymerization reactions of lignin [28].

1.5.2 Vanillin

The structure of vanillin includes the typical guaiacyl-residue that occurs in native lignin and is thus well suited as a model compound. It can be obtained from various substances, such as eugenol, isoeugenol, lignin, ferulic acid, sugars, aromatic amino acids, etc.. One of the main products, resulting from the oxidative degradation of lignin in an alkaline medium using oxidizing agents like nitrobenzene is vanillin [29]. Based on the scientific literature, several independent lignin degradation pathways have been identified in different microorganisms, and vanillin is found as an intermediate metabolite in the β -aryl ether cleavage pathway and the ferulate catabolic pathway [30].

1.5.3 Vanillyl alcohol

Vanillyl alcohol serves as a typical lignin model substance, as it is made up of an aromatic ring, an alcoholic hydroxy group, a phenolic hydroxy group, and a methoxy group. The phenolic hydroxy group and the methoxy group represent the guaiacyl-residue, which is highly abundant in native lignin.

1.5.4 Veratraldehyde and veratric acid

The treatment of lignin (and also veratrylglycerol- β -guaiacyl ether – a dimeric non-phenolic β -O-4-type lignin model compound) under alkaline oxygen or hydrogen peroxide bleaching conditions (O_2 or H_2O_2) at high pH-levels results in the formation of the degradation products veratraldehyde and veratric acid. Since the compounds veratraldehyde and veratric acid consist of the 3,4-dimethoxy aromatic nucleus, which does not exist in native lignin, reactions with these substances cannot be fully equated with those of native lignin. Veratraldehyde can be regarded as an analog of vanillin and veratric acid as an analog of vanillic acid [31].

1.5.5 Veratryl alcohol

For the depolymerization of lignin, specific lignolytic enzymes are required and lignin peroxidase plays a key role in the degradation of lignin. Veratryl alcohol is the main substrate of this important lignin-degrading enzyme and is present in the lignin degradation process [32].

1.5.6 *p*-Cresol

This model compound, a derivative of phenol, is one of the most abundant phenolic compounds formed by depolymerization reactions of lignin [28]. Furthermore, *p*-cresol has the phenolic hydroxy group typically found as *p*-hydroxyphenyl (H) residue in native lignin.

1.5.7 Coniferyl alcohol

Coniferyl alcohol, classified as a phenylpropanoid, is one of the three monolignols (*c.f.* Figure 3) of which native lignin is largely composed, making it a very suitable model compound.

1.5.8 Guaiacylglycerol- β -guaiacyl ether

Guaiacylglycerol- β -guaiacyl ether is one of the most important lignin model compounds that in particular represents the arylglycerol- β -aryl ether structure in lignin, which is an important interphenylpropane linkage in lignins. Since the β -O-4 substructure appears abundantly in lignin (50-70%), guaiacylglycerol- β -guaiacyl ether is indispensable as a model structure for lignin research [33].

1.5.9 Veratrylglycerol- β -guaiacyl ether

Veratrylglycerol- β -guaiacyl ether represents a dimeric non-phenolic lignin model compound of the β -O-4-linkage-type. Since a β -alkyl aryl ether bond occurs in the structure, which is considered to be the most common interunit linkage in native lignin, the dimeric component represents a very important model compound for experiments and research on lignin. However, unlike the other dimeric model compound (guaiacylglycerol- β -guaiacyl ether), this structure does not possess a phenolic hydroxy group.

1.5.10 Chromophoric compounds

It has been shown that apart from pure cellulose, for example, bacterial cellulose, cellulosic pulps, fibers, and derivatives minute amounts (mostly in ppb range) of chromophoric compounds are present. Chromophores in pulp and paper are triggered by oxidative damage to the polysaccharide matrix during processing, especially oxidative bleaching and subsequent aging processes or they are already present in the starting pulp [34], [35], [36].

1.5.10.1 2,5-Dihydroxy-1,4-benzoquinone (DHBQ)

DHBQ is a primary chromophore (originating from carbohydrate substances or the respective degradation products) and was found in all cellulosic materials investigated. This chromophoric compound was observed to be formed by cellulose degradation during thermal conditions of *Lyoce* processing. It can be regarded as a basic "chromophore precursor structure" that on the one hand can be easily degraded to smaller, reactive fragments and on the other hand can condense to larger structures, resulting in the formation of other chromophores and highly condensed structures of 2,5-dihydroxy-1,4-benzoquinone. This chromophore could also be found and isolated in the pulp that had been refluxed in DMAc and thoroughly washed afterward [35], [36].

1.5.10.2 5,8-Dihydroxy-1,4-naphtoquinone (DHNQ)

This chromophoric compound can be considered as a secondary chromophore (process chemicals are involved in their formation), which is formed by primary chromophores under the prevailing more drastic and oxidative conditions if the material has undergone prolonged thermal treatment in NMMO [35], [36].

1.5.10.3 2,5-Dihydroxyacetophenone (2,5-DHAP)

2,5-DHAP is also considered as a primary chromophore and is a typical condensation product from carbohydrates, which is obtained either by thermal, acidic, or alkaline treatment. It is also a cellulose degradation product, formed during the thermal conditions of *Lyocell* and *Viscose* processing. Also, 2,5-DHAP could be isolated, according to the novel chromophore isolation method, from pulp, which was heated under reflux in DMAc and then washed thoroughly [35], [36].

The three compounds mentioned above - DHNQ, DHBQ, and 2,5-DHAP - were found in all the analyzed materials and have become known as the three key cellulosic chromophores [34].

1.5.10.4 2,6-Dihydroxyacetophenone (2,6-DHAP)

2,6-DHAP is also considered a primary chromophore and was found in the *Viscose* pulping process only. This chromophore was isolated from pulp, which had been heated in DMAc under reflux and then washed thoroughly. This in turn indicates that these chromophores (2,6-DHAP, 2,5-DHAP, and DHBQ) are formed by thermal stress from cellulose largely independent of the reaction medium. [35], [36].

1.5.11 *N*-Methylmorpholine-*N*-oxide monohydrate

N-methylmorpholine-*N*-oxide monohydrate (NMMO) represents the solvent for cellulose in *Lyocell* technology, which can be considered as an environmentally friendly cellulose solvent, as it dissolves cellulose completely without the need for chemical derivatization.

1.5.12 Morpholine

As stated, NMMO serves as a solvent for cellulose in the *Lyocell* fiber-making process. Depending on the temperature, the duration of thermal stress, cellulose concentration, and the quality of the NMMO, morpholine can be formed as a degradation product of NMMO (monohydrate) in the dissolution process [37], [38], [39].

1.5.13 Imidazole and 1-Methyl imidazole

These two substances can be considered as ionic-liquid-related substances. Several ionic liquids are capable of fractionating lignocellulosic materials, with cellulose processing often performed in imidazolium-type ionic liquids. Imidazole and 1-methyl imidazole are formed as degradation products of 1-butyl-3-methyl-imidazolium (BMIM) and 1-ethyl-3-methyl-imidazolium (EMIM), which both represent ionic liquids with wide utilization [38],[40].

1.5.14 Rhodizonic acid dihydrate

As already stated above (*c.f.* chapter 1.5.10.1), 2,5-dihydroxy-1,4-benzoquinone (DHBQ) is considered as the most prominent representative of cellulosic key chromophores, occurring in almost all types of aged cellulose. Rhodizonic acid, which is a secondary chromophore, results from the degradation of DHBQ in the presence of excess chlorine dioxide. Especially in the form of its salt, rhodizonic acid is even more stable and more potent as a chromophore than DHBQ [41].

1.5.15 Gallic acid

Gallic acid is a natural phenolic compound that is found in many plants such as gallnuts, lacquer trees, oak bark, tea, and grapes [42]. Gallic acid represents the building block of the plant tannin group of gallic tannins.

1.5.16 Ellagic acid

Ellagic acid is a naturally occurring phenolic component produced by many different plants such as oaks, chestnuts, and walnuts and it also acts as a building block of ellagic tannins. The compound is a condensed dimer of gallic acid which is also the prevalent phenolic acid in plant tannins [43].

1.5.17 Propyl gallate

Propyl gallate is also part of the gallate group and represents an ester of gallic acid. It is not a natural compound and can only be obtained *via* chemical synthesis. In practice, propyl gallate is prepared either by biological (enzymatic) or chemical methods, whereas the latter has been dominant, focusing on the reaction between gallic acid and n-propanol [44].

2 EXPERIMENTAL PART

2.1 Materials and Methods

2.1.1 Reagents and solvents

The used reagents and solvents were bought from commercial sources with a purity of > 95%, and unless otherwise noted used without further purification.

2.1.2 Lignins

Two different native lignin samples (spruce and beech) were provided by a project partner. The samples were purified by precipitation (*c.f.* chapter 2.2.4) and freeze-dried.

2.1.3 NMR analysis

The NMR spectra were recorded on a Bruker Avance II 400 spectrometer (^1H resonance at 400.13 MHz, ^{13}C resonance at 100.61 MHz, and ^{31}P resonance at 161.98 MHz) equipped with a 5 mm N₂ cooled cryo probe head (Prodigy) with z-gradient at r.t. (standard Bruker pulse programs, shown in Table 3 below; Bruker, Rheinstetten, Germany). Data processing was performed with the software Bruker Topspin 3.6.3. Chemical shifts were referenced to the solvent signals for CDCl₃: δ (^1H) = 7.26 ppm, δ (^{13}C) = 77 ppm; DMSO: δ (^1H) = 2.49 ppm, δ (^{13}C) = 39.60 ppm; CD₃OD: δ (^1H) = 3.31 ppm, δ (^{13}C) = 49 ppm; C₅D₅N: δ (^1H) = 7.22, 7.58, 8.74 ppm, δ (^{13}C) = 123.87, 135.91, 150.35 ppm.

1D-NMR experiments (^1H , ^{13}C , and ^{31}P) and 2D-NMR experiments (COSY, HSQC, HMBQ, and TOCSY) were employed to evaluate the structures.

The respective NMR parameters for ^1H -, ^{13}C - and ^{31}P -experiments are listed in Table 3.

Table 3: NMR parameters listed for ^1H -NMR, ^{13}C -NMR, and ^{31}P -NMR respectively.

Experiment	Bruker pulse program	Acquisition parameter		Processing parameter	
^1H	zg30	TD	32.768	SI	32 k
		SW (ppm)	16	SF (MHz)	400.13
		SWH (Hz)	6400	WDW	gm
		O1P (ppm)	7	LB (Hz)	-0.3
		O1 (Hz)	2800	GB	0.3
		D1 (s)	1		
		P1 (μs)	11.7		
		PLW (W)	9		
^{13}C	jmod	TD	65.536	SI	32 k
		SW (ppm)	239	SF (MHz)	100.61
		SWH (Hz)	24000	WDW	em
		O1P (ppm)	110	LB (Hz)	1
		O1 (Hz)	11067.40		
		D1 (s)	1		
		P1 (μs)	10.2		
		PLW (W)	32		
		J(XH) (Hz)	145		
^{31}P	zg30 zgdc	TD	65.536	SI	32 k
		SW (ppm)	322	SF (MHz)	161.98
		SWH (Hz)	52083	WDW	em
		O1P (ppm)	60.000	LB (Hz)	2
		O1 (Hz)	9718.54		
		D1 (s)	1		
		P1 (μs)	11.90		
		PLW (W)	28		

2.2 Derivatization method I – Iodination

2.2.1 Solvent selection

The reactions were first carried out in deuterated methanol (CD_3OD). The reason for using deuterated methanol as a solvent rather than deuterated chloroform (CDCl_3), which would have been the first choice, is that the solubility of some model compounds in chloroform is not given. In addition, deuterated methanol was used for the reaction, so that NMR measurements could be directly carried out to monitor the reaction. Since solvent-dependent side reactions occurred in deuterated methanol, the solvent was changed, and normal methanol (CH_3OH) was used. Also, literature [20] suggested methanol as a suitable solvent for these reactions. However, the results obtained in this thesis showed that methanol also proved not to be the most suitable solvent for these reactions and caused some side reactions.

Therefore, an attempt was made to perform the reactions in chloroform (CHCl_3), despite the lower solubility of the components. To increase the solubility, the substances were mixed with the solvent and stirred overnight. As a result, a large part of the substance quantity was finally dissolved and the solubility requirement for successful reactions was fulfilled.

Initially, pyridine was avoided as a solvent because it was considered a disturbing factor in NMR evaluation due to the three solvent peaks in the aromatic region. Furthermore, it is more challenging to remove pyridine residues from a reaction mixture compared to the other solvents. However, it was subsequently chosen as the solvent for the reactions, due to the better solubility of the substances in pyridine. More specifically, deuterated pyridine ($\text{C}_5\text{D}_5\text{N}$) was utilized so that NMR measurements could be performed directly during the reactions.

The derivatization reactions with PyICl for the model compounds **8-14** were all carried out in either deuterated chloroform or deuterated pyridine, depending on the solubility of the model compounds. Given the solvent-related by-products encountered in the series of measurements previously carried out for model compounds **1-7** (especially with deuterated methanol and protonated methanol), it was decided to discontinue the use of these solvents. The extractions (*c.f.* chapter 2.2.3) were no longer performed with the subsequent model compounds either, and therefore, the solvent CHCl_3 was also no longer considered.

2.2.2 Sample preparation

Approximately 15 to 20 mg of the sample were dissolved in the respective solvent. If the dissolution was not complete, the sample was stirred overnight to ensure that a large part of the amount was dissolved. Since this study was a qualitative rather than a quantitative analysis, this approach was sufficient. The dissolved sample was mixed 1:1 (molar) with the iodination reagent (PyI₂). The reaction mixture was shaken and, if deuterated solvent was used, transferred directly into an NMR tube. In the case of non-deuterated solvent, the solvent was evaporated *in vacuo* and the solid remaining reaction mixture was redissolved in a deuterated solvent.

2.2.3 Workup

For the first derivatization reactions with PyI₂ (model compounds **1-7** and **12-14**), extraction was carried out as a purification step to get rid of salts possibly formed during the reaction (e.g., pyridinium salts of PyI₂). The reaction mixture was mixed with chloroform (CHCl₃) and deionized water and extracted twice. The organic phases were combined, and the solvent was evaporated *in vacuo*. The remaining reaction mixture was subsequently dissolved in a deuterated solvent and transferred to an NMR tube. Since no salt formation was observed for model compounds **8-11** resulting in well-resolved NMR spectra without a purification step, the extraction was no longer performed on these samples.

2.2.4 Lignin purification

Approximately 400 mg of the lignin samples were dissolved in the minimum required amount (approximately 3 ml) of 75 Vol.-% acetic acid and stirred at the vortex mixer until complete solubility of the samples was achieved. The sample solution was then introduced drop by drop into a large excess (12x) of deionized water (approximately 36 ml). After storing the formed dispersion of lignin in water at 4°C overnight it was centrifuged 3 times at 5000 rpm at -5°C. The supernatant was separated from the solid residue and redispersed in deionized water (12 ml) for washing purposes and centrifuged again two times. The combined solid lignin precipitates were freeze-dried overnight.

The dry lignin was again dissolved in the minimum required amount (approx. 1.5-2 ml for spruce and 1-1.5 ml for beech) of a mixture of 1,2-dichloroethane/ethanol (2:1) and stirred at the vortex mixer until complete dissolution of the samples was achieved (dissolution was time demanding). The solution was introduced slowly into an excess (approx. 25 ml) of diethyl ether, resulting in precipitation. The suspension was centrifuged at 5000 rpm for 10 min at 15°C. The diethyl ether was decanted, and the lignin was suspended by stirring with ether and centrifuged again. This washing step was repeated four times. The pure lignin was dried under vacuum for several days.

2.3 Derivatization method II – Phosphitylation

2.3.1 Solvent selection

The first measurement series was carried out in a solvent mixture of deuterated chloroform and deuterated pyridine (CDCl_3 : pyr- d_5 = 1:1.6), as this has already been proven for this method according to the literature. However, the use of the solvent mixture had a negative influence on the homogeneity of the magnet system and the quality of shimming procedure was limited. The addition of chloroform to the solvent mixture usually serves to dissolve the sample (along with the added pyridine), prevents precipitation of the pyridine-HCl salt (formed by the HCl liberated during the reaction and pyridine (c.f. Scheme 3)), and provides the deuterated signal required for NMR signal locking [22].

However, since most of the model compounds show good solubility in pure pyridine (in comparison to pure chloroform) and the possible formation of pyridine-HCl salt should not create any decisive problems, it was decided to repeat the measurements in pure pyridine (deuterated).

2.3.2 Sample preparation

In the first series of measurements, 15-20 mg of sample were dissolved in 600 μl of a 1:1.6 mixture of CDCl_3 and deuterated pyridine (the solvent mixture was dried over a molecular sieve). In the second series, the samples were dissolved in 600 μl deuterated pyridine. The samples were then shaken to ensure dissolution. The solubility of the model compounds in the solvent mixture was in some cases not always complete, but it was sufficient for NMR measurements to be carried out (except for rhodizonic acid dihydrate **23**, which was very poorly soluble). After thorough mixing, 50 μl phosphitylation reagent (2-chloro-4,4,5,5-tetramethyl-1,3,2-dioxaphospholane) was added through a septum into the vial to avoid any contact between reagents and moisture. After the addition of TMDP, the sample was shaken for 1 h at room temperature and subsequently transferred into an NMR tube.

3 RESULTS AND DISCUSSION

3.1 NMR analysis of the pure model compounds

In the following tables, ^1H - and ^{13}C - chemical shifts of the pure model compounds are given. The multiplicity of the peaks is only indicated if it was apparent in the NMR spectra.

3.1.1 Methyl isoeugenol

Table 4: ^1H - and ^{13}C -shifts of methyl isoeugenol (NMR-solvent: CD_3OD).

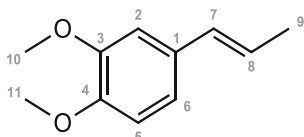
Atom number	^1H		^{13}C
	δ (ppm)	J (Hz)	δ (ppm)
1			132.83
2	6.94 (d)		110.22
3			149.60
4			150.44
5	6.82 (br.s)		112.88
6	6.85 (dd)		119.99
7	6.31 (dq)	15.7; 1.6	131.94
8	6.11 (qd)	15.7; 6.6	124.37
9	1.83 (dd)	6.6; 1.6	18.52
10	3.79 (s)		56.43
11	3.81 (s)		56.34

^1H -NMR (400 MHz, CD_3OD):

δ [ppm] 1.83 (dd, $J = 6.6, 1.6$ Hz, 3H), 3.81 (s, 3H), 3.79 (s, 3H), 6.11 (dq, $J = 15.7, 6.6$ Hz, 1H), 6.31 (dq, $J = 15.7, 1.6$ Hz, 1H), 6.82 (br. s, 1H), 6.85 (dd, 1H), 6.94 (d, 1H).

^{13}C -NMR (101 MHz, CD_3OD):

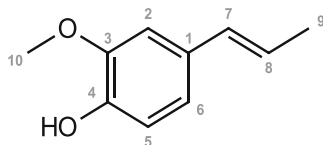
δ [ppm] 18.52 (q), 56.34 (q), 56.43 (q), 110.22 (d), 112.88 (d), 119.99 (d), 124.37 (d), 131.94 (d), 132.83 (s), 149.60 (s), 150.44 (s).



3.1.2 Isoeugenol

Table 5: ^1H - and ^{13}C -shifts of isoeugenol (NMR-solvent: CD_3OD).

Atom number	^1H		^{13}C
	δ (ppm)	J (Hz)	δ (ppm)
1			131.66
2	6.91 (d)	2.0	110.00
3			148.97
4			146.72
5	6.69 (d)	8.2	116.08
6	6.75 (dd)	8.2; 2.0	120.10
7	6.29 (dq)	15.7; 1.6	132.20
8	6.07 (qd)	15.7; 6.6	123.38
9	1.83 (dd)	6.6; 1.6	18.48
10	3.84 (s)		56.27



^1H -NMR (400 MHz, CD_3OD):

δ [ppm] 1.83 (dd, J = 6.6, 1.6 Hz, 3H), 3.84 (s, 3H), 6.07 (qd, J = 15.7, 6.6 Hz, 1H), 6.29 (dq, J = 15.7, 1.6 Hz, 1H), 6.69 (d, J = 8.2 Hz, 1H), 6.75 (dd, J = 8.2, 2.0 Hz, 1H), 6.91 (d, J = 2.0 Hz, 1H).

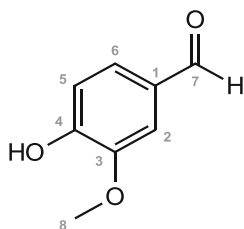
^{13}C -NMR (101 MHz, CD_3OD):

δ [ppm] 18.48 (q), 56.27 (q), 110.00 (d), 116.08 (d), 120.10 (d), 123.38 (d), 131.66 (s), 132.20 (d), 146.72 (s), 148.97 (s).

3.1.3 Vanillin

Table 6: ^1H - and ^{13}C -shifts of vanillin (NMR-solvent: CD_3OD).

Atom number	^1H		^{13}C
	δ (ppm)	J (Hz)	δ (ppm)
1			130.64
2	7.43 (s)		111.22
3			149.65
4			n.d.
5	6.94 (dd)	7.7	116.28
6	7.42 (dd)	7.7; 1.9	127.91
7	9.74 (s)		192.86
8	3.91 (s)		56.35



^1H -NMR (400 MHz, CD_3OD):

δ [ppm] 3.91 (s, 3H), 6.94 (dd, $J = 7.7$ Hz, 1H), 7.42 (dd, $J = 7.7, 1.9$ Hz, 1H), 7.43 (s, 1H), 9.74 (s, 1H).

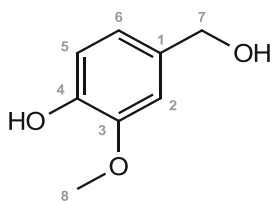
^{13}C -NMR (101 MHz, CD_3OD):

δ [ppm] 56.35 (q), 111.22 (d), 116.28 (d), 127.91 (d), 130.64 (s), 149.65 (s), 192.86 (s).

3.1.4 Vanillyl alcohol

Table 7: ^1H - and ^{13}C -shifts of vanillyl alcohol (NMR-solvent: CD_3OD).

Atom number	^1H		^{13}C
	δ (ppm)	J (Hz)	δ (ppm)
1			134.18
2	6.94 (d)	1.6	112.05
3			148.91
4			146.91
5	6.75 (d)	8.0	115.93
6	6.78 (dd)	8.0; 1.6	121.06
7	4.50 (s)		65.31
8	3.85 (s)		56.27



^1H -NMR (400 MHz, CD_3OD):

δ [ppm] 3.85 (s, 3H), 4.50 (s, 2H), 6.75 (d, $J = 8.0$ Hz, 1H), 6.78 (dd, $J = 8.0, 1.6$ Hz, 1H), 6.94 (d, $J = 1.6$ Hz, 1H).

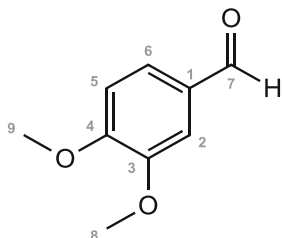
^{13}C -NMR (101 MHz, CD_3OD):

δ [ppm] 56.27 (q), 65.31 (t), 112.05 (d), 115.93 (d), 112.05 (d), 115.93 (d), 121.06 (d), 134.18 (s), 146.91 (s), 148.91 (s).

3.1.5 Veratraldehyde

Table 8: ^1H - and ^{13}C -shifts of veratraldehyde (NMR-solvent: CD_3OD).

Atom number	^1H		^{13}C
	δ (ppm)	J (Hz)	δ (ppm)
1			131.48
2	7.43 (d)	2.0	110.54
3			151.06
4			156.27
5	7.11 (d)	8.3	112.02
6	7.53 (dd)	8.3; 2.0	127.80
7	9.80 (s)		192.92
8	3.88 (s)		56.35
9	3.92 (s)		56.58



^1H -NMR (400 MHz, CD_3OD):

δ [ppm] 3.88 (s, 3H), 3.92 (s, 3H), 7.11 (d, $J= 8.3$ Hz, 1H), 7.43 (d, $J= 2.0$ Hz, 1H), 7.53 (dd, $J= 8.3, 2.0$ Hz, 1H), 9.80 (s, 1H).

^{13}C -NMR (101 MHz, CD_3OD):

δ [ppm] 56.35 (q), 56.58 (q), 110.54 (d), 112.02 (d), 127.80 (d), 131.48 (s), 151.06 (s), 156.27 (s), 192.92 (d).

3.1.6 Veratryl alcohol

Table 9: ^1H - and ^{13}C -shifts of veratryl alcohol (NMR-solvent: CD_3OD).

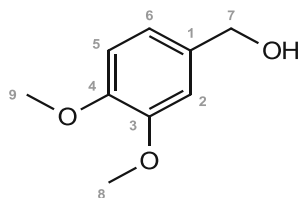
Atom number	^1H		^{13}C
	δ (ppm)	J (Hz)	δ (ppm)
1			135.60
2	6.97 (br.s)		112.17
3			150.42
4			149.78
5	6.89 (m)		112.75
6	6.89 (m)		120.69
7	4.53 (s)		65.10
8	3.83 (d)		56.33
9	3.81 (d)		56.47

^1H -NMR (400 MHz, CD_3OD):

δ [ppm] 3.81 (d, 3H), 3.83 (d, 3H), 4.53 (s, 2H), 6.89 (m, 1H), 6.89 (m, 1H), 6.97 (br.s, 1H).

^{13}C -NMR (101 MHz, CD_3OD):

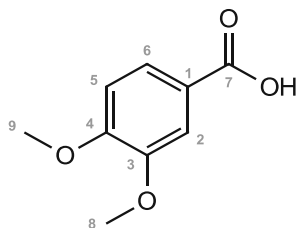
δ [ppm] 56.33 (q), 56.47 (q), 65.10 (t), 112.17 (d), 112.75 (d), 120.69 (d), 135.60 (s), 149.78 (s), 150.42 (s).



3.1.7 Veratric acid

Table 10: ^1H - and ^{13}C -shifts of veratric acid (NMR-solvent: CD_3OD).

Atom number	^1H		^{13}C
	δ (ppm)	J (Hz)	δ (ppm)
1			124.22
2	7.56 (d)	2.0	113.52
3			150.06
4			154.67
5	7.01 (d)	8.4	111.79
6	7.67 (dd)	8.4; 2.0	125.05
7			169.76
8	3.86 (s)		56.38
9	3.89 (s)		56.42



^1H -NMR (400 MHz, CD_3OD):

δ [ppm] 3.86 (s, 3H), 3.89 (s, 3H), 7.01 (d, J = 8.4 Hz, 1H), 7.56 (d, J = 2.0 Hz, 1H), 7.67 (dd, J = 8.4, 2.0 Hz, 1H).

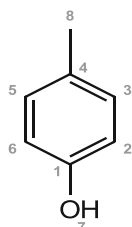
^{13}C -NMR (101 MHz, CD_3OD):

δ [ppm] 56.38 (q), 56.42 (q), 111.79 (d), 113.52 (d), 124.22 (s), 125.05 (d), 150.06 (s), 154.67 (s), 169.76 (s).

3.1.8 *p*-Cresol

Table 11: ^1H - and ^{13}C -shifts of *p*-cresol (NMR-solvent: CDCl_3).

Atom number	^1H		^{13}C
	δ (ppm)	J (Hz)	δ (ppm)
1			153.11
2, 6	6.74 (d)	8.6	115.04
3, 5	7.05 (d)	8.6	130.04
4			129.99
7	4.79 (s)		
8	2.29 (s)		20.43



^1H -NMR (400 MHz, CDCl_3):

δ [ppm] 2.29 (s, 3H), 4.79 (s, 1H), 6.74 (d, J = 8.6 Hz, 2H), 7.05 (d, J = 8.6 Hz, 2H).

^{13}C -NMR (101 MHz, CDCl_3):

δ [ppm] 20.43 (q), 115.04 (d), 129.99 (s), 130.04 (d), 153.11 (s).

3.1.9 Coniferyl alcohol

Table 12: ^1H - and ^{13}C -shifts of coniferyl alcohol (NMR-solvent: CDCl_3).

Atom number	^1H		^{13}C
	δ (ppm)	J (Hz)	δ (ppm)
1			129.20
2	6.92 (d)	1.8	108.27
3			146.59
4			145.56
5	6.86 (d)	8.1	114.42
6	6.89 (dd)	8.1; 1.8	120.30
7	6.53 (dt)	15.8; 1.4	131.38
8	6.22 (dt)	15.8; 5.9	126.12
9	4.30 (dd)	5.9; 1.4	63.86
10			
11	3.90 (s)		55.85
12	5.66 (s)		

^1H -NMR (400 MHz, CDCl_3):

δ [ppm] 3.90 (s, 3H), 4.30 (dd, J = 5.9, 1.4 Hz, 2H), 5.66 (s, 1H), 6.22 (dt, J = 15.8, 5.9 Hz, 1H), 6.53 (dt, J = 15.8, 1.4 Hz, 1H), 6.86 (d, J = 8.1 Hz, 1H), 6.89 (dd, J = 8.1, 1.8 Hz, 1H), 6.92 (d, J = 1.8 Hz).

^{13}C -NMR (101 MHz, CDCl_3):

δ [ppm] 55.85 (q), 63.86 (t), 108.27 (d), 114.42 (d), 120.30 (d), 126.12 (d), 129.20 (s), 131.38 (d), 145.56 (s), 146.59 (s).

3.1.10 Veratrylglycerol- β -guaiacyl etherTable 13: ^1H - and ^{13}C -shifts of veratrylglycerol- β -guaiacyl ether (NMR-solvent: CDCl_3).

Atom number	^1H		^{13}C
	δ (ppm)	J (Hz)	δ (ppm)
1			132.36
1'	6.91		121.62
2	6.97 (d)		109.10
2'	6.97 (m)	2.0	121.09
3			148.98
3'			146.82
4			148.42
4'			151.62
5	6.83 (d)	8.3	110.95
5'	6.94		112.12
6	6.90 (dd)	8.3; 2.0	118.34
6'	7.06 (ddd)	8.4; 7.2; 1.9	124.26
7	4.16 (ddd)	5.8; 4.7; 3.4	87.48
8a	3.91 (ddd)	12.2; 5.8; 5.4	60.71
8b	3.66 (ddd)	12.2; 7.7; 3.5	60.71
9	4.98 (dd)	4.7; 3.3	72.62
10	3.868 (s)		55.88*
11	3.874 (s)		55.88*
12	3.88 (s)		55.85*
13	3.51 (d)	3.3	
14	2.76 (dd)	7.7; 5.4	

*... exchangeable

 ^1H -NMR (400 MHz, CDCl_3):

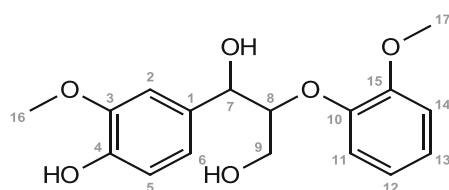
δ [ppm] 2.76 (dd, $J=7.7, 5.4$ Hz, 1H), 3.51 (d, $J=3.3$ Hz, 1H), 3.66 (ddd, $J=12.2, 7.7, 3.5$ Hz, 1H), 3.87 (s, 3H), 3.868 (s, 3H), 3.874 (s, 3H), 3.91 (ddd, $J=12.2, 5.8, 5.4$ Hz, 1H), 4.16 (ddd, $J=5.8, 4.7, 3.4$ Hz, 1H), 4.98 (dd, $J=4.7, 3.3$ Hz, 1H), 6.83 (d, $J=8.3$ Hz, 1H), 6.90 (dd, $J=8.3, 2.0$ Hz, 1H), 6.91 (1H), 6.94 (1H), 6.97 (d, 1H), 6.97 (m, 1H), 7.06 (ddd, $J=8.4; 7.2; 1.9$ Hz, 1H).

 ^{13}C -NMR (101 MHz, CDCl_3):

δ [ppm] 55.85 (q), 55.88 (q), 55.88 (q), 60.71 (d), 60.71 (d), 72.62 (d), 87.48 (d), 109.10 (d), 110.95 (d), 112.12 (d), 118.34 (d), 121.09 (d), 121.62 (d), 124.26 (d), 132.36 (s), 146.82 (s), 148.42 (s), 148.98 (s), 151.62 (s).

3.1.11 Guaiacylglycerol- β -guaiacyl etherTable 14: ^1H - and ^{13}C -shifts of guaiacylglycerol- β -guaiacyl ether (NMR-solvent: CDCl_3).

Atom number	^1H		^{13}C
	δ (ppm)	J (Hz)	δ (ppm)
1			131.73
2	6.97 (d)	1.8	108.58
3			146.59
4			145.09
5	6.88 (d)	8.1	114.24
6	6.83 (dd)	8.1; 1.8	118.99
7	4.97 (d)	4.6	72.72
8	4.16 (ddd)	6.1; 4.6; 3.3	87.51
9a	3.66 (dd)	12.2; 3.3	60.71
9b	3.91 (dd)	12.2; 6.1	60.71
10			146.84
11	6.98 (dd)	8.0; 1.7	121.12
12	6.92 (m)		121.64
13	7.07 (m)		124.29
14	6.94 (m)		112.15
15			151.64
16	3.88 (s)		55.97
17	3.89 (s)		55.88

 ^1H -NMR (400 MHz, CDCl_3):

δ [ppm] 3.66 (dd, $J = 12.2, 3.3$ Hz, 1H), 3.88 (s, 3H), 3.89 (s, 3H), 3.91 (dd, $J = 12.2, 6.1$ Hz, 1H), 4.16 (ddd, $J = 6.1, 4.6, 3.3$ Hz, 1H), 4.97 (d, $J = 4.6$ Hz, 1H), 6.83 (dd, $J = 8.1, 1.8$ Hz, 1H), 6.88 (d, $J = 8.1$ Hz, 1H), 6.92 (m, 1H), 6.94 (m, 1H), 6.97 (d, $J = 1.8$ Hz, 1H), 6.98 (dd, $J = 8.0, 1.7$ Hz, 1H), 7.07 (m, 1H).

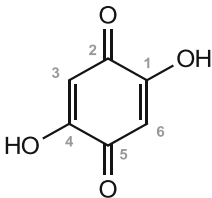
 ^{13}C -NMR (101 MHz, CDCl_3):

δ [ppm] 55.88 (q), 55.97 (q), 60.71 (d, 2C), 72.72 (d), 87.51 (d), 108.58 (d), 112.15 (d), 114.24 (d), 118.99 (d), 121.12 (d), 121.64 (d), 124.29 (d), 131.73 (s), 146.59 (s), 146.84 (s), 151.64 (s).

3.1.12 2,5-Dihydroxy-1,4-benzoquinone

Table 15: ^1H - and ^{13}C -shifts of DHBQ (NMR-solvent: $\text{C}_5\text{D}_5\text{N}$).

Atom number	^1H		^{13}C
	δ (ppm)	J (Hz)	δ (ppm)
1, 2, 4, 5			174.50
3, 6	6.29 (s)		105.70



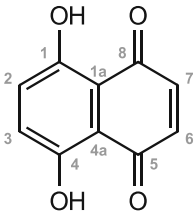
^1H -NMR (400 MHz, $\text{C}_5\text{D}_5\text{N}$): δ [ppm] 6.29 (s, 2H).

^{13}C -NMR (101 MHz, $\text{C}_5\text{D}_5\text{N}$): δ [ppm] 105.70 (d), 174.50 (s).

3.1.13 5,8-Dihydroxy-1,4-naphtoquinone

Table 16: ^1H - and ^{13}C -shifts of DHNQ (NMR-solvent: $\text{C}_5\text{D}_5\text{N}$).

Atom number	^1H		^{13}C
	δ (ppm)	J (Hz)	δ (ppm)
1a, 4a			112.90
1, 4, 8, 5			173.49
2, 3, 6, 7	7.19 (s)		135.20



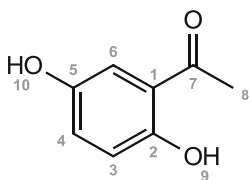
^1H -NMR (400 MHz, $\text{C}_5\text{D}_5\text{N}$): δ [ppm] 7.19 (s, 4H).

^{13}C -NMR (101 MHz, $\text{C}_5\text{D}_5\text{N}$): δ [ppm] 112.90 (s), 135.20 (d), 173.49 (s).

3.1.14 2,5-Dihydroxyacetophenone

Table 17: ^1H - and ^{13}C -shifts of 2,5-DHAP (NMR-solvent: $\text{C}_5\text{D}_5\text{N}$).

Atom number	^1H		^{13}C
	δ (ppm)	J (Hz)	δ (ppm)
1			120.98
2			156.22
3	7.11 (d)	8.8	119.64
4	7.39 (dd)	8.8; 2.9	126.29
5			151.32
6	7.56 (d)	2.9	116.99
7			205.16
8	2.52 (s)		27.41
9	12.25 (s)		
10	11.37 (s)		



^1H -NMR (400 MHz, $\text{C}_5\text{D}_5\text{N}$):

δ [ppm] 2.52 (s, 3H), 7.11 (d, J = 8.8 Hz, 1H), 7.39 (dd, J = 8.8, 2.9 Hz, 1H), 7.56 (d, J = 2.9 Hz, 1H), 11.37 (s, 1H), 12.25 (s, 1H).

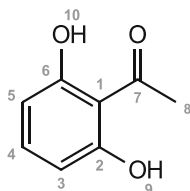
^{13}C -NMR (101 MHz, $\text{C}_5\text{D}_5\text{N}$):

δ [ppm] 27.41 (q), 116.99 (d), 119.64 (d), 120.98 (s), 126.29 (d), 151.32 (s), 156.22 (s), 205.16 (s).

3.1.15 2,6-Dihydroxyacetophenone

Table 18: ^1H - and ^{13}C -shifts of 2,6-DHAP (NMR-solvent: CDCl_3).

Atom number	^1H		^{13}C
	δ (ppm)	J (Hz)	δ (ppm)
1			110.17
2, 6			161.21
3, 5	6.40 (d)	8.2	108.35
4	7.24 (t)	8.2	136.06
7			205.25
8	2.75 (s)		33.46
9, 10	9.51 (s)		



^1H -NMR (400 MHz, CDCl_3):

δ [ppm] 2.75 (s, 3H), 6.40 (d, J = 8.2 Hz, 2H), 7.24 (t, J = 8.2 Hz, 1H), 9.51 (s, 2H).

^{13}C -NMR (101 MHz, CDCl_3):

δ [ppm] 33.46 (q), 108.35 (d), 110.17 (s), 136.06 (d), 161.21 (s), 205.25 (s).

3.1.16 Imidazole

Table 19: ^1H - and ^{13}C -shifts of imidazole (NMR-solvent: CDCl_3).

Atom number	^1H		^{13}C
	δ (ppm)	J (Hz)	δ (ppm)
1	12.53 (s)		
2	7.73 (t)	1.0	135.07
3, 4	7.12 (d)	1.0	121.75

^1H -NMR (400 MHz, CDCl_3):

δ [ppm] 7.12 (d, $J=1.0$ Hz, 2H), 7.73 (t, $J=1.0$ Hz, 1H), 12.53 (s, 1H).

^{13}C -NMR (101 MHz, CDCl_3):

δ [ppm] 121.75 (d), 135.07 (d).

3.1.17 1-Methyl imidazole

Table 20: ^1H - and ^{13}C -shifts of 1-Methylimidazole (NMR-solvent: CDCl_3).

Atom number	^1H		^{13}C
	δ (ppm)	J (Hz)	δ (ppm)
1	3.66 (s)		33.24
2	7.44 (br. s)		137.70
3	7.02 (br. t)	1.0	129.24
4	6.85 (t)	1.0	120.00

^1H -NMR (400 MHz, CDCl_3):

δ [ppm] 3.66 (s, 3H), 6.85 (t, $J=1.0$ Hz, 1H), 7.02 (br. t, $J=1.0$ Hz, 1H), 7.44 (br. s, 1H).

^{13}C -NMR (101 MHz, CDCl_3):

δ [ppm] 33.24 (q), 120.00 (d), 129.24 (d), 137.70 (d).

3.1.18 Morpholine

Table 21: ^1H - and ^{13}C -shifts of morpholine (NMR-solvent: CDCl_3).

Atom number	^1H		^{13}C
	δ (ppm)	J (Hz)	δ (ppm)
1	1.99 (s)		
2, 5	2.85 (m)		46.39
3, 4	3.66 (m)		67.97

^1H -NMR (400 MHz, CDCl_3): δ [ppm] 1.99 (s, 1H), 2.85 (m, 2H), 3.66 (m, 2H).

^{13}C -NMR (101 MHz, CDCl_3): δ [ppm] 46.39 (d), 67.97 (d).

3.1.19 N-Methylmorpholine-N-oxide

Table 22: ^1H - and ^{13}C -shifts of NMMO (NMR-solvent: CDCl_3).

Atom number	^1H		^{13}C
	δ (ppm)	J (Hz)	δ (ppm)
1	3.22 (s)		60.92
2, 5*	3.32 (tm)	11.4; 3.0	65.78
	3.09 (dm)	11.4	
3, 4*	3.72 (dm)	12.6	61.58
	4.34 (ddd)	12.6; 11.4; 2.2	

*... The peaks could not be exactly assigned from which of the two H-atoms they originate.

^1H -NMR (400 MHz, CDCl_3): δ [ppm] 3.09 (dm, $J = 11.4$ Hz, 1H), 3.22 (s, 3H), 3.32 (tm, $J = 11.4, 3.0$ Hz, 1H), 3.71 (dm, $J = 12.6$ Hz, 1H), 4.34 (ddd, $J = 12.6, 11.4, 2.2$ Hz, 1H).

^{13}C -NMR (101 MHz, CDCl_3): δ [ppm] 60.92 (q), 61.58 (d), 65.78 (d).

3.1.20 Ellagic acid

Table 23: ^1H - and ^{13}C -shifts of ellagic acid (NMR-solvent: CDCl_3)*.

Atom number	^1H		^{13}C
	δ (ppm)	J (Hz)	δ (ppm)
1, 1'			112.46
2, 2'			136.48
3, 3'			139.83
4, 4'			148.24
5, 5'	7.44 (s)		110.27
6, 6'			107.63
7, 7'			159.28

*... Literature [45] was used for the allocation of this component.

^1H -NMR (400 MHz, CDCl_3):

δ [ppm] 7.44 (s, 2H).

^{13}C -NMR (101 MHz, CDCl_3):

δ [ppm] 107.63 (s), 110.27 (d), 112.46 (s), 136.48 (s), 139.83 (s), 148.24 (s), 159.28 (s).

3.1.21 Gallic acid

Table 24: ^1H - and ^{13}C -shifts of gallic acid (NMR-solvent: CDCl_3).

Atom number	^1H		^{13}C
	δ (ppm)	J (Hz)	δ (ppm)
1			120.61
2, 6	6.91 (s)		108.90
3, 5			145.60
4			138.18
7			167.68
8	12.24 (br. s)		
9, 11	9.19 (br. s)		
10	8.83 (br. s)		

^1H -NMR (400 MHz, CDCl_3):

δ [ppm] 6.91 (s, 2H), 8.83 (br. s, 1H), 9.19 (br. s, 1H), 12.24 (br. s, 1H).

^{13}C -NMR (101 MHz, CDCl_3):

δ [ppm] 108.90 (d), 120.61 (s), 138.18 (s), 145.60 (s), 167.68 (s).

3.1.22 Propyl gallate

Table 25: ^1H - and ^{13}C -shifts of propyl gallate (NMR-solvent: CDCl_3).

Atom number	^1H		^{13}C
	δ (ppm)	J (Hz)	δ (ppm)
1			119.71
2, 6	6.95 (s)		108.60
3, 5			146.09
4			138.50
7			166.02
8	4.10 (t)	6.6	65.59
9	1.65 (qt)	7.4; 6.6	21.86
10	0.93 (t)	7.4	10.54

 ^1H -NMR (400 MHz, CDCl_3): δ [ppm] 0.93 (t, $J=7.4$ Hz, 3H), 1.65 (qt, $J=7.4$, 6.6 Hz, 2H), 4.10 (t, $J=6.6$ Hz, 2H), 6.95 (s, 2H). ^{13}C -NMR (101 MHz, CDCl_3): δ [ppm] 10.54 (q), 21.86 (t), 65.59 (t), 108.60 (d), 119.71 (s), 138.50 (s), 146.09 (s), 166.02 (s).

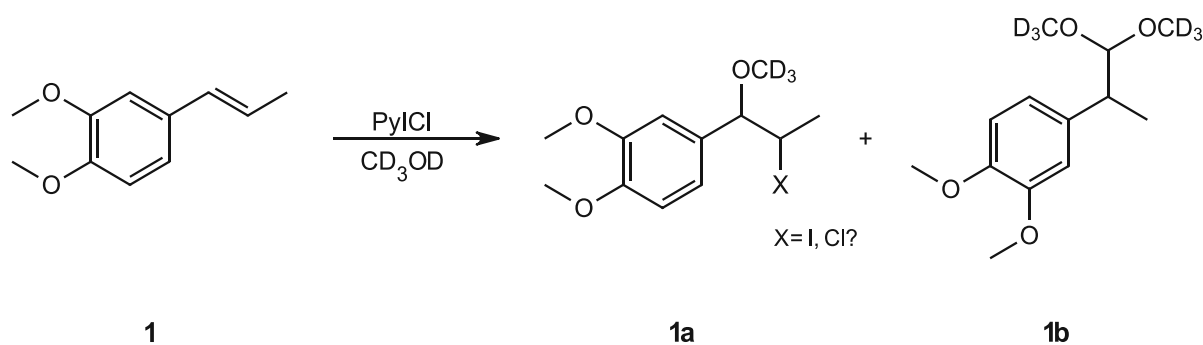
3.2 Derivatization method I – Iodination

In this chapter, the reaction schemes, and the ^1H - and ^{13}C - chemical shifts of the newly formed derivatives, resulting from derivatization reactions with PyICl are given. It was not always possible to elucidate the structure of all the components that were formed, in particular, whether the attached substituents involved iodine or chlorine, and the elucidation of minor products also posed a challenge due to low signal/noise or partial signal overlap with those of the main compounds. Therefore, it is important to emphasize that some of the structures and mechanisms mentioned are conjectures that have not been scientifically confirmed. For incomplete reactions, the ratio between the still available starting material and the product is quoted.

3.2.1 Methyl isoeugenol

Given the fact that methyl isoeugenol **1** is not a hydroxy-substituted molecule, one would not expect the characteristic iodination at the aromatic ring according to theory [20]. Nevertheless, it is of great interest how the molecule behaves in this reaction.

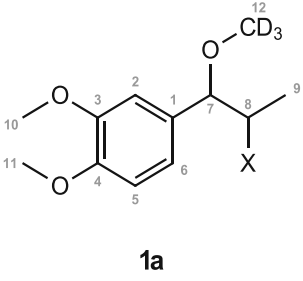
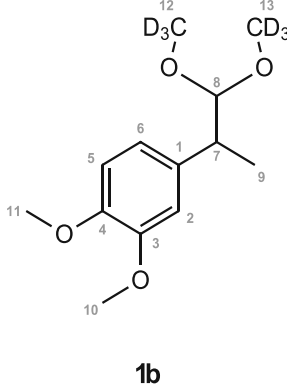
3.2.1.1 In deuterated methanol (CD_3OD)



Scheme 4: Reaction of methyl isoeugenol **1** with PyICl in CD_3OD and the products formed correspondingly where **1a** is the main component and **1b** is the secondary component. **1a:1b** ca. 4:1.

As indicated in Scheme 4, it is not known which substituent X is involved in component **1a**. Based on the use of PyICl as an iodinating reagent, it is suspected that the substituent could be either an iodine or a chlorine atom. Following Table 26 contains the ^1H - and ^{13}C - chemical shifts of components **1a** and **1b**.

Table 26: ^1H - and ^{13}C -shifts of the main component **1a** (left) and the secondary component **1b** (right) resulting from the reaction of methyl isoeugenol **1** and PylCl in CD_3OD . (NMR-solvent: CD_3OD).

							
Atom number	^1H		^{13}C	Atom number	^1H		^{13}C
	δ (ppm)	J (Hz)	δ (ppm)		δ (ppm)	J (Hz)	δ (ppm)
1			132.79	1			137.31
2	6.94 (d)	2.0	112.02	2	6.85 (d)	2.1	113.23
3			150.32 ^a	3			150.12
4			150.28 ^a	4			148.98
5	6.93 (d)	8.2	112.36	5	6.85 (d)	8.2	112.89
6	6.88 (dd)	8.2; 2.0	121.59	6	6.78 (dd)	8.2; 2.1	121.37
7	4.18 (d)	5.3	88.77	7	2.92 (qi)	7.0	43.85
8	4.39 (m)	7.0; 5.3	32.39	8	4.35 (d)	6.9	110.15
9	1.77 (d)	7.0	23.55	9	1.22 (d)	7.1	17.32
10	3.84 ^b (s)		56.44	10	3.82 (s)		56.36 ^c
11	3.83 ^b (s)		56.44	11	3.80 (s)		56.50 ^c
12			56.9	12, 13			54.0

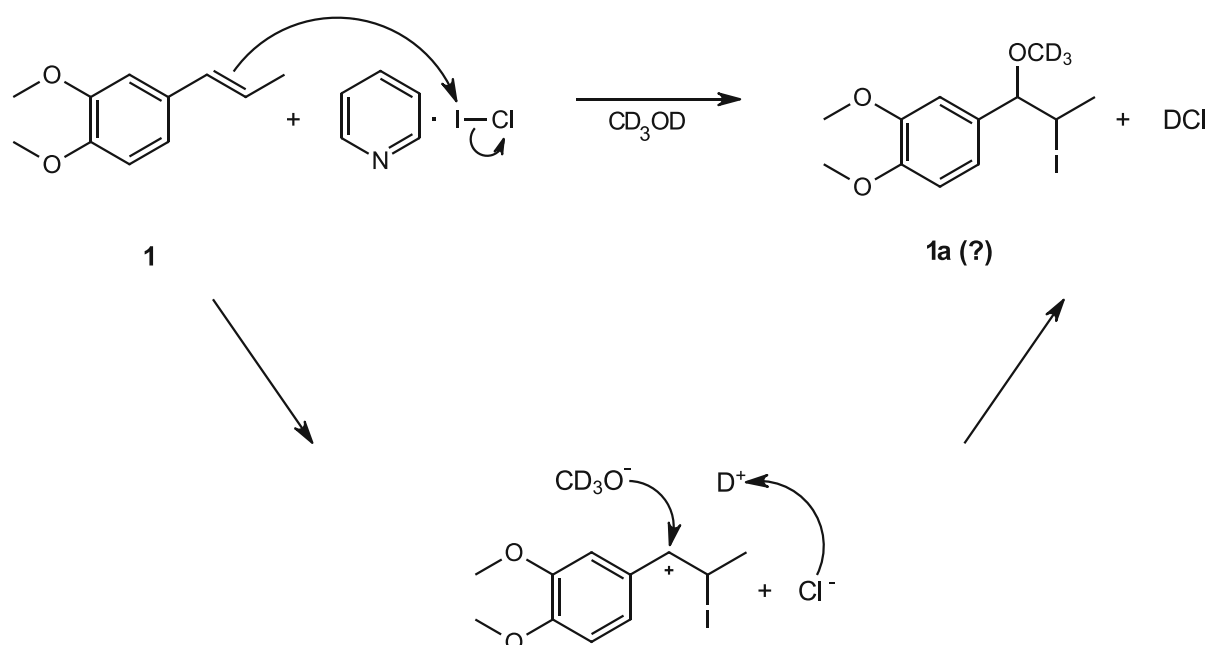
^{a,b,c}... exchangeable

The substituent X of component **1a** could neither be explicitly determined by mass spectrometry nor with the aid of NMR predict server "CSEARCH" [46] (*c.f.* Table 30). The addition of deuterated methanolate to the molecule was, however, confirmed by mass spectrometry (*c.f.* chapter 3.3.1). In component **1a**, the ^1H -shifts of atoms H7 (4.18 ppm) and H8 (4.39 ppm) indicate that the double bond is removed (compared to the starting material, see Table 4, where the shifts of these two H-atoms are in the region of the double bond protons at about 6 ppm). The ^{13}C -shifts of C7 (88.77 ppm) and C8 (32.39 ppm) also indicate a change in the electronic environment. The disappearance of the electron-rich double bond in the molecule causes a shift of the signals to lower frequencies. Chlorine and iodine exhibit a negative inductive effect, which in general is responsible for a shift to higher frequencies due to deshielding. However, the effect is very small. Both halogen atoms exhibit a +M-effect, which increases the electron density at the nucleus and thus leads to shielding, accompanied by a shift to

lower frequencies. In the case of the iodine atom, however, this effect is considerably weakened owing to its size. In the case of component **1a**, the conversion from an olefinic bond to an electron-poorer aliphatic bond and the +M effect of the presumed substituents probably predominate, resulting in an overall shift to lower frequencies.

Based on the cross-peak of H7 and C12 in the $^1\text{H}/^{13}\text{C}$ -HMBC spectrum, the reaction with deuterated methanol was confirmed for **1a**.

The following reaction mechanism, shown in Scheme 5 could represent a potential mechanism for the formation of component **1a** if the substituent X would be iodine. As already mentioned, this is a hypothesis since confirmation of the substituent is still outstanding.



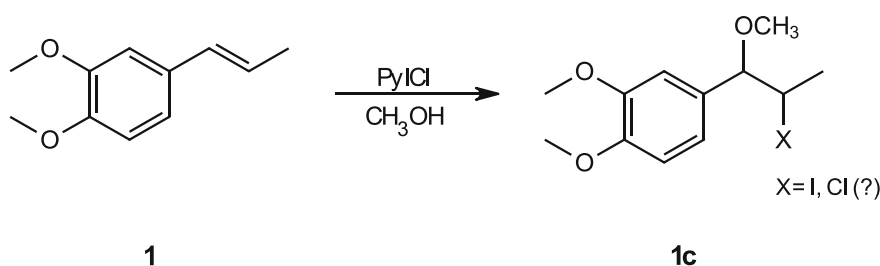
*Scheme 5: Potential reaction mechanism of methyl isoeugenol **1** with $\text{PyI}\cdot\text{Cl}$ resulting in the presumed structure **1a**. The first step of the reaction represents an electrophilic addition, where the double bond attacks the iodochloride ($\text{I}\cdot\text{Cl}$), resulting in the addition of iodine to the molecule and the formation of Cl^- . The next step is initiated by a nucleophilic attack of deuterated methanol (CD_3O^-) on the positively charged position, resulting in **1a** and DCI .*

A fragment of the structure of component **1b** was confirmed by mass spectrometric analysis, presented in chapter 3.3.1. In this reaction, a rearrangement of the side chain occurred, which was deduced by the $^1\text{H}/^{13}\text{C}$ -HMBC experiment. Based on the cross-peak of the methyl protons H9 (1.22 ppm) to C1 (137.31 ppm) this rearrangement could be proved. In the starting material, the distance of the methyl protons to C1 is 3 bonds, whereas after the rearrangement it is only two bonds, and therefore, the respective coupling of H9 to C1 via three bonds could be observed in the $^1\text{H}/^{13}\text{C}$ -HMBC spectrum. In addition, H7 is present as a quintet, which revealed the coupling with H8 (4.35 ppm) and

H9 (1.22 ppm) via 3 bonds respectively. In addition, because of the rearrangement of the side chain, proton H7 displays long-range cross-peaks to the aromatic carbons C2 and C6.

The ^1H -shifts of the atoms H7 (2.92 ppm) and H8 (4.35 ppm) were again decisive for the conclusion that the double bond is no longer present. Based on the observed cross-peak of H8 (4.35 ppm) and C12/13 (54.0 ppm) in the $^1\text{H}/^{13}\text{C}$ -HMBC the addition of deuterated methanolate to the molecule was inferred.

3.2.1.2 In methanol (CH_3OH)



Scheme 6: Reaction of methyl isoeugenol **1** with PyI in CH_3OH and the product **1c** formed correspondingly. **1c**:SM ca. 1:0.2.

As indicated in Scheme 6, the substituent X could not be identified for component **1c** either. However, as with component **1a** above (c.f. chapter 3.2.1.1), based on the iodination reagent (PyI), it is assumed that either an iodine or chlorine substituent is involved. Table 27 lists the ^1H - and ^{13}C -chemical shifts of component **1c**.

Table 27: ^1H - and ^{13}C -shifts of the main component **1c** resulting from the reaction of methyl isoeugenol **1** and PyI in CH_3OH . (NMR-solvent: CDCl_3).

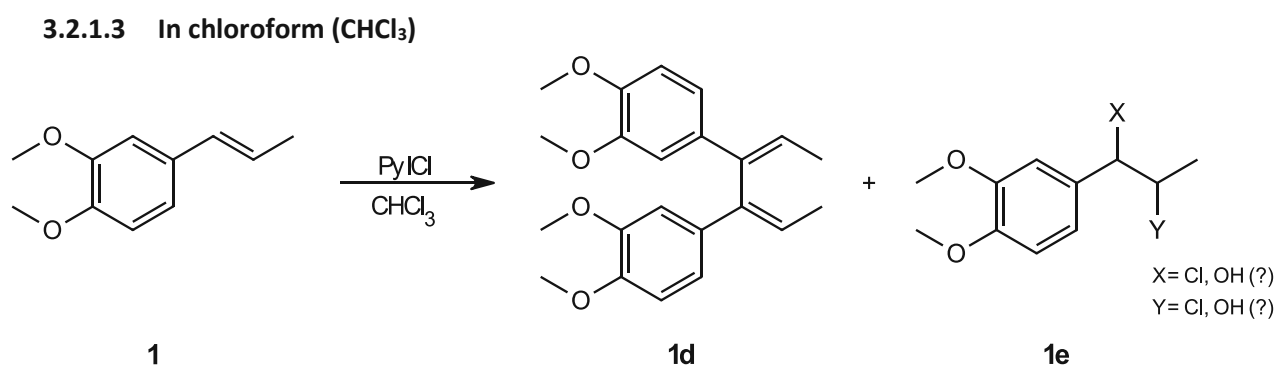
Atom number	^1H		^{13}C
	δ (ppm)	J (Hz)	δ (ppm)
1			130.99
2	6.85 (m)		109.91
3			148.79 ^a
4			148.73 ^a
5	6.84 (m)		110.51
6	6.83 (m)		120.13
7	4.16 (d)	5.0	87.59
8	4.32 (qd)	7.0; 5.0	31.87
9	1.79 (d)	7.0	22.72
10	3.88 ^b (s)		55.88 ^c
11	3.89 ^b (s)		55.80 ^c
12	3.31 (s)		57.55

^a, ^b, ^c ... exchangeable

Component **1c** can be regarded as analogous to component **1a** (c.f. chapter 3.2.1.1), with the difference that **1a** results from a reaction in deuterated methanol (CD_3OD) and **1c** in protonated methanol (CH_3OH).

The shifts of H7 (4.16 ppm) and H8 (4.32 ppm) correspond to aliphatic protons, which explains the disappearance of the double bond. The attachment of the methanolate (CH_3O^-) to the molecule is detected by a cross-peak of H7 (4.16 ppm) and C12 (57.55 ppm) in the $^1\text{H}/^{13}\text{C}$ -HMBC spectrum. The significant shift to lower frequencies of C8 (31.87 ppm), to which the substituent is attached, can probably be attributed to the +M effect of the substituent X.

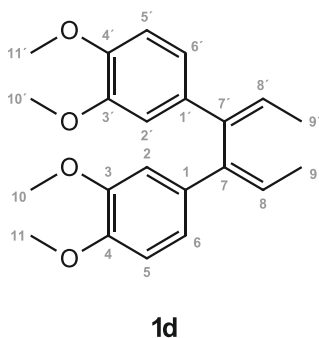
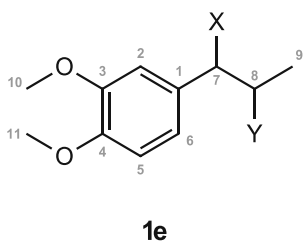
The possible reaction mechanism considered for component **1a** (c.f. Scheme 5) could also be responsible for the formation of component **1c** in an analogous form (with CH_3OH instead of CD_3OD). However, substituent X is not identified and therefore the mechanism remains a hypothesis.



Scheme 7: Reaction of methyl isoeugenol **1** with PyICl in CHCl_3 and the products formed correspondingly. **1d** is component I, and **1e** is component II formed in this reaction. SM:**1d:1e** ca. 1:0.9:0.4.

Component **1d** was formed by dimerization of methyl isoeugenol, which could be confirmed by mass spectrometric analysis (c.f. 3.3.1). Component **1e** is attached with substituents, whereas neither X nor Y could be identified. Given the solvent (CHCl_3) and the corresponding ^{13}C -shifts, it is reasonable to assume that either chlorine or oxygen is involved. Table 28 contains the ^1H - and ^{13}C - chemical shifts of components **1d** and **1e**.

Table 28: ^1H - and ^{13}C -shifts of component **1d** (left) and component **1e** (right) resulting from the reaction of methyl isoeugenol **1** and PyICl in CHCl_3 . (NMR-solvent: CDCl_3).

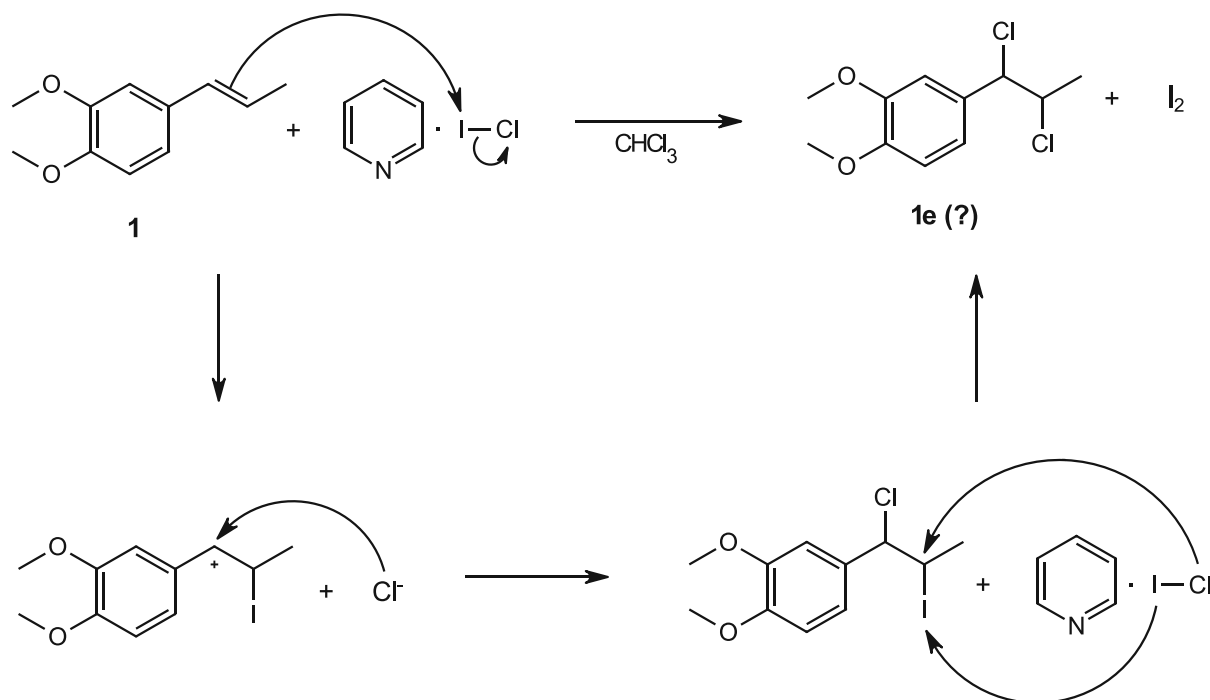
							
Atom number	^1H		^{13}C	Atom number	^1H		^{13}C
	δ (ppm)	J (Hz)	δ (ppm)		δ (ppm)	J (Hz)	δ (ppm)
1, 1'			123.25	1			131.00
2, 2'	6.87 (m)		112.40	2	6.92		110.46
3, 3'			149.67	3			n.d.
4, 4'			150.88	4			n.d.
5, 5'	7.00 (d)	8.1	111.87	5	n.d.		n.d.
6, 6'	6.93 (m)		123.34	6	6.93		120.33
7, 7'			142.60	7	4.86 (d)	7.8	67.51
8, 8'	6.58 (br. q)	6.5	130.41	8	4.37 (m)	7.8; 6.5	60.35
9, 9'	2.11 (d)	6.5	15.75	9	1.70 (d)	6.5	22.29
10, 10'	3.89 (s)		56.84	10	n.d.		n.d.
11, 11'	3.93 (s)		56.19	11	n.d.		n.d.

For component **1d**, the presence of the double bond can be inferred by considering the ^1H -shift of H8 (6.58 ppm), emerging in the olefinic ppm range. Given that only one olefinic H-atom could be detected for this substance, indicates a substitution at the double bond. The ^{13}C -shift of C7 (142.60 ppm) is shifted slightly to higher frequencies compared to C7 (131.94 ppm) of pure methyl isoeugenol (*c.f.* Table 4). However, the corresponding C-atom to which the substituent is attached does not exhibit a ^{13}C -chemical shift characteristic for a particular substituent. The assumption that it is a magnetically equivalent dimer was subsequently confirmed by mass spectrometry (*c.f.* chapter 3.3.1), although the prediction-server CSEARCH showed deviations of the respective shifts (*c.f.* Table 30).

In component **1e**, the absence of the double bond is evident from the two protons H7 (4.86 ppm) and H8 (4.37 ppm), emerging in the aliphatic ppm range. According to the ^{13}C -spectrum, C7 and C8 each represent doublets (CH) - their shifts at 67.51 ppm (C7) and 60.35 ppm (C8) favor a chlorine or even oxygen as substituents. NMR-spectroscopy enabled the evaluation of the basic structure of **1e**, while the identification of the substituents remains inconclusive despite mass spectrometry.

Since component **1e** is only present in smaller quantities and the peaks of the other components predominate, this component could unfortunately not be completely evaluated and therefore could not be inspected using CSEARCH. The undetectable signals are labeled “n.d.” in Table 28. However, the decisive signals could be assigned to propose this structure.

A hypothetically occurring mechanism that could provide component **1e** is given in Scheme 8:



*Scheme 8: Hypothetical reaction mechanism of methyl isoeugenol **1** with PyICl resulting in the presumed structure **1e**. The first step of the reaction is an electrophilic addition, where the double bond attacks the iodochloride (ICl), resulting in the addition of iodine to the molecule and the formation of Cl⁻. In the next step, the negative chloride ion attacks the side chain and attaches to the positively charged C-atom, followed by another attack of PyICl. The chloride ion attaches to the side chain and I₂ is released.*

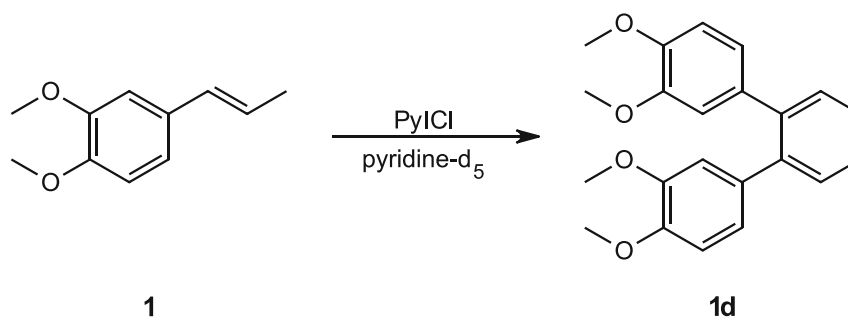
3.2.1.4 In deuterated pyridine (C_5D_5N)Scheme 9: Reaction of methyl isoeugenol **1** with PyICl in C_5D_5N and the resulting product **1d**. *SM:1d* ca. 2:1.

Table 29 lists the 1H - and ^{13}C - chemical shifts of component **1d**.

Table 29: 1H - and ^{13}C -shifts of component **1d** resulting from the reaction of methyl isoeugenol **1** and PyICl in C_5D_5N . (NMR-solvent: C_5D_5N).

Atom number	1H		^{13}C
	δ (ppm)	J (Hz)	δ (ppm)
1, 1'			124.90
2, 2'	7.10 (d)	2.0	113.79
3, 3'			150.73
4, 4'			151.95
5, 5'	7.07 (d)	8.4	112.90
6, 6'	7.03 (dd)	8.4; 2.0	124.01
7, 7'			143.63
8, 8'	6.59 (q)	7.2	129.72
9, 9'	1.99 (d)	7.2	15.62
10, 10'	3.76 (s)		56.77
11, 11'	3.85 (s)		56.52

Component **1d**, dimerized methyl isoeugenol, which results from the reaction of methyl isoeugenol **1** and PyICl in deuterated pyridine was also formed in the derivatization reaction in chloroform (*c.f.* Scheme 7). Thus, a more detailed description of this component can be found in chapter 3.2.1.3. It can be concluded that the component is formed independently of the solvent.

As expected, no reaction occurred at the aromatic system with methyl isoeugenol **1**, but the double bond exhibited very reactive behavior.

3.2.1.5 CSEARCH-prediction

Only those derivatives, for which all signals were detectable in the NMR-spectra, could be inspected by the NMR-predict server CSEARCH [46].

For component **1a** (c.f. chapter 3.2.1.1) CSEARCH was used to investigate whether the substituent X could be iodine or chlorine and for component **1d** (c.f. chapter 3.2.1.3), whether the dimer was formed. Table 30 lists the chemical shifts of the ^{13}C -atoms, including the experimental value and predictions from CSEARCH. The shifts marked in green show good agreement with the predictions. Unfortunately, more significant deviations were found exactly for those respective ^{13}C -shifts, where the substituent is attached or adjacent (yellow-, red-marked).

Table 30: Deviations of the respective ^{13}C -atoms in components **1a** (X= I), **1a** (X= Cl), and **1d** (dimer) predicted by the NMR-predict server CSEARCH. The experimental value, the neural network prediction, and the HOSE-code prediction of the NMR chemical shifts in ppm of the ^{13}C -atoms are given.

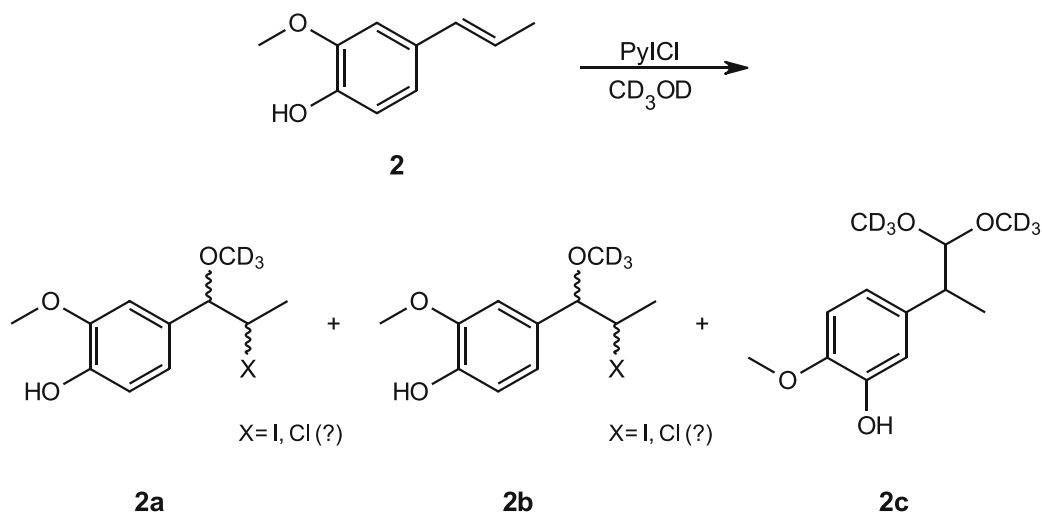
Component	C-atom	Experimental value (ppm)	Neural network prediction (ppm)	HOSE-code prediction (ppm)
1a (X= I)	C1	132.8	133.2	134.2
	C2	112.0	111.9	110.7
	C3	150.3	149.9	148.9
	C4	150.3	147.4	148.7
	C5	112.4	111.9	110.7
	C6	121.6	121.0	120.0
	C7	88.8	87.9	75.3
	C8	32.4	69.8	32.1
	C9	23.5	25.9	23.1
	C10	56.4	56.8	55.9
	C11	56.4	56.8	56.0
	C12	56.9	58.3	57.3
1a (X= Cl)	C1	132.8	132.8	134.2
	C2	112.0	112.5	110.7
	C3	150.3	150.1	148.9
	C4	150.3	147.1	148.7
	C5	112.4	111.7	111.4
	C6	121.6	121.3	120.0
	C7	88.8	88.7	75.3
	C8	32.4	57.7	57.9
	C9	23.5	18.8	19.8
	C10	56.4	56.8	55.9
	C11	56.4	56.8	56.0
	C12	56.9	58.3	57.3

1d (dimer)	C1/1'	123.3	132.6	132.3
	C2/2'	112.4	113.9	113.0
	C3/3'	149.7	149.7	148.5
	C4/4'	150.9	148.8	148.8
	C5/5'	111.9	113.2	111.2
	C6/6'	123.3	121.6	123.5
	C7/7'	142.6	137.0	111.2
	C8/8'	130.4	139.5	140.0
	C9/9'	15.8	16.9	15.4
	C10/10'	56.8	56.8	56.1
	C11/11'	56.2	56.8	56.0

3.2.2 Isoeugenol

Isoeugenol possesses a hydroxy group on the aromatic ring, which would allow iodination at the *ortho*-position according to the literature [20].

3.2.2.1 In deuterated methanol (CD₃OD)

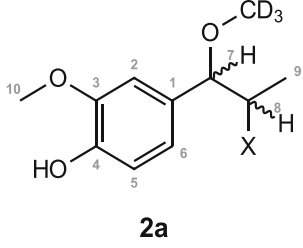
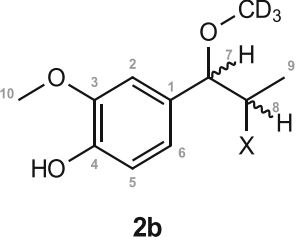


Scheme 10: Reaction of isoeugenol **2** with PyICl in CD₃OD and the products formed correspondingly. The structures of **2a** and **2b** are represented with wavy lines since these two components are most likely diastereomers. **SM:2a:2b:2c** ca. 1:0.2:0.3:0.1.

As indicated in Scheme 10, it is not known which substituent X is involved in components **2a** and **2b**. Based on the use of PyICl as an iodinating reagent, it is suspected that the substituent X represents either iodine or chlorine. In this reaction, it is noticeable that the solvent applied (CD₃OD) has a strong influence on the formation of the products. The incorporation of deuterated methanol was detected in all three components **2a**, **2b**, and **2c**.

Table 31 contains the ¹H- and ¹³C- chemical shifts of components **2a** and **2b**.

Table 31: ^1H - and ^{13}C -shifts of component **2a** (left) and component **2b** (right) resulting from the reaction of isoeugenol **2** and PyICl in CD_3OD . (NMR-solvent: CD_3OD).

 2a				 2b			
Atom number	^1H		^{13}C	Atom number	^1H		^{13}C
	δ (ppm)	J (Hz)	δ (ppm)		δ (ppm)	J (Hz)	δ (ppm)
1			131.30	1			130.92
2	6.89		111.74	2	n. d.		n. d.
3			n. d.	3			n. d.
4			n. d.	4			n. d.
5	6.72		115.95	5	n. d.		n. d.
6	6.73		121.61	6	n. d.		n. d.
7	4.12 (d)	5.2	88.68	7	3.90 (d)	7.4	90.09
8	4.36 (dq)	7.0; 5.2	32.79	8	4.22 (dq)	7.4; 7.0	33.15
9	1.74 (d)	7.0	23.50	9	1.65 (d)	7.0	25.79
10	3.89		56.8	10	n. d.		n. d.

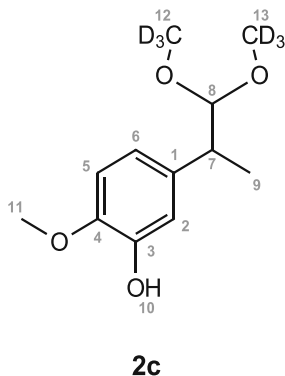
Components **2a** and **2b** are illustrated with wavy bonds since they presumably represent diastereomers. Based on the coupling constants of H7 and H8 (5.2 Hz in **2a** and 7.4 Hz in **2b**), it could be concluded that the two protons in component **2b** (larger coupling constant) are positioned at an angle more deviating from 90° than the two protons in component **2a** (*c.f.* Karplus curve). More precise information about the conformation of the substituents is not provided by the NMR evaluation.

For a more detailed description of these two components **2a** and **2b**, a reference can be made to chapter 3.2.1.1 since the structure and the NMR shifts of component **1a** exhibit great similarity and can be considered analogous. Therefore, the proposed hypothetical mechanism (*c.f.* Scheme 5) could proceed in the same way for the reaction of isoeugenol **2** in deuterated methanol as for methyl isoeugenol **1**. Due to partial overlaps because of the very small amounts of the resulting components in the reaction mixture, not all associated signals could be detected in the spectrum ("n.d." for "not detected" in Table 31), but the decisive signals for the structure could be assigned.

Table 32 contains the ^1H - and ^{13}C - chemical shifts of component **2c**.

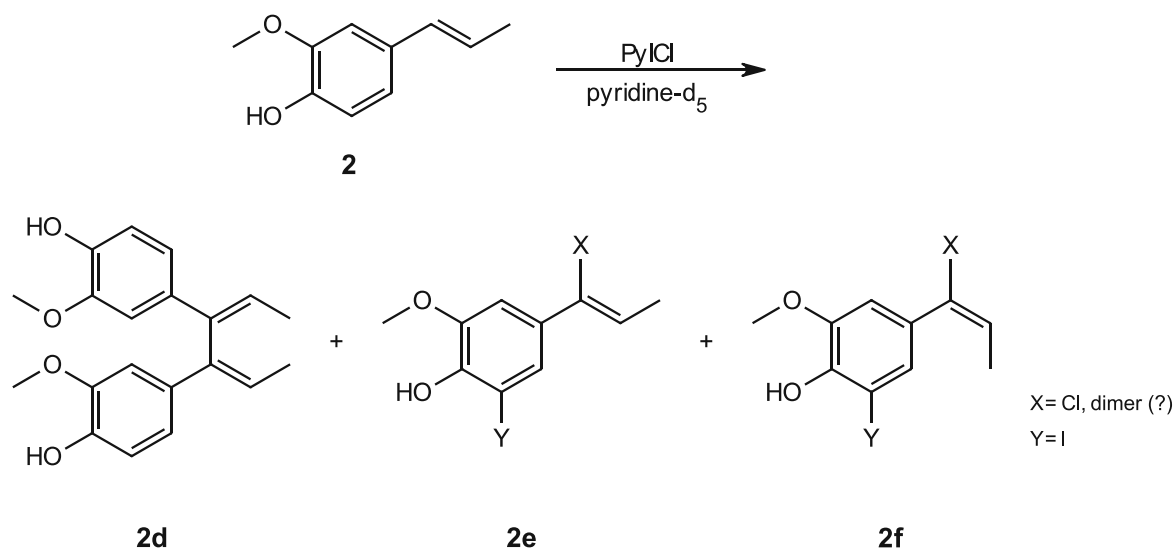
Table 32: ^1H - and ^{13}C -shifts of component **2c** resulting from the reaction of isoeugenol **2** and PyICl in CD_3OD . (NMR-solvent: CD_3OD).

Atom number	^1H		^{13}C
	δ (ppm)	J (Hz)	δ (ppm)
1			135.80
2	6.79		112.75
3	n. d.		n. d.
4			n.d.
5	n. d.		n. d.
6	6.66		121.35
7	2.88 (dq)	7.0; 6.9	43.79
8	4.33 (d)	6.9	110.19
9	1.20 (d)	7.0	17.38
10	n. d.		
11	n. d.		n. d.
12, 13			54.30



Component **2c** is an isoeugenol derivative analog to methyl isoeugenol derivative **1b** derived from the reaction in deuterated methanol. Due to the very similar structure and chemical shifts (comparison of Table 32 and right side of Table 26), reference can be made to chapter 3.2.1.1 for a more detailed description. Since component **2c** was formed in very small amounts and signal overlapping from the other components occurred, it was not possible to determine all NMR shifts associated with the component (marked with “n.d.”). The incorporation of deuterated methanol in the molecule was detected by a cross-peak of H8 (2.88 ppm) and C12/13 (54.30 ppm) in the $^1\text{H}/^{13}\text{C}$ -HMBC spectrum. A fragment of structure **2c** was confirmed by mass spectrometric analysis (c.f. chapter 3.3.2).

Unfortunately, it was not possible to evaluate the products formed in the derivatization reactions of isoeugenol **2** with PyICl in the solvents chloroform (CHCl_3) and methanol (CH_3OH). Presumably, many side reactions, possibly dimerization and/or decompositions, occurred during these reactions, resulting in very complex spectra. Due to severe signal overlap, a reasonable evaluation was not possible.

3.2.2.2 In deuterated pyridine (C₅D₅N)

Scheme 11: Reaction of isoeugenol **2** with PyI₂ in C₅D₅N and the resulting products **2d**, **2e**, and **2f**. **2d:2e:2f** ca. 1:0.3:0.2.

Analogous to component **1d** (c.f. chapter 3.2.1.4), component **2d** was identified as a dimer of isoeugenol by mass spectrometry (c.f. chapter 3.3.2) but showed deviations in the CSEARCH-prediction (c.f. Table 35).

Despite mass analysis and the use of the NMR predict server CSEARCH [46], substituent X could not be identified for components **2e** and **2f**, but Y was identified as iodine (c.f. Table 35).

Considering the respective ¹³C-shifts where substitution occurred (C7 in Table 34 below), dimerization could also be assumed for **2e** and **2f**, but unfortunately, this could not be confirmed by mass spectrometric analysis.

Since this reaction was performed in deuterated pyridine and regarding the associated ¹³C-shifts, it is also reasonable to assume that the substituent X could involve chlorine originating from the iodinating reagent (PyI₂) and that the products were formed independently of the solvent. As indicated in Scheme 11, components **2e** and **2f** probably represent *E/Z* isomers, since they are otherwise not remarkably different, and the chemical shifts are very similar. In Table 33 the ¹H- and ¹³C- chemical shifts of isoeugenol derivative **2d** are listed and Table 34 shows the ¹H- and ¹³C- chemical shifts of components **2e** and **2f**.

Table 33: ^1H - and ^{13}C -shifts of the presumed component **2d** resulting from the reaction of isoeugenol **2** and PyICl in $\text{C}_5\text{D}_5\text{N}$. (NMR-solvent: $\text{C}_5\text{D}_5\text{N}$).

Atom number	^1H		^{13}C
	δ (ppm)	J (Hz)	δ (ppm)
1, 1'			123.48
2, 2'	7.14 (d)	2.0	114.41
3, 3'			149.80
4, 4'			151.10
5, 5'	7.42 (d)	8.2	117.85
6, 6'	6.91 (dd)	8.2; 2.0	124.47
7, 7'			144.08
8, 8'	6.55 (q)	7.2	129.15
9, 9'	1.97 (d)	7.2	15.79
10, 10'	3.79 (s)		57.04

The detection of only one olefinic H-atom (H8 at 6.55 ppm) led to the conclusion that a substitution on the double bond is involved. Component **2d** is a derivative of isoeugenol analogous to component **1d**, a derivative of methyl isoeugenol **1**, both formed by dimerization. The chemical shifts and structures of both **2d** and **1d** are very similar, whereby reference can be made to chapter 3.2.1.3 for further explanation.

Table 34: ^1H - and ^{13}C -shifts of the presumed components **2e** (left) and **2f** (right) resulting from the reaction of isoeugenol **2** and PyICl in $\text{C}_5\text{D}_5\text{N}$. (NMR-solvent: $\text{C}_5\text{D}_5\text{N}$).

2e				2f			
Atom number	^1H		^{13}C	Atom number	^1H		^{13}C
	δ (ppm)	J (Hz)	δ (ppm)		δ (ppm)	J (Hz)	δ (ppm)
1			126.52	1			128.16
2	7.20 (d)	2.0	114.07	2	7.10 (d)	2.2	110.49
3			148.88	3			149.80
4			142.68	4			n.d.
5			86.94*	5			86.90*
6	7.60 (d)	2.0	133.08	6	7.22 (d)	2.2	128.99
7			143.80	7			142.41
8	6.65 (q)	7.2	124.06	8	6.71 (q)	7.2	126.01
9	1.64 (d)	7.2	14.15	9	1.69 (d)	7.2	14.33
10	3.76 (s)		57.29	10	3.85 (s)		57.01

* ... exchangeable

As mentioned above, components **2e** and **2f** are probably *E/Z* isomers. However, NMR evaluation cannot determine in which component substituent X is *cis*- and in which *trans*-orientated to the methyl group. For illustration purposes, in Scheme 11 above, **2e** is shown as *cis*-orientated and **2f** as *trans*-orientated, but this is not confirmed.

In both cases, only one olefinic proton H8 (**2e**: 6.65 ppm and **2f**: 6.71 ppm) was detected, which in turn led to the assumption that a substituent X is attached to the double bond or that the components have undergone dimerization. The ^{13}C -chemical shifts of C7 (**2e**: 143.80 ppm and **2f**: 142.41 ppm) are very similar to those of component **1d** (C7: 143.63 ppm) and **2d** (C7: 144.08 ppm), where the formation of the dimer was confirmed. However, due to insufficient scientific evidence, unfortunately, the substituent question for components **2e/2f** needs to be declared as unsolved.

In both components, only two aromatic H-atoms were detected, which suggests a substitution at the aromatic ring. The respective ^{13}C -shifts of the C5-atoms (**2e**: 86.94 ppm and **2f**: 86.90 ppm) are a promising indication that iodine has been attached to the molecule. Comparison with published iodinated structures [13] shows that the ^{13}C -shifts of the respective C-atoms are in the same range. In the next chapter 3.2.3, for instance, this will be discussed in more detail. In addition, it should be noted

that these components occur in very small amounts in the reaction mixture, and therefore not all the associated signals were identifiable.

3.2.2.3 CSEARCH-prediction

CSEARCH was applied to investigate whether chlorine was involved in substituent X for component **2e** (c.f. chapter 3.2.2.2) and whether dimerization occurred in component **2d** (c.f. chapter 3.2.2.2). Table 35 shows the chemical shifts of the ^{13}C -atoms, including the experimental value and predictions from CSEARCH. The shifts marked in green show good agreement with the predictions. Unfortunately, more significant deviations were found exactly for those respective ^{13}C -shifts, where the substituent is attached or adjacent (yellow-, red-marked).

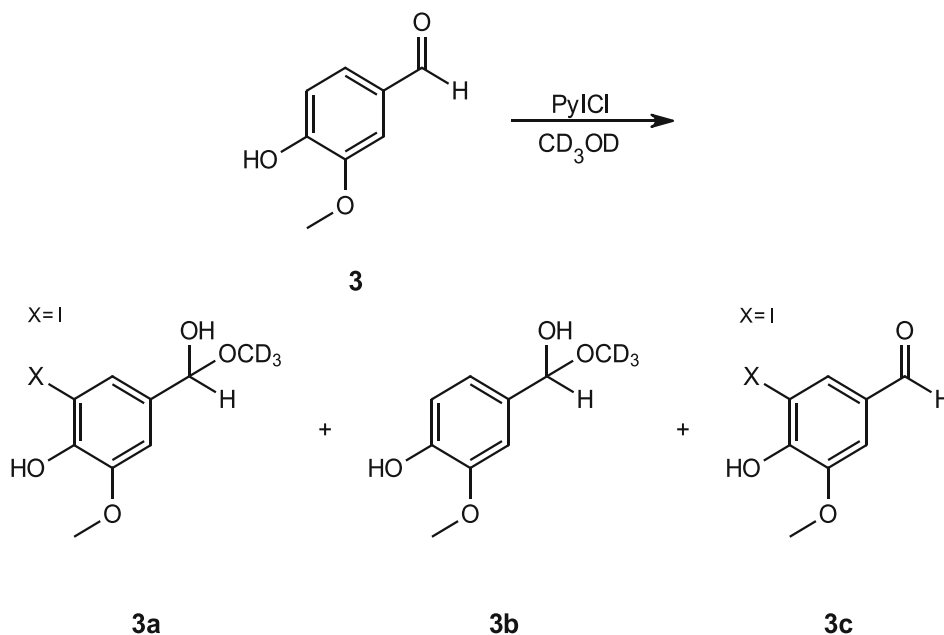
Table 35: Deviations of the respective ^{13}C -atoms in components **2d** (dimer) and **2e** (X= Cl) predicted by the NMR-predict server CSEARCH. The experimental value, the neural network prediction, and the HOSE-code prediction of the NMR chemical shifts in ppm of the ^{13}C -atoms are given.

Component	C-atom	Experimental value (ppm)	Neural network prediction (ppm)	HOSE-code prediction (ppm)
2d (dimer)	C1/1'	123.5	131.7	132.3
	C2/2'	114.4	113.3	113.0
	C3/3'	149.8	147.1	147.2
	C4/4'	151.1	147.6	147.3
	C5/5'	117.8	115.2	115.4
	C6/6'	124.5	121.8	123.5
	C7/7'	144.1	137.0	111.2
	C8/8'	129.1	139.5	140.0
	C9/9'	15.8	16.9	15.4
	C10/10'	57.0	58.8	56.1
2e (X= Cl)	C1	126.5	136.2	124.7
	C2	114.1	113.9	112.4
	C3	148.9	147.6	151.6
	C4	142.7	151.5	153.1
	C5	86.4	96.8	85.9
	C6	133.1	133.2	140.0
	C7	143.8	131.2	137.6
	C8	124.1	127.1	123.5
	C9	14.2	14.9	14.5
	C10	57.3	56.8	56.4

3.2.3 Vanillin

Vanillin features a hydroxylated aromatic structure (c.f. Figure 1), meeting the conditions for successful iodination according to the protocol [20].

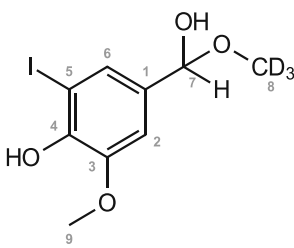
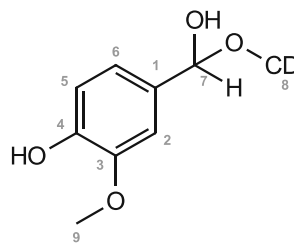
3.2.3.1 In deuterated methanol (CD₃OD)



Scheme 12: Reaction of vanillin **3** with PyI₂ in CD₃OD and the products formed correspondingly. **3a** is the main component, **3b** represents the secondary component I, and **3c** represents secondary component II. **3a:3b:3c:SM** ca. 1:0.3:0.1:0.1.

Solvent-related side reactions also occurred in the derivatization reaction of vanillin **3** in deuterated methanol, as can be seen in Scheme 12 from products **3a** and **3b**. For these derivatives, the substituent X could be identified as iodine. Table 36 contains the ¹H- and ¹³C- chemical shifts of vanillin derivatives **3a** and **3b**.

Table 36: ^1H - and ^{13}C -shifts of the main component **3a** (left) and the side product **3b** (right) resulting from the reaction of vanillin **3** and PyICl in CD_3OD . (NMR-solvent: CD_3OD).

 3a				 3b			
Atom number	^1H		^{13}C	Atom number	^1H		^{13}C
	δ (ppm)	J (Hz)	δ (ppm)		δ (ppm)	J (Hz)	δ (ppm)
1			132.47	1			131.03
2	6.96 (d)	1.9	110.75	2	6.98 (d)	1.9	111.06
3			148.16*	3			148.79
4			148.03*	4			147.86
5			82.92	5	6.77 (d)	8.1	115.66
6	7.31 (dd)	1.9; 0.6	130.01	6	6.86 (ddd)	8.1; 1.9; 0.6	120.70
7	5.26 (br. t)		103.64	7	5.28 (br. t)		104.76
8			52.37 (m)	8			52.21
9	3.86 (s)		56.58	9	3.85 (s)		56.31

*... exchangeable

The main component **3a** formed in the reaction of vanillin **3** with PyICl resulted from the disappearance of the aldehyde, which is indicated by the ^{13}C high field shift of the C7 (103.64 ppm). In addition, only two aromatic H-atoms (H2 and H6) were detected, which suggests a substitution at the aromatic ring. This assumption is subsequently supported by the ^{13}C -shift of C5 (82.92).

The high field shift of C5 to the ppm range of about 80-90 ppm is a strong indication that iodine has been attached to the molecule. C5 represents the *ortho*-position to the OH group in this case, and as predicted in the literature [20], iodination has occurred at this position. As mentioned earlier, iodine exhibits a positive mesomeric effect that leads to shielding and thus a shift to lower frequencies. However, due to the large atomic size of iodine, the overlap of the orbitals between iodine and the directly bonded C -atom becomes smaller, weakening the mesomeric effect. The reason why iodine causes such a characteristic high field shift on the directly bound C-atom could lie in the "heavy atom effect" in addition to the +M effect. The heavy atom effect describes a relativistic effect, which can drastically alter the NMR shifts of the neighboring nuclei due to the presence of a nearby atom with a high atomic number. The effect involves the perturbation of the spin-orbit coupling in an atom or molecule by this neighboring atom of a heavy element [47], [48].

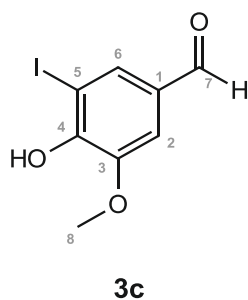
Further, the addition of deuterated methanolate was confirmed by a cross-peak of H7 (5.26 ppm) and C8 (52.37 ppm) in the $^1\text{H}/^{13}\text{C}$ -HMBC spectrum.

For component **3b**, no aromatic substitution was concluded due to the presence of three aromatic proton signals (H2, H5, and H6). The $^1\text{H}/^{13}\text{C}$ -HMBC cross-peak of H7 (5.28 ppm) to C8 (52.21 ppm) indicates the incorporation of deuterated methanolate resulting in the formation of a hemiacetal. Based on the chemical shifts of C7 (104.76 ppm) and H7 (5.28 ppm), the absence of the aldehyde group is proven. Since MeO- d_4 was used as solvent its high concentration of course favors the formation of the hemiacetal.

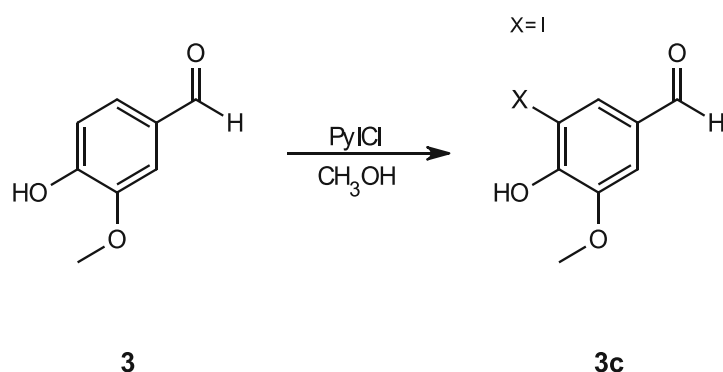
Table 37 shows the ^1H - and ^{13}C - chemical shifts of the third derivative **3c** of vanillin.

Table 37: ^1H - and ^{13}C -shifts of the secondary component II **3c** resulting from the reaction of vanillin **3** and PyI₂ in CD_3OD . (NMR-solvent: CD_3OD).

Atom number	^1H		^{13}C
	δ (ppm)	J (Hz)	δ (ppm)
1			131.73
2	7.43 (t)	1.8	110.87
3			148.80
4			154.22
5			83.15
6	7.86 (d)	1.8	136.62
7	9.70 (s)		191.60
8	3.93 (s)		56.73



Compound **3c** still contains the aldehyde group, indicated by ^1H -shift of H7 (9.7 ppm) and ^{13}C -shift of C7 (191.60 ppm). The absence of the third aromatic proton (H5) implies an aromatic substitution at C5 (83.15 ppm), *ortho* to the hydroxy group. This structure evaluated by NMR spectroscopy was confirmed by mass spectrometry (*c.f.* chapter 3.3.3), which proves that the substituent X is iodine. Thus, the characteristic ^{13}C -shift of the respective quaternary C-atoms, induced by iodine is confirmed and occurs in the range of approximately 80-90 ppm.

3.2.3.2 In methanol (CH₃OH)

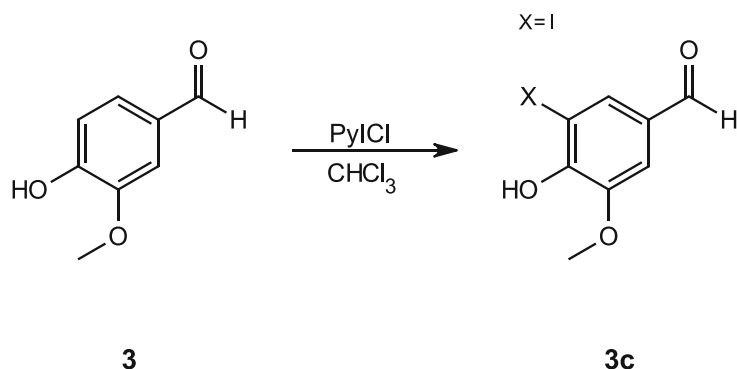
Scheme 13: Reaction of vanillin **3** with PyI₂ in CH₃OH and the product **3c** formed correspondingly. **3c** represents the iodinated derivative formed. **3c:SM** ca. 1:0.3.

The reaction of vanillin **3** and PyI₂ in methanol proved successful and an iodinated vanillin derivative **3c** was formed. Its ¹H- and ¹³C- chemical shifts can be found in Table 38.

Table 38: ¹H- and ¹³C-shifts of component **3c** resulting from the reaction of vanillin **3** and PyI₂ in CH₃OH. (NMR-solvent: CDCl₃ + DMSO-d₆).

Atom number	¹ H		¹³ C
	δ (ppm)	J (Hz)	δ (ppm)
1			130.03
2	7.21 (d)	1.73	108.93
3			146.81
4			152.07
5			81.80
6	7.68 (d)	1.73	135.61
7	9.61 (s)		189.31
8	3.81 (s)		56.07

Component **3c** was also formed during the reaction of vanillin **3** in deuterated methanol (CD₃OD), thus reference can be made to chapter 3.2.3.1 for a more detailed description. However, in comparison to the reaction in deuterated methanol, no hemiacetal formation was observed in protonated methanol.

3.2.3.3 In chloroform (CHCl₃)

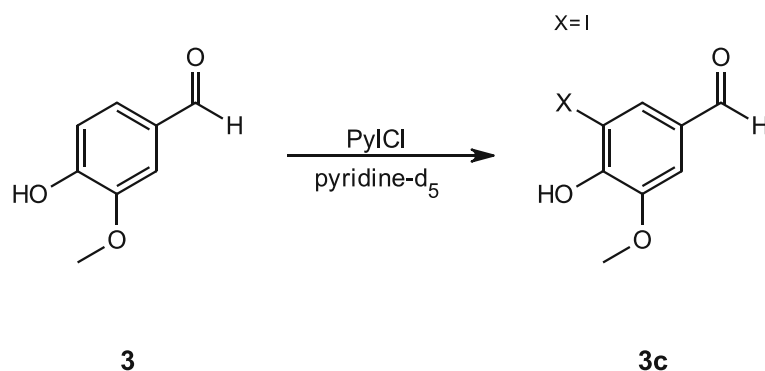
Scheme 14: Reaction of vanillin **3** with PyICl in CHCl₃ and the product **3c** formed correspondingly. **3c** represents the main component formed. **3c:SM** ca. 1:0.1.

The derivatization reaction with PyICl of vanillin **3** in chloroform (CHCl₃) yielded *ortho*-iodinated vanillin **3c** as a product. The corresponding ¹H- and ¹³C- shifts of component **3c** from this reaction are given in Table 39.

Table 39: ¹H- and ¹³C-shifts of the main component **3c** resulting from the reaction of vanillin **3** and PyICl in CHCl₃. (NMR-solvent: CDCl₃ + DMSO-d₆).

Atom number	¹ H		¹³ C
	δ (ppm)	J (Hz)	δ (ppm)
1			130.23
2	7.26 (d)	1.8	108.90
3			146.82
4			152.04
5			81.64
6	7.72 (d)	1.8	135.78
7	9.65 (s)		189.38
8	3.85 (s)		56.18

For a more detailed description of component **3c**, a reference can be made to chapter 3.2.3.1.

3.2.3.4 In deuterated pyridine (C_5D_5N)

Scheme 15: Reaction of vanillin **3** with PyICl in C_5D_5N and the product **3c** formed correspondingly. **3c:SM** ca. 1:0.3.

Derivatization reaction of vanillin **3** proved successful in pyridine (C_5D_5N) and again iodination at the *ortho*-position took place successfully. The corresponding ^1H - and ^{13}C - shifts of component **3c** are shown in Table 40.

Table 40: ^1H - and ^{13}C -shifts of the main component **3c** resulting from the reaction of vanillin **3** and PyICl in C_5D_5N . (NMR-solvent: C_5D_5N).

Atom number	^1H		^{13}C
	δ (ppm)	J (Hz)	δ (ppm)
1			131.13
2	7.55 (d)	1.79	111.02
3			148.80
4			155.00
5			85.95
6	8.14 (d)	1.79	136.80
7	9.96 (s)		190.36
8	3.68 (s)		56.50

For a more detailed description of component **3c**, a reference can be made to chapter 3.2.3.1.

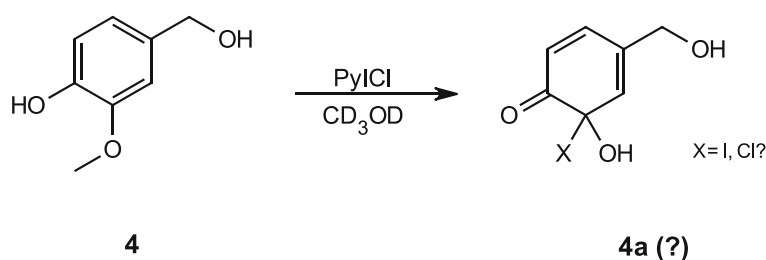
Since component **3c** (*ortho*-iodinated vanillin) was formed in all four solvents, it can be claimed that the iodination reaction is solvent independent. The reaction mechanism leading to *ortho*-iodinated vanillin **3c** corresponds to an electrophilic aromatic substitution and is shown in a generalized form in Scheme 2.

3.2.4 Vanillyl alcohol

Model compound vanillyl alcohol **4** (*c.f.* Figure 1) possesses a hydroxy group on the aromatic ring, which means that the conditions for successful iodination with PyI₂ at the *ortho*-position to the OH-group are fulfilled according to the literature [20].

3.2.4.1 In deuterated methanol (CD₃OD)

Observations showed that the reaction of vanillyl alcohol **4** and PyI₂ takes place very rapidly and that decomposition of the substance probably occurs after longer reaction times. The product **4a** shown below in Scheme 16 is only a conjecture since the OH-group at position C3 could not be detected with the aid of the NMR spectra.

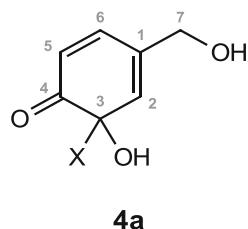


Scheme 16: Reaction of vanillyl alcohol **4** with PyI₂ in CD₃OD and the corresponding presumably formed product **4a**. Starting material is still available in great quantity. **SM:4a** ca. 1:0.8.

Table 41 lists the ¹H- and ¹³C- chemical shifts from the assumed structure of component **4a**.

Table 41: ¹H- and ¹³C-shifts of the presumably resulting product **4a** from the reaction of vanillyl alcohol **4** and PyI₂ in CD₃OD. (NMR-solvent: CD₃OD).

Atom number	¹ H		¹³ C
	δ (ppm)	J (Hz)	δ (ppm)
1			139.4
2	6.33 (m)		129.7
3			92.5
4			197.4
5	6.02 (d)	10.0	126.2
6	6.97 (dd)	10.0; 2.1	141.7
7	4.22 (d)	1.8	63.4

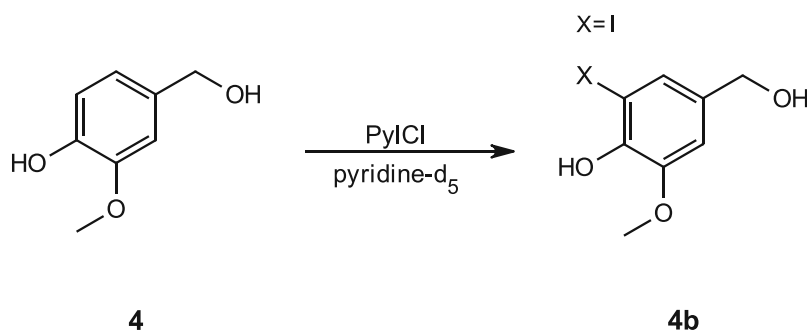


The proposed structure **4a**, resulting from the derivatization reaction of vanillyl alcohol **4** with PyICl, needs to be declared a conjecture (hence the question mark in Scheme 16), as the structure fits best to the observed chemical shifts and coupling constants. Unfortunately, there are also no reference values for similar structures.

Starting from H7 (4.22 ppm), cross-peaks to C1 (139.4 ppm), C2 (129.7 ppm), and C6 (141.7 ppm) were detected in the $^1\text{H}/^{13}\text{C}$ -HMBC spectrum, indicating that there was no modification of the hydroxymethyl side chain. A quaternary carbon signal at δ_{C} 92.5 ppm was assigned to C3 due to its long-range cross-peak to H5 at δ_{H} 6.02 ppm. This carbon shows no cross-peak to any methoxy protons leading to the assumption that the methoxy group is no longer present. In addition, H2 and H5 give cross-peaks to a low-field carbon at δ_{C} 197.4 ppm, which was therefore assigned to an oxidized C4.

The ^{13}C -peak of C3 appears at 92.5 ppm, which is a slight deviation from the other iodinated C-atoms. But considering the electronic environment, deviations can occur, and it would be possible that X represents iodine here as well. Since three olefinic proton signals were found in the ^1H -NMR spectrum, a substitution at the *ortho*-position is excluded. The H-atoms H5 and H6 exhibit a coupling constant 3J of 10 Hz, which is too large for coupling protons over three bonds in the aromatic system. While a pyran structure, which was initially considered, would explain the observed coupling of 10 Hz, it contradicts with the six detected C-atoms (C1-C6). Possibly the electronic environment resulting from the double bond and the oxygen atom on C4 could be decisive for the untypically large coupling constant (10 Hz) of H5 and H6. However, these are only considerations for which no supporting evidence exists.

Unfortunately, the reactions of vanillyl alcohol **4** with PyICl in the solvents methanol (CH_3OH) and chloroform (CHCl_3) did not provide any valuable information. Vanillyl alcohol reacted very rapidly, and obviously, decomposition and the formation of many components occurred so that it was neither possible nor useful to evaluate the NMR spectra.

3.2.4.2 In deuterated pyridine (C₅D₅N)

Scheme 17: Reaction of vanillyl alcohol **4** with PyI₂ in C₅D₅N and the product **4b** formed correspondingly. **4b:SM** ca. 1:0.5.

Derivatization reaction of vanillyl alcohol **4** proved successful in deuterated pyridine and iodination at the *ortho*-position took place. The corresponding ¹H- and ¹³C- shifts are listed in Table 42.

Table 42: ¹H- and ¹³C-shifts of component **4b** resulting from the reaction of vanillyl alcohol **4** and PyI₂ in C₅D₅N. (NMR-solvent: C₅D₅N).

Atom number	¹ H		¹³ C
	δ (ppm)	J (Hz)	δ (ppm)
1			136.96
2	7.24 (d)		111.72
3			148.58
4			147.51
5			85.77
6	7.77 (dt)	1.9; 0.6	129.83
7	4.92 (br. t)		64.20
8	3.68 (s)		56.51

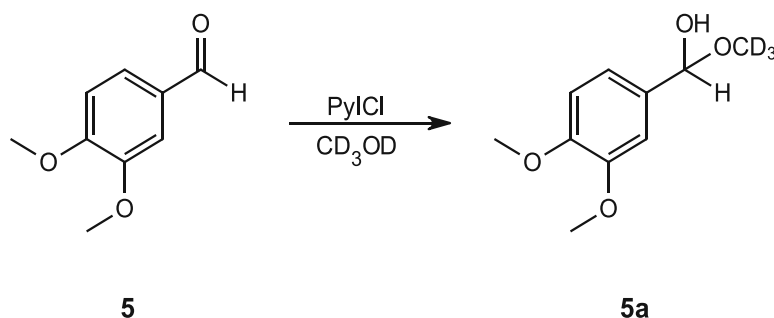
The derivatization reaction of vanillyl alcohol **4** with PyI₂ in deuterated pyridine performed significantly better compared to the other solvents. The ¹³C-shift from C5 with 85.77 ppm can be regarded as a clear indication of iodine addition (X= I) and product **4b** with its structure was confirmed by mass spectrometry (c.f. chapter 3.3.4).

In the case of vanillyl alcohol **4**, deuterated pyridine proved to be the best solvent, as it enabled the successful iodination reaction and hardly any by-products occurred.

3.2.5 Veratraldehyde

Regarding the model compound veratraldehyde **5** (c.f. Figure 1) it should be noted that this structure does not possess an OH-group on the aromatic ring but is provided with two methyl groups. According to the literature [20], no iodination should therefore be expected in the iodination reaction with PyI₂.

3.2.5.1 In deuterated methanol (CD₃OD)



Scheme 18: Reaction of veratraldehyde **5** with PyI₂ in CD₃OD and the corresponding formed product **5a**. The starting material **5** is still present. **5a:SM** ca. 1:1.

As can be seen in Scheme 18 the derivatization reaction of veratraldehyde **5** with PyI₂ in deuterated methanol resulted in a product **5a** which, as expected, was not subjected to iodination but was derived from a reaction with the solvent (CD₃OD). ¹H- and ¹³C- chemical shifts of **5a** are shown in Table 43.

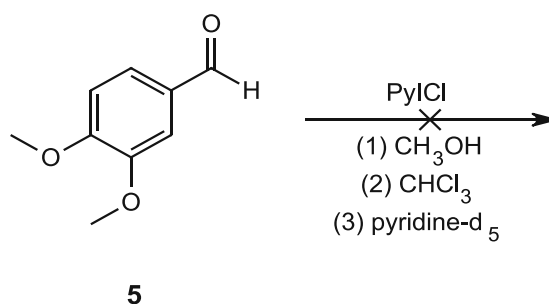
Table 43: ¹H- and ¹³C-shifts of component **5a** resulting from the reaction of veratraldehyde **5** and PyI₂ in CD₃OD. (NMR-solvent: CD₃OD).

Atom number	¹ H		¹³ C
	δ (ppm)	J (Hz)	δ (ppm)
1			132.36
2	7.01 (d)	1.9	111.27
3			150.26
4			150.62
5	6.93 (d)	8.2	112.28
6	6.98 (dd)	8.2; 1.9	120.58
7	5.31 (s)		104.54
8	3.82 (s)		56.36*
9	3.83 (s)		56.41*
10			52.39

* ... exchangeable

The signals of the atoms H7 (5.31 ppm) and C7 (104.54 ppm) shifted to high fields indicating the formation of the hemiacetal. A cross-peak of H7 (5.31 ppm) to C10 (52.39 ppm) in the $^1\text{H}/^{13}\text{C}$ -HMBC spectrum indicates the addition of deuterated methanolate to the molecule.

No reactive behavior of veratraldehyde **5** was observed in the other solvents, methanol (CH_3OH), chloroform (CHCl_3), and deuterated pyridine ($\text{C}_5\text{D}_5\text{N}$), so no derivatization occurred, as shown in Scheme 19.

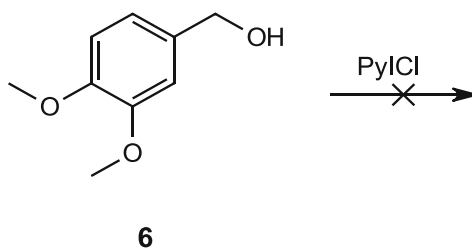


Scheme 19: No reaction occurred between veratraldehyde **5** and the iodinating reagent PyI_2 in the solvents methanol (CH_3OH), chloroform (CHCl_3), and deuterated pyridine ($\text{C}_5\text{D}_5\text{N}$).

As indicated in the literature, no iodinated derivative was expected for the model compound veratraldehyde **5** due to the absence of the OH-group, as confirmed by experimental results. The only product **5a** formed in these reactions was a result of a reaction with the solvent (CD_3OD) used. In protonated methanol (CH_3OH), on the other hand, no hemiacetal formation has occurred. A possible explanation could be that the reasonable amounts of H_2O present in protonated methanol leads to immediate hydrolysis of the hemiacetal – if ever formed.

3.2.6 Veratryl alcohol

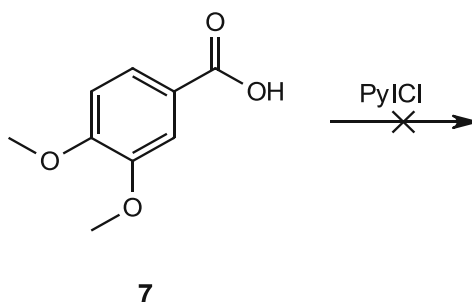
No reaction occurred between veratryl alcohol **6** and PyICl, regardless of the solvent (the reaction was performed in deuterated methanol, methanol, chloroform, and deuterated pyridine. According to the literature [20], iodination with PyICl occurs preferentially when the molecule possesses an aromatic OH-group, which is not the case with veratryl alcohol (c.f. Figure 1). Thus, the result is not unexpected.



Scheme 20: No reaction occurred between veratryl alcohol **6** and the iodinating reagent PyICl.

3.2.7 Veratric acid

As mentioned above, the prerequisite for successful iodination using PyICl is the presence of an OH-group on the aromatic compound. Since veratric acid **7** does not have a phenolic OH-group either (c.f. Figure 1), it is not surprising that no iodination occurred with this model compound, independent of the solvent used. The reaction was performed in deuterated methanol, methanol, chloroform, and deuterated pyridine.

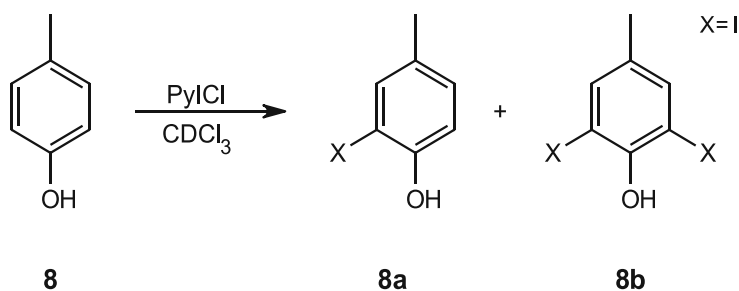


Scheme 21: No reaction occurred between veratric acid **7** and the iodinating reagent PyICl.

3.2.8 *p*-Cresol

The structure of the model compound *p*-cresol **8** (c.f. Figure 1) possesses an aromatic OH-group to which both *ortho*-positions are unsubstituted and both, according to the literature [20], show great potential to be iodinated by PyI₂.

3.2.8.1 In deuterated chloroform (CDCl₃)



Scheme 22: Reaction of *p*-cresol **8** with PyI₂ in CDCl₃ and the corresponding formed products **8a** and **8b**. Component **8a** represents the single-iodinated *p*-cresol, and component **8b** the double-iodinated *p*-cresol. SM:**8a:8b** ca. 1:0.9:0.4.

As can be seen in Scheme 22, the derivatization reaction of *p*-cresol with PyI₂ proved successful and resulted in two iodinated derivatives. The ¹H- and ¹³C- chemical shifts of the two derivatives **8a** and **8b** are shown in Table 44.

Table 44: ¹H- and ¹³C-shifts of single-iodinated component **8a** (left) and double-iodinated component **8b** (right) resulting from the reaction of *p*-cresol **8** and PyI₂ in CDCl₃. (NMR-solvent: CDCl₃).

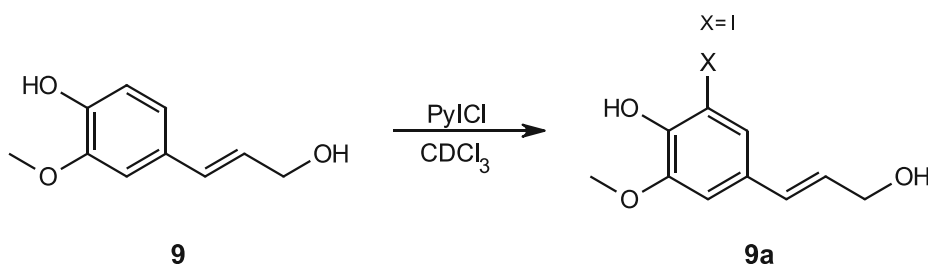
Atom number	¹ H		¹³ C	Atom number	¹ H		¹³ C
	δ (ppm)	J (Hz)	δ (ppm)		δ (ppm)	J (Hz)	δ (ppm)
1			153.26	1			151.43
2			84.47	2, 6			82.29
3	7.44 (d)	1.5	138.56	3, 5	7.46 (s)		139.46
4			131.18	4			133.76
5	6.95 (dd)	8.3; 1.5	130.29	7	2.19 (s)		19.27
6	6.93 (br. d)	8.3	114.95				
7	2.22 (s)		20.35				

Component **8a** represents the single iodinated derivative of *p*-cresol **8**. It can be identified by the ^{13}C high field shift of C2 to 84.47 ppm, which implies the characteristic ppm range of quaternary C-atoms attached with the substituent iodine. Component **8b** is the double iodinated derivative, where iodine has substituted both *ortho*-positions to the OH-group, again evident from the ^{13}C shifts of C2 and C6 to 82.29 ppm. Also, the detection of only two aromatic H-atoms (H3 and H5 at 7.46 ppm), which are magnetically equivalent, indicates double substitution.

3.2.9 Coniferyl alcohol

The model compound coniferyl alcohol **9** carries a hydroxy and a methoxy group on the aromatic ring (c.f. Figure 1). The *ortho*-position to the OH-group is unsubstituted and, according to the literature [20], should undergo iodination through the reaction with PyI₂.

3.2.9.1 In deuterated chloroform (CDCl₃)



Scheme 23: Reaction of coniferyl alcohol **9** with PyI₂ in CDCl₃ and the corresponding formed iodinated product **9a**. The main product is still the starting material **9**, and component **9a** represents the iodinated coniferyl alcohol. **SM:9a** ca. 1:0.4.

Scheme 23 depicts the successful derivatization reaction of coniferyl alcohol **9** with PyI₂ resulting in an iodinated derivative of coniferyl alcohol **9a**. The corresponding ¹H- and ¹³C- chemical shifts are shown in Table 45.

Table 45: ¹H- and ¹³C-shifts of iodinated component **9a** resulting from the reaction of coniferyl alcohol **9** and PyI₂ in CDCl₃. (NMR-solvent: CDCl₃).

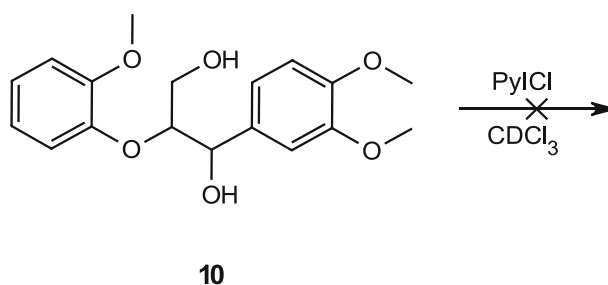
Atom number	¹ H		¹³ C
	δ (ppm)	J (Hz)	δ (ppm)
1			129.28
2	6.82 (d)	1.9	107.09
3			146.6
4			141.72
5			77.8
6	6.98 (d)	1.9	120.43
7	6.48 (dt)	15.8; 1.5	129.91
8	6.24 (dt)	15.8; 5.6	127.73
9	4.31 (dd)	5.6; 1.5	63.52
10			
11	3.91 (s)		56.30

The ¹³C-shift from C5 (77.8 ppm) and the absence of the third aromatic H-signal (H5) are crucial indications for the iodination at the *ortho*-position to the OH-group.

3.2.10 Veratrylglycerol- β -guaiacyl ether

The model compound veratrylglycerol- β -guaiacyl ether **10** (c.f. Figure 1) does not include a hydroxy group on the aromatic ring, but two methoxy groups, which, however, should not have a directing effect on iodine substitution. Therefore, according to the literature [20], no iodination with PyICl is expected in this reaction.

3.2.10.1 In deuterated chloroform (CDCl_3)



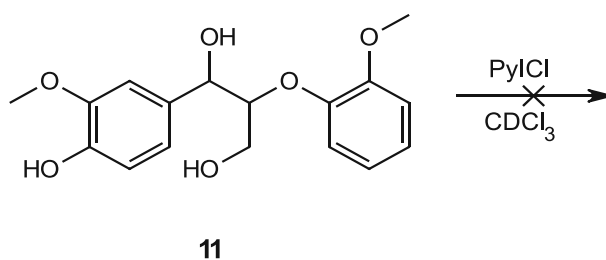
Scheme 24: No reaction occurred between veratrylglycerol- β -guaiacyl ether **10** and the iodinating reagent PyICl in CDCl_3 .

The model compound veratrylglycerol- β -guaiacyl ether **10** exhibited no reactive behavior towards the iodinating reagent PyICl and no derivatives were formed.

3.2.11 Guaiacylglycerol- β -guaiacyl ether

Contrary to the previously discussed β -ether lignin model compound (veratrylglycerol- β -guaiacyl ether **10**), the structure of the dimeric model compound guaiacylglycerol- β -guaiacyl ether **11** (c.f. Figure 1) shows a hydroxylated aromatic structure, and a reaction with PyICl could result in an iodinated derivative, as the literature suggests [20].

3.2.11.1 In deuterated chloroform (CDCl_3)



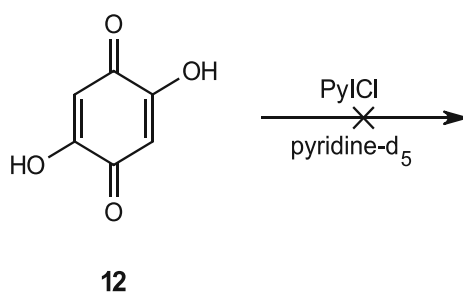
Scheme 25: No reaction occurred between guaiacylglycerol- β -guaiacyl ether **11** and the iodinating reagent PyICl in CDCl_3 .

However, evaluation employing NMR spectroscopy revealed that this model compound also did not undergo a reaction with the iodinating reagent PyICl, and no iodinated derivative could be detected. The reason for the unsuccessful iodination, despite the presence of an aromatic OH-group, is not known.

3.2.12 2,5-Dihydroxy-1,4-benzoquinone

As can be seen from the structure of DHBQ **12** (c.f. Figure 1) two aromatic hydroxy groups are present, and the respective *ortho*-positions are not substituted. According to theory [20], the *ortho*-positions would therefore be available for the addition of iodine in the iodination reaction with PyI₂.

3.2.12.1 In deuterated pyridine (C₅D₅N)



Scheme 26: No reaction occurred between 2,5-Dihydroxy-1,4-benzoquinone **12** and the iodinating reagent PyI₂ in C₅D₅N.

However, NMR analysis indicated that no reaction occurred between DHBQ **12** and PyI₂.

A possible reason for the non-occurring iodination could lie in the formation of a very stable, strongly resonance-stabilized dianion **12a**, which is formed in a neutral to alkaline medium (the milieu of this reaction was alkaline owing to the use of pyridine) [38], [49]. The strong stabilization could be the explanation for the non-occurring iodination on the molecule and may be the reason why the directing effect of the hydroxy groups for iodination at the *ortho*-position is lost.

The dianion DHBQ²⁻ **12a** is characterized by extensive double bond delocalization and is depicted in Figure 10.

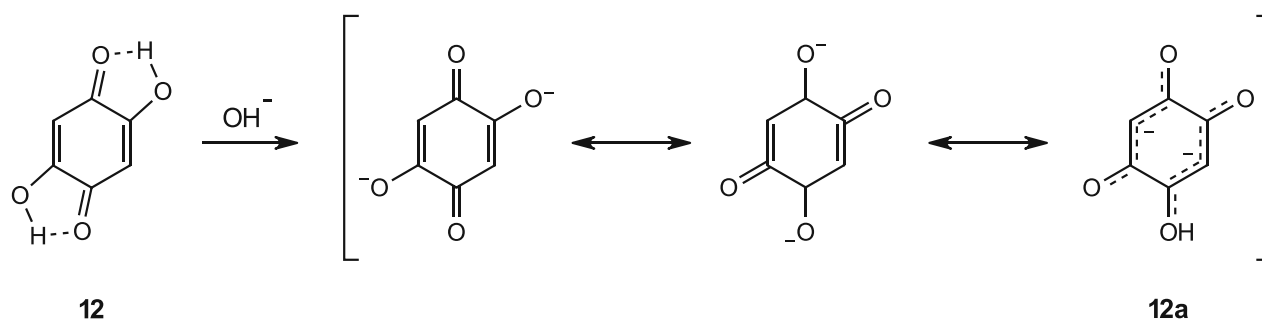
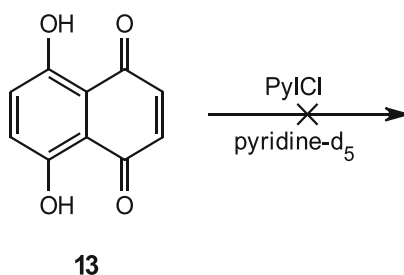


Figure 10: In an acidic medium, DHBQ exhibits a special stabilization by hydrogen bonding, while in a neutral to alkaline medium, the compound is stabilized in the form of its dianion **12a** by resonance.

3.2.13 5,8-Dihydroxy-1,4-naphthoquinone

The structure of the model compound DHNQ **13** (c.f. Figure 1) has similar properties as DHBQ, discussed in 3.2.12. It contains two aromatic OH-groups, and the *ortho*-positions are unsubstituted, where the addition of iodine could take place.

3.2.13.1 In deuterated pyridine (C₅D₅N)



Scheme 27: No reaction occurred between 5,8-Dihydroxy-1,4-naphthoquinone **13** and the iodinating reagent PyI₂ in C₅D₅N.

However, also for DHNQ **13**, no reaction could be observed. The reason is not known, but similar to DHBQ resonance stabilization could prevent iodination. DHNQ **13** also exhibits particular stabilization in neutral and alkaline medium (like pyridine in this reaction) by resonance stabilization of its dianion **13a** [49]. This stabilization causes the reactive character of the molecule to be lost and was probably responsible for the failed iodination at DHNQ.

The stabilizing structures of DHNQ in acidic and neutral/alkaline milieus are presented in Figure 11.

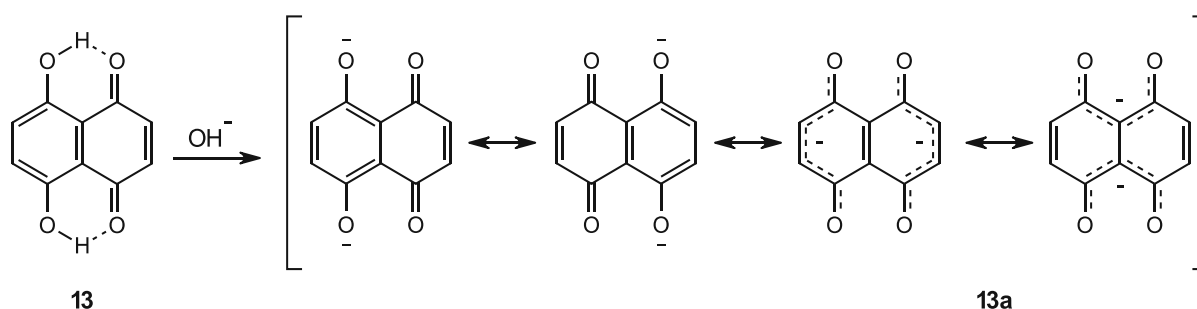
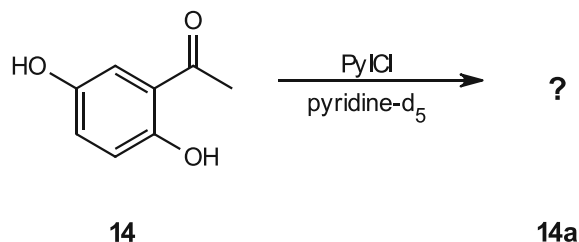


Figure 11: In an acidic medium, DHNQ **13** exhibits a special stabilization by hydrogen bonding, while in a neutral to alkaline medium, the compound is stabilized in the form of its dianion **13a** by resonance.

3.2.14 2,5-Dihydroxyacetophenone

The structure of 2,5-DHAP **14** (c.f. Figure 1) provides three unsubstituted *ortho*-positions next to its two aromatic hydroxy groups, which, theoretically [20], show potential for iodination.

3.2.14.1 In deuterated pyridine (C_5D_5N)



Scheme 28: Reaction of 2,5-Dihydroxyacetophenone **14** with PyI_2 in C_5D_5N and the unidentified product **14a** formed correspondingly. The ratio between the undefined main component **14a** and the still available starting material in the reaction mixture is approximately 1:0.54.

The derivatization reaction of 2,5-dihydroxyacetophenone **14** with the iodinating reagent PyI_2 , resulted in a product **14a** formed in large quantity but its structure could not be elucidated. Analysis by NMR spectroscopy and mass spectrometry were both unsuccessful, thus no final conclusion can be drawn. However, there was no indication of iodination of the component, nor could a ^{13}C -signal be detected in the ppm range characteristic of iodine substitution (approx. 80-90 ppm). Based on this finding, it can probably be claimed that no iodination has occurred in this substance.

2,5-DHAP has a special feature concerning the integration of substituents since the molecule possesses both substituents with an activating effect on the aromatic system (hydroxy groups) and the acetyl group, which exerts a deactivating effect on the aromatic system [49]. This inherent inconsistency between the substituents could be one possible reason why iodination at 2,5-DHAP did not occur.

Further, 2,5-DHAP **14** tends to the formation of stable intramolecular hydrogen bonds and tautomerization, with the *ortho*-quinoid tautomer **14b** being easily formed, as shown in Figure 12. As suggested for DHBQ **12** and DHNQ **13**, the lack of reactivity with PyI_2 is probably attributed to these types of stabilization in the molecule.

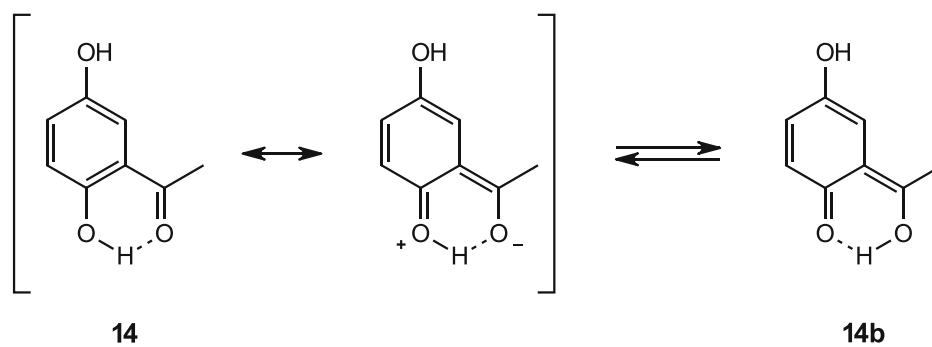


Figure 12: Stabilization of 2,5-DHAP **14** by hydrogen bonds and keto-enol-tautomerism with the formation of the ortho-quinoid tautomer **14b**.

3.2.15 Native lignins

To evaluate the potential of the derivatization method in terms of application to lignins, the reactions with PyICl were performed with native lignin. Iodination with PyICl of lignins is theoretically only supported by G-units that are unsubstituted at the *ortho*-position to the phenyl group (e.g., terminal groups).

A spruce sample served as softwood lignin and a beech sample as hardwood lignin, both consisting of monolignols with G units, among others.

3.2.15.1 Spruce

Two $^1\text{H}/^{13}\text{C}$ -HSQC spectra, before and after iodination are shown in Figure 13. The left spectrum corresponds to pure spruce lignin and the right spectrum results from the derivatization reaction of spruce lignin with PyICl.

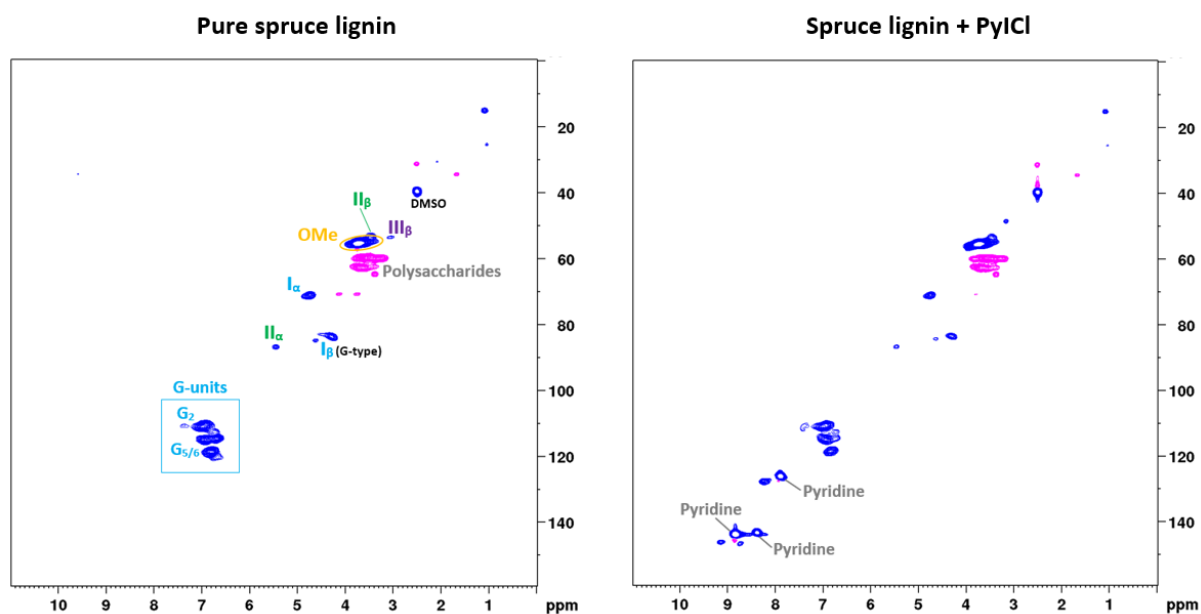


Figure 13: $^1\text{H}/^{13}\text{C}$ -HSQC spectrum of pure spruce lignin (left) and spruce lignin reacted with PyICl (right). The two spectra differ mainly in the pyridine residue (see right spectrum), otherwise, all peaks are very similar. The assignments inserted in the left spectrum also apply to the right spectrum but were not inserted again for better visibility.

In the aromatic range ($\approx 6-8$ ppm), the cross-peaks typical for the G-unit are visible. As mentioned earlier (chapter 1.2), softwood lignins consist mainly of G-unit monolignols (guaiacyl-residue). The cross-peaks in the aliphatic region ($\approx 2.5-5.5$ ppm) correspond to the side chains of different linkage types. For a detailed description of the respective linkage types, a reference can be made to chapter 1.4.3. I_{α} and I_{β} (marked in blue) correspond to the side chains in β -O-4-linkages and II_{α} and II_{β} (marked in green) in β -5-bonds. β - β -linkage side chains are represented by the cross-peak marked with III_{β} (purple). The cross-peaks circled in yellow represent methoxy groups and the pink cross-peaks are unassigned polysaccharides, solvents, etc. Only the most distinct peaks in the spectra have been assigned, other small peaks appearing in the spectrum probably correspond to polysaccharides or fatty acids.

Comparing the two spectra in Figure 13, no significant difference, except for the pyridine residues originating from PyICl (right spectrum), can be observed. This suggests that no successful iodination of spruce lignin has occurred. Of course, these $^1\text{H}/^{13}\text{C}$ -HSQC spectra represent the one-bond relationship between ^1H -atoms and ^{13}C -atoms, implying that the cross-peak of the theoretically iodinated quaternary C-atom would not even be visible in these spectra.

To figure out whether a successful iodination reaction with PyICl occurred, the $^1\text{H}/^{13}\text{C}$ -HMBC spectrum needs to be analyzed, as this provides more information concerning possible iodination. In the case of successful iodination, a cross-peak of the C-atom with the attached iodine to the aromatic protons of the G-units should be visible in the $^1\text{H}/^{13}\text{C}$ -HMBC spectrum. From the previous experiments performed on the model compounds, it is reasonable to assume that the corresponding ^{13}C -peak would appear around 80 ppm. However, the evaluation and the comparison of the $^1\text{H}/^{13}\text{C}$ -HMBC spectra from the spruce sample before and after reaction with PyICl supported the assumption of unsuccessful iodination since no cross-peak indicated iodine substitution.

3.2.15.2 Beech

Two $^1\text{H}/^{13}\text{C}$ -HSQC spectra of hardwood lignin are shown in Figure 14. The left spectrum corresponds to pure beech lignin and the right spectrum results from the derivatization reaction of beech lignin with PyICl.

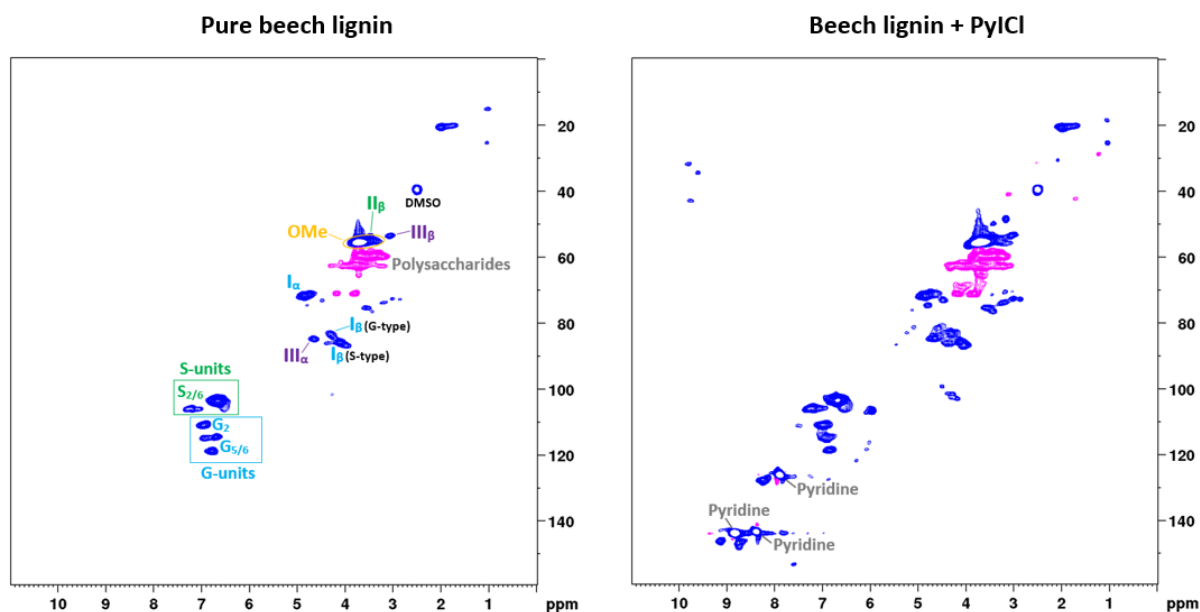


Figure 14: $^1\text{H}/^{13}\text{C}$ -HSQC spectrum of pure spruce lignin (left) and spruce lignin reacted with PyICl (right). The right spectrum shows pyridine residues originating from PyICl. The two spectra are very similar, yet some peaks appear in the right spectrum that are not present in the pure beech lignin spectrum (left), indicating that some reaction may have occurred. The assignments inserted in the left spectrum also apply to the right spectrum but were not inserted again for better visibility.

Comparing the two $^1\text{H}/^{13}\text{C}$ -HSQC spectra, the emerging peaks of pyridine, which in the right spectrum originate from the reaction with PyICl, are striking.

These spectra display cross-peaks in the aromatic region ($\approx 6-8$ ppm) of both G-units and S-units, a not unexpected finding since, as mentioned earlier (*c.f.* chapter 1.2), hardwood lignins are mainly composed of coniferyl- (G) and sinapyl- (S) types. In the aliphatic region ($\approx 2.5-5.5$ ppm) clearly visible are peaks corresponding to the side chains in different linkage types in beech lignin. The peaks labeled with I_α and I_β in blue correspond to side chains in β -O-4 linkage types, the peak labeled with II_β in green originate from chains in β -5 linkages, and those labeled with III_α and III_β in purple correspond to side chains in β - β -linkage types. For a detailed description of the respective linkage types, a reference can be made to chapter 1.4.3. The cross-peaks circled in yellow represent methoxy groups and the pink cross-peaks originate from unassigned polysaccharides, solvents, etc. To investigate whether iodination has occurred in the beech sample, the corresponding $^1\text{H}/^{13}\text{C}$ -HMBC spectrum (Figure 15) is analyzed.

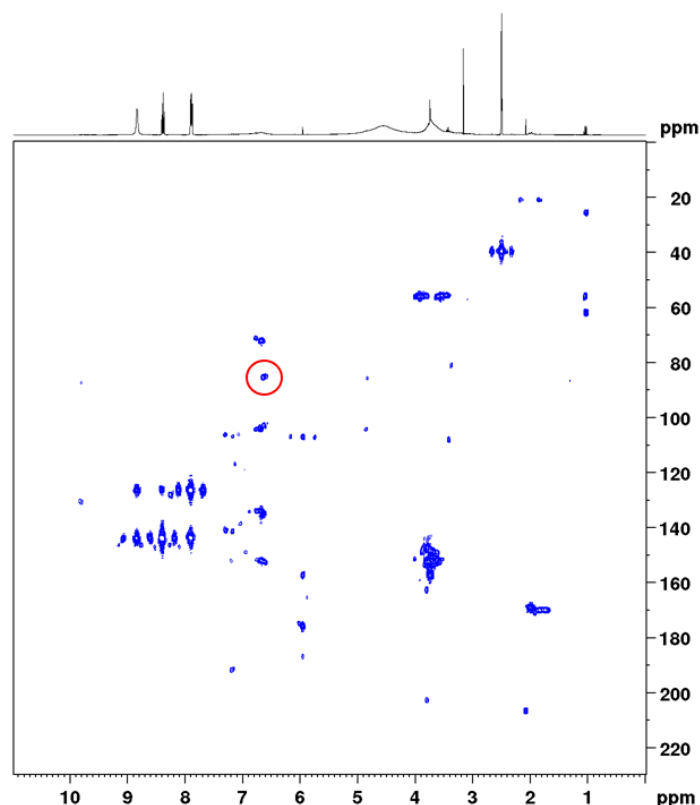


Figure 15: $^1\text{H}/^{13}\text{C}$ -HMBC spectrum resulting from the reaction of beech lignin with PyICl . The peak framed in red could be an indication that iodination has occurred.

As mentioned in the previous chapter 3.2.15.1, it is reasonable to assume that in case of successful iodination, a quaternary C-atom is expected to appear in the range of approximately 80 ppm in the $^1\text{H}/^{13}\text{C}$ -spectrum. The $^1\text{H}/^{13}\text{C}$ cross-peak at 6.64/85.6 ppm, circled in red in Figure 15, could be attributed to the successful iodination of the native lignin. 85.6 ppm would represent a characteristic chemical shift for iodinated quaternary aromatic C-atoms. Furthermore, the labeled C-atom couples merely to the aromatic region and does not exhibit any other couplings. However, this cross-peak could possibly also be attributed to the correlation of aromatic protons to α -protons of the side chains in lignin. Thus, based on this one cross-peak it is not justified to draw firm conclusions that iodination has been successful and additional investigations for unequivocal confirmation are needed.

3.3 Mass spectrometry

The products derived from the derivatization reactions, described in chapter 3.2, were analyzed by mass spectrometry. The supplementary analytical method enables substances already identified by NMR spectroscopy to be confirmed or new valuable information to be gathered. The primary intention to apply mass spectrometry was to identify the attached heteroatoms to ensure whether iodination, chlorination, or dimerization had taken place or not.

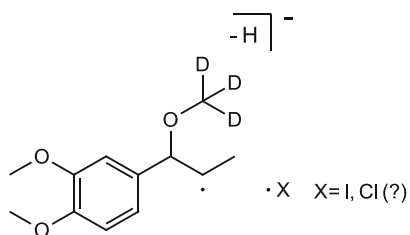
The analysis by mass spectrometry, however, proved to be challenging, since some reaction mixtures consisted of several components owing to possible decomposition or polymerization products. In addition, residues of the iodination reagent (PyI₂) were usually still present. Therefore, only a few of the structures could be analyzed reasonably by mass spectrometry.

Mass spectrometry was applied to those compounds where structure elucidation by NMR analysis was uncertain, or questions remained unresolved (derivatives of model compounds **1-7** and **12-14**). Mass analysis was unsuccessful for most components owing to the above-mentioned factors. However, structures or fragmented structures of the derivatives of methyl isoeugenol **1**, isoeugenol **2**, vanillin **3**, and vanillyl alcohol **4** were successfully confirmed.

3.3.1 Methyl isoeugenol

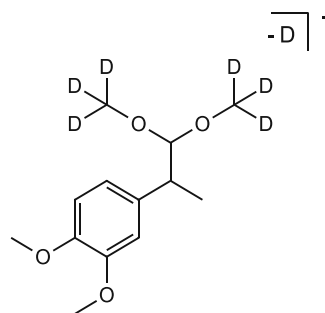
Components **1a** and **1b**, which both resulted from the reaction of methyl isoeugenol **1** and PyI₂ in deuterated methanol (*c.f.* Scheme 4) were detected as fragments by mass spectrometry. The monoisotopic mass and the fragmented structure of **1a** are represented in Figure 16 and of **1b** in Figure 17. Regarding component **1a**, unfortunately, the substituent X which would be of most interest in this analysis has been split off from the molecule during ionization in the mass spectrometric analysis. Therefore, it is still unclear which substituent has been attached to C8. At least the addition of deuterated methanol to the double bond of methyl isoeugenol was verified.

During the NMR evaluation of component **1b**, it was already suspected that this product originates from a solvent-influenced reaction only, the addition of deuterated methanol. Figure 18 shows the corresponding liquid chromatography-mass spectrometry chromatogram (LC-MS chromatogram) (positive mode), with the respective peaks marked with arrows.



Monoisotopic Mass: **211.13 amu**

Figure 16: Monoisotopic mass and structure of the fragmented component **1a**.



Monoisotopic Mass: **244.16 amu**

Figure 17: Monoisotopic mass and structure of the fragmented component **1b**.

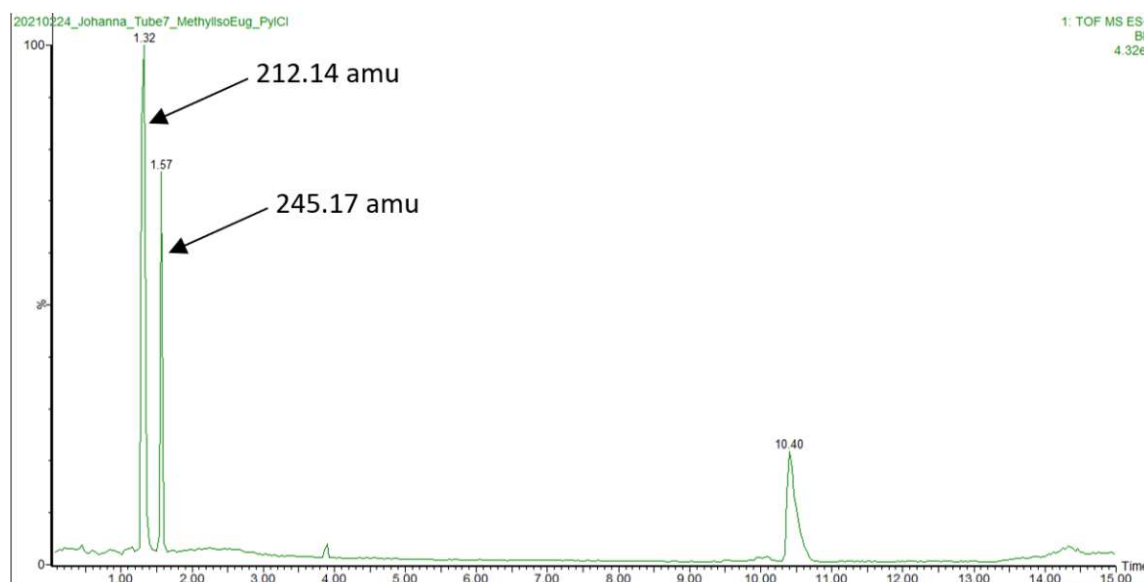
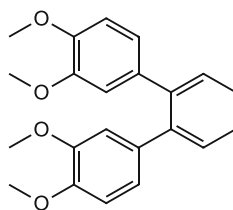


Figure 18: LC-MS chromatogram (positive mode) of the reaction mixture resulting from the reaction of methyl isoeugenol **1** and PyI in CD_3OD . The two marked mass peaks represent the fragmented components **1a** (left) and **1b** (right). Unfortunately, the other detected mass peaks could not be identified.

Component **1d** was identified in the mass spectrometric analysis as a dimer of methyl isoeugenol. Figure 19 shows the structure and monoisotopic mass of the component and the corresponding LC- MS chromatogram, measured in the positive mode, is shown in Figure 20.



Monoisotopic Mass = **354.18 amu**

Figure 19: Monoisotopic mass and structure of component **1d**.

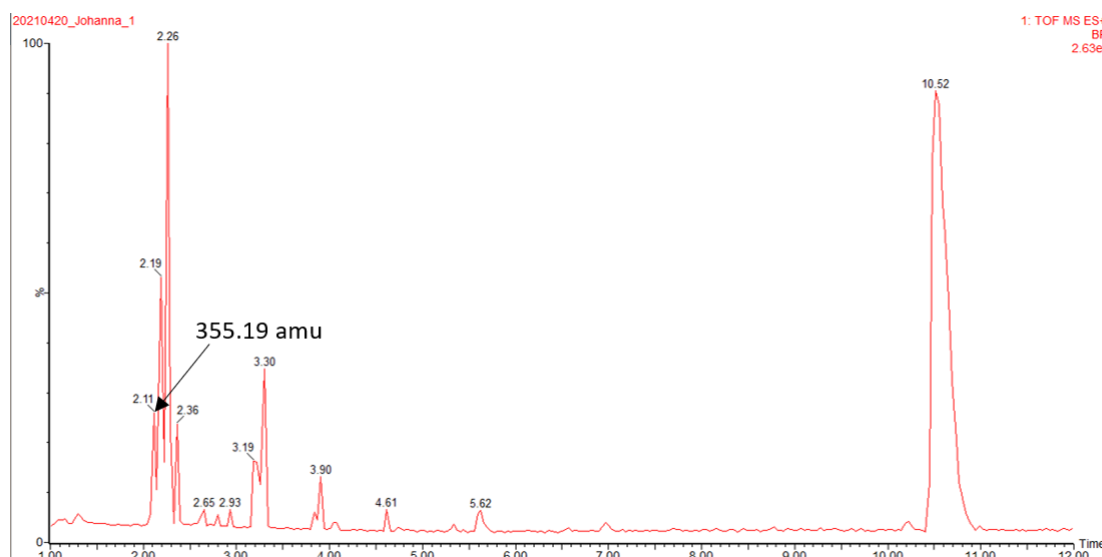
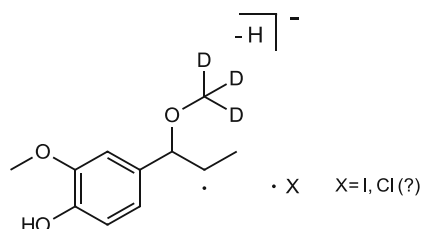


Figure 20: LC-MS chromatogram (positive mode) of the reaction mixture resulting from the reaction of methyl isoeugenol **1** and PyICl in C_5D_5N . The marked mass peak represents component **1d**. Unfortunately, the other detected mass peaks could not be identified.

3.3.2 Isoeugenol

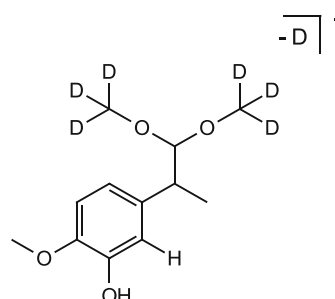
Fragments of the components **2a** and **2c**, both resulting from the reaction of isoeugenol **2** with PyICl in deuterated methanol (c.f. Scheme 10) were confirmed by mass spectrometry. As with component **1a**, component **2a** could only be detected in mass spectrometry as a fragment in which the interesting part, the substituent, has been split off during ionization. The addition of deuterated methanol could be confirmed but unfortunately, the attached substituent on C8 is still unknown. A fragment of component **2c** was detected at mass spectrometric analysis.

The fragmented structures and monoisotopic masses are shown in Figure 21 for **2a** and Figure 22 for **2c**, while the respective LC-MS chromatogram, measured in positive mode is shown in Figure 23.



Monoisotopic Mass: **197.11 amu**

Figure 21: Monoisotopic mass and structure of the fragmented component **2a**.



Monoisotopic Mass: **230.14 amu**

Figure 22: Monoisotopic mass and structure of the fragmented component **2c**.

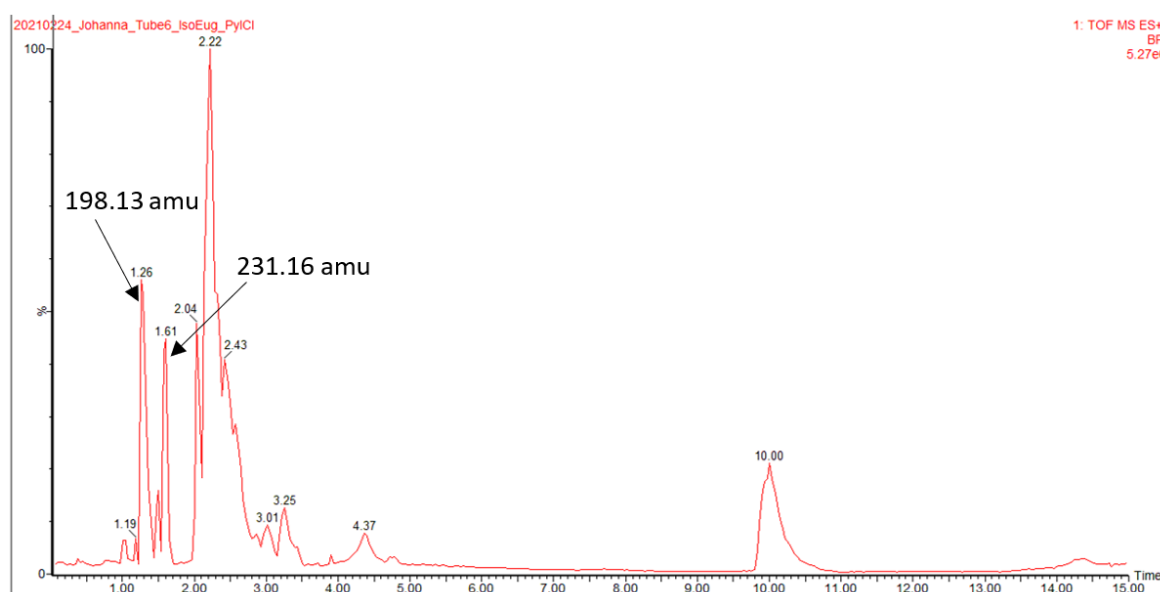
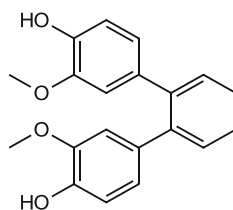


Figure 23: LC-MS chromatogram (positive mode) of the reaction mixture resulting from the reaction of isoeugenol **2** and PyIcI in CD_3OD . The two marked mass peaks represent the fragmented components **2a** (left) and **2c** (right). Unfortunately, the other detected mass peaks could not be identified.

Component **2d**, which represents a dimer of isoeugenol, was formed in the reaction of isoeugenol **2** with PyIcI (*c.f.* Scheme 11) and could be confirmed by mass spectrometry. Figure 24 shows the monoisotopic mass of **2d**, Figure 25 the corresponding LC-MS chromatogram, measured in positive mode and Figure 26 illustrates the corresponding mass spectrum (positive mode), where the respective m/z -peak of the dimer (marked with an arrow) is visible.



Monoisotopic Mass = 326.15 amu

Figure 24: Monoisotopic mass and structure of the component **2d**.

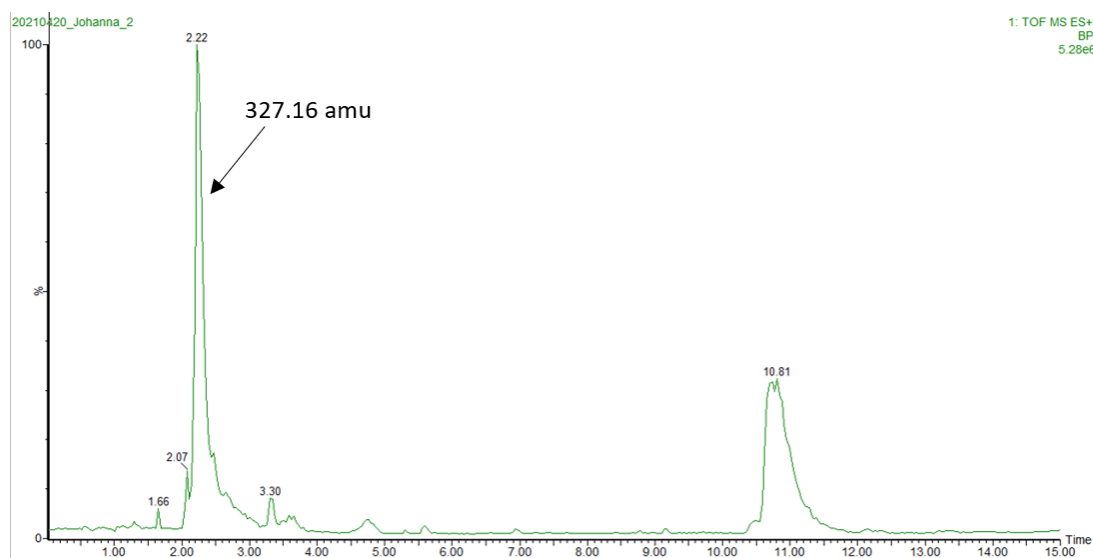


Figure 25: LC-MS chromatogram (positive mode) of the reaction mixture resulting from the reaction of isoeugenol **2** and PylCI in C_5D_5N . The marked mass peak represents component **2d**. Unfortunately, the other detected mass peaks could not be identified.

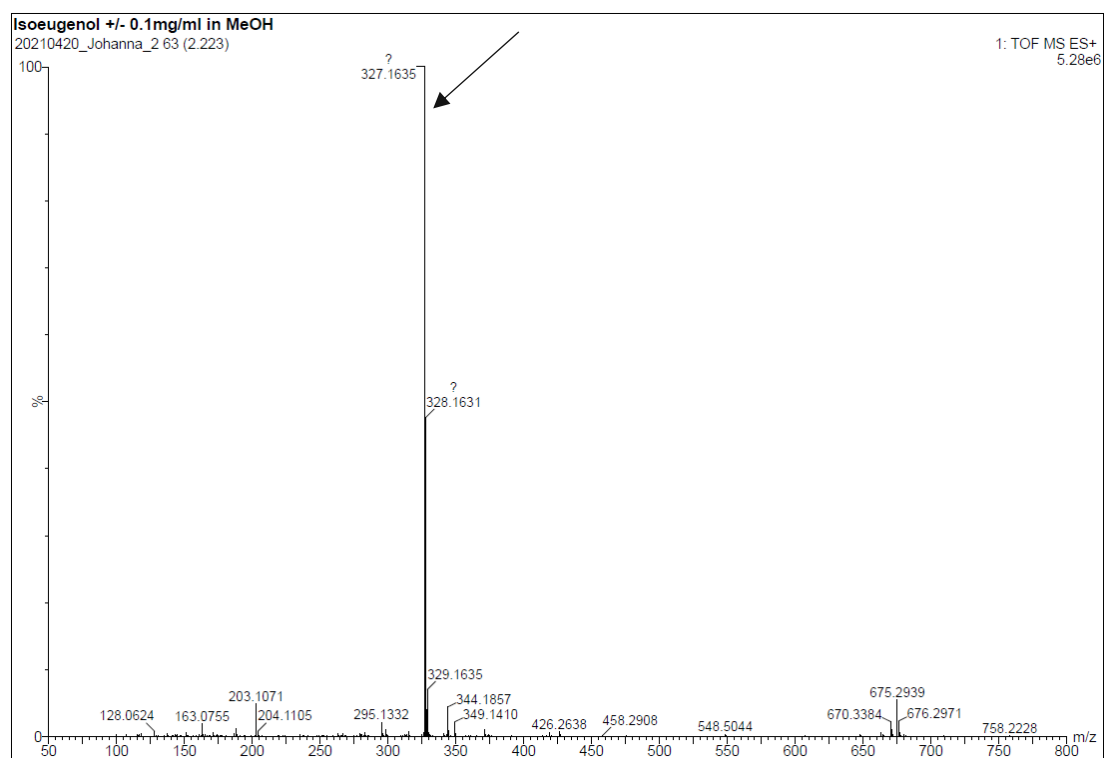
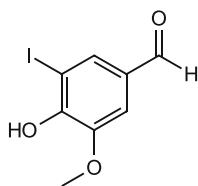


Figure 26: Mass spectrum (positive mode) of the reaction mixture resulting from the reaction of isoeugenol **2** and PyICl in C_5D_5N . The marked m/z -peak represents component **2d**.

3.3.3 Vanillin

The structure of component **3c** (c.f. chapter 3.2.3), which was determined by NMR evaluation, was confirmed by mass spectrometry. Regardless of the solvent, this component was formed in every reaction of vanillin **3** with PyICl. The monoisotopic mass and the corresponding structure of **3c** are shown in Figure 27 and Figure 28 displays the LC-MS chromatogram, measured in negative mode, with the marked peak originating from component **3c**.



Monoisotopic Mass = **277.94 amu**

Figure 27: Monoisotopic mass and structure of component **3c**.

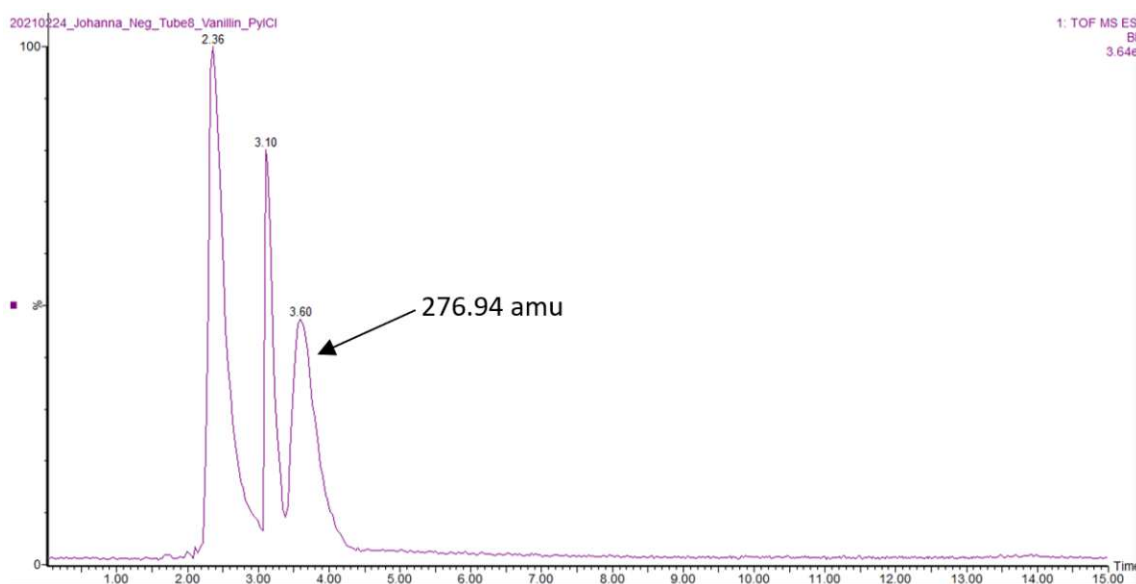
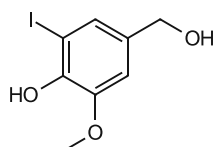


Figure 28: LC-MS chromatogram (negative mode) of the reaction mixture resulting from the reaction of vanillin **3** and PyICl in CD₃OD. The mass peak marked (the right of the three peaks) represents component **3c**. Unfortunately, the other visible mass peaks could not be identified.

3.3.4 Vanillyl alcohol

The iodinated derivative of vanillyl alcohol **4**, designated as component **4b**, resulting from the reaction with the PyICl in deuterated pyridine (*c.f.* Scheme 17) was confirmed by mass spectrometry.

Figure 29 shows the monoisotopic mass and the structure of component **4b**, while Figure 30 depicts the LC-MS chromatogram (negative mode) in which the marked mass peak corresponds to component **4b**.



Monoisotopic Mass = **279.96 amu**

Figure 29: Monoisotopic mass and structure of component **4b**.

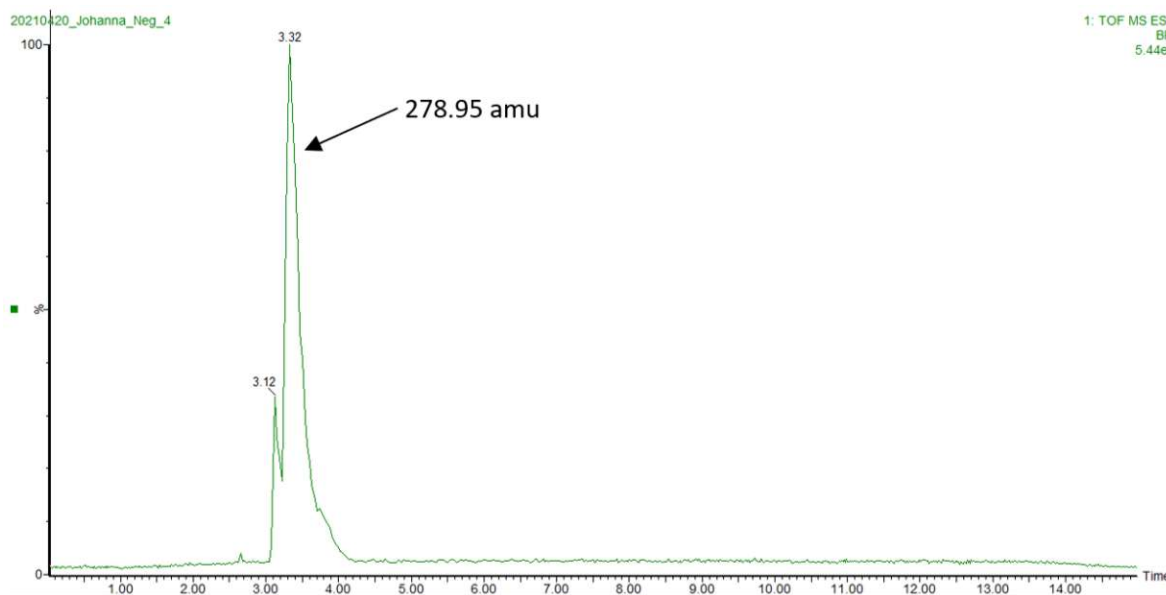


Figure 30: LC-MS chromatogram (negative mode) of the reaction mixture resulting from the reaction of vanillyl alcohol **4** and PyICl in C_5D_5N . The large, marked mass peak belongs to component **4b**.

Mass spectrometric analysis of the reaction mixtures derived from the derivatization reactions with the model compounds confirmed the successful iodination of vanillin **3** and vanillyl alcohol **4** at the *ortho*-position.

3.4 NMR-Measurements - Iodination

The NMR shifts of the resulting derivatives from iodination are listed below. Only those chemical shifts that were definable in the spectra are included in the NMR codes and only one NMR code of each component is given below, even if the same component was formed in different solvents.

3.4.1 Methyl isoeugenol

1a

¹H-NMR (400 MHz, CD₃OD): δ [ppm] 1.77 (d, *J* = 7.0 Hz, 3H), 3.83^a (s, 3H), 3.84^a (s, 3H), 4.18 (d, *J* = 5.3 Hz, 1H), 4.39 (m, *J* = 7.0, 5.3 Hz, 1H), 6.88 (dd, *J* = 8.2, 2.0 Hz, 1H), 6.93 (d, *J* = 8.2 Hz, 1H), 6.94 (d, *J* = 2.0 Hz, 1H).

¹³C-NMR (101 MHz, CD₃OD): δ [ppm] 23.55 (q), 32.39 (d), 56.44 (q), 56.44 (q), 56.9 (s), 88.77 (d), 112.02 (d), 112.36 (d), 121.59 (d), 132.79 (s), 150.28^b (s), 150.32^b (s).
^{a,b} ... exchangeable

1b

¹H-NMR (400 MHz, CD₃OD): δ [ppm] 1.22 (d, *J* = 7.1 Hz, 3H), 2.92 (qi, *J* = 7.1 Hz, 1H), 3.80 (s, 3H), 3.82 (s, 3H), 4.35 (d, *J* = 6.9 Hz, 1H), 6.78 (dd, *J* = 8.2, 2.1 Hz, 1H), 6.85 (d, *J* = 8.2 Hz, 1H), 6.85 (d, *J* = 2.1 Hz, 1H).

¹³C-NMR (101 MHz, CD₃OD): δ [ppm] 17.32 (q), 43.85 (d), 54.00 (s), 56.36^a (q), 56.50^a (q), 110.15 (d), 112.89 (d), 113.23 (d), 121.37 (d), 137.31 (s), 148.98 (s), 150.12 (s).
^a... exchangeable

1c

¹H-NMR (400 MHz, CDCl₃): δ [ppm] 1.79 (d, *J* = 7.0 Hz, 3H), 3.31 (s, 3H), 3.88^a (s, 3H), 3.89^a (s, 3H), 4.16 (d, *J* = 5.0 Hz, 1H), 4.32 (qd, *J* = 7.0, 5.0, 1H), 6.83 (m, 1H), 6.84 (m, 1H), 6.85 (m, 1H).

¹³C-NMR (101 MHz, CDCl₃): δ [ppm] 22.72 (q), 31.87 (d), 55.80^b (q), 55.88^b (q), 57.55 (q), 87.59 (d), 109.91 (d), 110.51 (d), 120.13 (d), 130.99 (s), 148.73^c (s), 148.79^c (s).
^{a,b,c} ... exchangeable

1d

¹H-NMR (400 MHz, CDCl₃):	δ [ppm] 2.11 (d, <i>J</i> = 6.5 Hz, 3H), 3.89 (s, 3H), 3.93 (s, 3H), 6.58 (br. q, <i>J</i> = 6.5 Hz, 1H), 6.87 (m, 1H), 6.93 (m, 1H), 7.00 (d, <i>J</i> = 8.1 Hz, 1H).
¹³C-NMR (101 MHz, CDCl₃):	δ [ppm] 15.75 (q), 56.19 (q), 56.84 (q), 111.87 (d), 112.40 (d), 123.25 (s), 123.34 (d), 130.41 (d), 142.6 (s), 149.67 (s), 150.88 (s).

1e

¹H-NMR (400 MHz, CDCl₃):	δ [ppm] 1.70 (d, <i>J</i> = 6.5 Hz, 3H), 4.37 (m, <i>J</i> = 7.8, 6.5 Hz, 1H), 4.86 (d, <i>J</i> = 7.8, 1H), 6.92 (1H), 6.93 (1H).
¹³C-NMR (101 MHz, CDCl₃):	δ [ppm] 22.29 (q), 60.35 (d), 67.51 (d), 110.46 (d), 120.33 (d), 131.00 (s).

3.4.2 Isoeugenol**2a**

¹H-NMR (400 MHz, CD₃OD):	δ [ppm] 1.74 (d, <i>J</i> = 7.0 Hz, 3H), 4.12 (d, <i>J</i> = 5.2 Hz, 1H), 4.36 (dq, <i>J</i> = 7.0, 5.2 Hz, 1H), 6.72 (1H), 6.73 (1H), 6.89 (1H).
¹³C-NMR (101 MHz, CD₃OD):	δ [ppm] 23.50 (q), 32.79 (d), 56.8 (q), 88.68 (d), 111.74 (d), 115.95 (d), 121.61 (d), 131.30 (s).

2b

¹H-NMR (400 MHz, CD₃OD):	δ [ppm] 1.65 (d, <i>J</i> = 7.0 Hz, 3H), 3.90 (d, <i>J</i> = 7.4 Hz, 1H), 4.22 (dq, <i>J</i> = 7.4, 7.0 Hz, 1H).
¹³C-NMR (101 MHz, CD₃OD):	δ [ppm] 25.79 (q), 33.15 (d), 90.09 (d), 130.92 (s).

2c

¹H-NMR (400 MHz, CD₃OD): δ [ppm] 1.20 (d, *J* = 7.0 Hz, 3H), 2.88 (dq, *J* = 7.0, 6.9 Hz, 1H), 4.33 (d, *J* = 6.9 Hz, 1H), 6.79 (1H).

¹³C-NMR (101 MHz, CD₃OD): δ [ppm] 17.38 (q), 43.79 (d), 54.3 (s), 110.19 (d), 112.75 (d), 121.35 (d), 135.80 (s).

2d

¹H-NMR (400 MHz, C₅D₅N): δ [ppm] 1.97 (d, *J* = 7.2 Hz, 3H), 3.79 (s, 3H), 6.55 (q, *J* = 7.2 Hz, 1H), 6.91 (dd, *J* = 8.2, 2.0 Hz, 1H), 7.14 (d, *J* = 2.0 Hz, 1H), 7.42 (d, *J* = 8.2 Hz, 1H).

¹³C-NMR (101 MHz, C₅D₅N): δ [ppm] 15.79 (q), 57.04 (q), 114.41 (d), 117.85 (d), 123.48 (s), 124.47 (d), 129.15 (d), 144.08 (s), 149.80 (s), 151.10 (s).

2e

¹H-NMR (400 MHz, C₅D₅N): δ [ppm] 1.64 (d, *J* = 7.2 Hz, 3H), 3.76 (s, 3H), 6.65 (q, *J* = 7.2 Hz, 1H), 7.20 (d, *J* = 2.0 Hz, 1H), 7.60 (d, *J* = 2.0 Hz, 1H).

¹³C-NMR (101 MHz, C₅D₅N): δ [ppm] 14.15 (q), 57.29 (q), 86.94* (s), 114.07 (d), 124.06 (d), 126.52 (s), 133.08 (d), 142.68 (s), 143.80 (s), 148.88 (s).
* ... exchangeable

2f

¹H-NMR (400 MHz, C₅D₅N): δ [ppm] 1.69 (d, *J* = 7.2 Hz, 3H), 3.85 (s, 3H), 6.71 (q, *J* = 7.2 Hz, 1H), 7.10 (d, *J* = 2.2 Hz, 1H), 7.22 (d, *J* = 2.2 Hz, 1H).

¹³C-NMR (101 MHz, C₅D₅N): δ [ppm] 14.33 (q), 57.01 (q), 86.90* (s), 110.49 (d), 126.01 (d), 128.16 (s), 128.99 (d), 142.41 (s), 149.80 (s).
* ... exchangeable

3.4.3 Vanillin

3a

¹H-NMR (400 MHz, CD₃OD): δ [ppm] 3.86 (s, 3H), 5.26 (br. t, 1H), 6.96 (d, *J* = 1.9 Hz, 1H), 7.31 (dd, *J* = 1.9, 0.6 Hz, 1H).

¹³C-NMR (101 MHz, CD₃OD): δ [ppm] 52.37 (m), 56.58 (q), 82.92 (s), 103.64 (d), 110.75 (d), 130.01 (d), 132.47 (s), 148.03^a (s), 148.16^a (s).
^a... exchangeable

3b

¹H-NMR (400 MHz, CD₃OD): δ [ppm] 3.85 (s, 3H), 5.28 (br. t, 1H), 6.77 (d, *J* = 8.1 Hz, 1H), 6.86 (ddd, *J* = 8.1, 1.9, 0.6 Hz, 1H), 6.98 (d, *J* = 1.9 Hz, 1H).

¹³C-NMR (101 MHz, CD₃OD): δ [ppm] 42.21 (s), 56.31 (q), 104.76 (d), 111.06 (d), 115.66 (d), 120.70 (d), 131.03 (s), 147.86 (s), 148.79 (s).

3c

¹H-NMR (400 MHz, CD₃OD): δ [ppm] 3.93 (s, 3H), 7.43 (t, *J* = 1.8 Hz, 1H), 7.86 (d, *J* = 1.8 Hz, 1H), 9.70 (s, 1H).

¹³C-NMR (101 MHz, CD₃OD): δ [ppm] 56.73 (q), 83.15 (s), 110.87 (d), 131.73 (s), 136.62 (d), 148.80 (s), 154.22 (s), 191.60 (d).

3.4.4 Vanillyl alcohol

4a (?)

¹H-NMR (400 MHz, CD₃OD): δ [ppm] 4.22 (d, *J*= 1.8 Hz, 2H), 6.02 (d, *J*= 10 Hz, 1H), 6.33 (m, 1H), 6.97 (dd, *J*= 10.0, 2.1 Hz, 1H).

¹³C-NMR (101 MHz, CD₃OD): δ [ppm] 63.4 (t), 92.5 (s), 126.2 (d), 129.7 (d), 139.4 (s), 141.7 (d), 197.4 (s).

4b

¹H-NMR (400 MHz, C₅D₅N): δ [ppm] 3.68 (s, 3H), 4.92 (br. t, 2H), 7.24 (d, 1H), 7.77 (dt, *J*= 1.9, 0.6 Hz, 1H).

¹³C-NMR (101 MHz, C₅D₅N): δ [ppm] 56.51 (q), 64.20 (t), 85.77 (s), 111.72 (d), 129.83 (d), 136.96 (s), 147.51 (s), 148.58 (s).

3.4.5 Veratraldehyde

5a

¹H-NMR (400 MHz, CD₃OD): δ [ppm] 3.82 (s, 3H), 3.83 (s, 3H), 5.31 (s, 1H), 6.93 (d, *J*= 8.3 Hz, 1H), 6.98 (dd, *J*= 8.2, 1.9 Hz, 1H), 7.01 (d, *J*= 1.9 Hz, 1H).

¹³C-NMR (101 MHz, CD₃OD): δ [ppm] 52.39 (s), 56.36^a (q), 56.41^a (q), 104.54 (d), 111.27 (d), 112.28 (d), 120.58 (d), 132.36 (s), 150.26 (s), 150.62 (s).

^a... exchangeable

3.4.6 *p*-Cresol

8a

¹H-NMR (400 MHz, CDCl₃): δ [ppm] 2.22 (s, 3H), 6.93 (br. d, *J*= 8.3 Hz, 1H), 6.95 (dd, *J*= 8.3, 1.5 Hz, 1H), 7.44 (d, *J*= 1.5 Hz, 1H).

¹³C-NMR (101 MHz, CDCl₃): δ [ppm] 20.35 (q), 84.47 (s), 114.95 (d), 130.29 (d), 131.18 (s), 138.56 (d), 153.26 (s).

8b

¹H-NMR (400 MHz, CDCl₃): δ [ppm] 2.19 (s, 3H), 7.46 (s, 2H).

¹³C-NMR (101 MHz, CDCl₃): δ [ppm] 19.27 (q), 82.29 (s, 2C), 133.76 (s), 139.46 (d, 2C), 151.43 (s).

3.4.7 Coniferyl alcohol

9a

¹H-NMR (400 MHz, CDCl₃): δ [ppm] 3.91 (s, 3H), 4.31 (dd, *J*= 5.6, 1.5 Hz, 2H), 6.24 (dt, *J*= 15.8, 5.6 Hz, 1H), 6.48 (dt, *J*= 15.8, 1.5 Hz, 1H), 6.82 (d, *J*= 1.9 Hz, 1H), 6.98 (d, *J*= 1.9 Hz, 1H).

¹³C-NMR (101 MHz, CDCl₃): δ [ppm] 56.30 (q), 63.52 (t), 77.80 (s), 107.09 (d), 120.43 (d), 127.73 (d), 129.28 (s), 129.91 (d), 141.72 (s), 146.60 (s).

3.5 Derivatization Method II – Phosphitylation

3.5.1 In deuterated chloroform/deuterated pyridine (CDCl₃: C₅D₅N = 1: 1.6)

Table 46 lists which model compounds were successfully phosphitylated (+) in the first series of measurements in the solvent mixture of deuterated chloroform and deuterated pyridine (CDCl₃:C₅D₅N = 1:1.6) and which were not (-).

Table 46: Overview of which model compounds resulted in a phosphitylated product (+) from the phosphitylation reaction in the solvent mixture (CDCl₃: C₅D₅N = 1:1.6) and which did not (-).

	Model compound	Phosphitylation
12	2,5-Dihydroxy-1,4-benzoquinone	+
13	5,8-Dihydroxy-1,4-naphthoquinone	+
14	2,5-Dihydroxyacetophenone	+
15	2,6-Dihydroxyacetophenone	+
16	Imidazole	-
17	1-Methylimidazole	-
18	Morpholine	+
19	<i>N</i> -Methylmorpholine <i>N</i> -oxide	-
20	Ellagic acid	+
21	Gallic acid	+
22	Propyl gallate	+
23	Rhodizonic acid dihydrate	-

Those model compounds which yielded a phosphitylated derivative, were carried out again in another series of measurements in pure deuterated pyridine (*c.f.* chapter 3.5.2). The underlying reason for this approach is that most of the model compounds show very good solubility in pure pyridine and chloroform is not necessarily required for this purpose. In addition, using a pure solvent has a beneficial effect on the NMR evaluation (*c.f.* chapter 2.3.1).

For four of the model compounds applied, imidazole **16**, 1-methyl imidazole **17**, *N*-methylmorpholine *N*-oxide **19**, and rhodizonic acid dihydrate **23** no phosphitylated product was detected.

3.5.1.1 Imidazole

According to theory, phosphitylation should take place during the reaction of imidazole **16** with the phosphitylation reagent (phospholane), since its structure shows an exchangeable proton (NH) required for this purpose. It is suspected that in the case of imidazole, the starting material may have been moist since the phosphitylation reagent (TMDP) apparently reacted with water, and no phosphitylated product was formed. Nevertheless, the measurement was repeated in pure pyridine and will be discussed in more detail in chapter 3.5.2.5.

3.5.1.2 1-Methyl imidazole

It is not unexpected that the phosphitylation reaction of 1-methylimidazole **17** with TMDP did not yield a phosphitylated derivative, since the molecule (*c.f.* Figure 2) is not provided with a labile proton where the phosphitylation reagent could attack but carries a methyl group at the N1-atom, instead.

3.5.1.3 N-Methylmorpholine N-oxide (NMMO)

It is reasonable to assume that NMMO **19** is too strong an oxidizing agent and probably oxidized the phosphitylation reagent (TMDP) before any phosphitylation of the component itself occurred.

3.5.1.4 Rhodizonic acid dihydrate

The solubility of rhodizonic acid dihydrate **23** in the CDCl_3 /pyridine- d_5 solvent mixture (as in the other solvents) was very low despite mixing overnight. Even after the addition of the phosphitylation reagent (TMDP), solubility did not improve. It can be assumed that too little of the component was dissolved for successful phosphitylation.

3.5.2 In deuterated pyridine (C_5D_5N)

The resulting phosphorylation products were analyzed by ^{31}P -NMR. For a more detailed analysis also all the $^1H/^{13}C$ -datasets were acquired.

Despite the combinatorial evaluation employing 1H -, ^{13}C - and ^{31}P -NMR, it was challenging to evaluate the spectra in detail. Due to many overlapping signals and by-products, a complete evaluation and assignment of all peaks were not possible for all derivatives.

3.5.2.1 2,5-Dihydroxy-1,4-benzoquinone

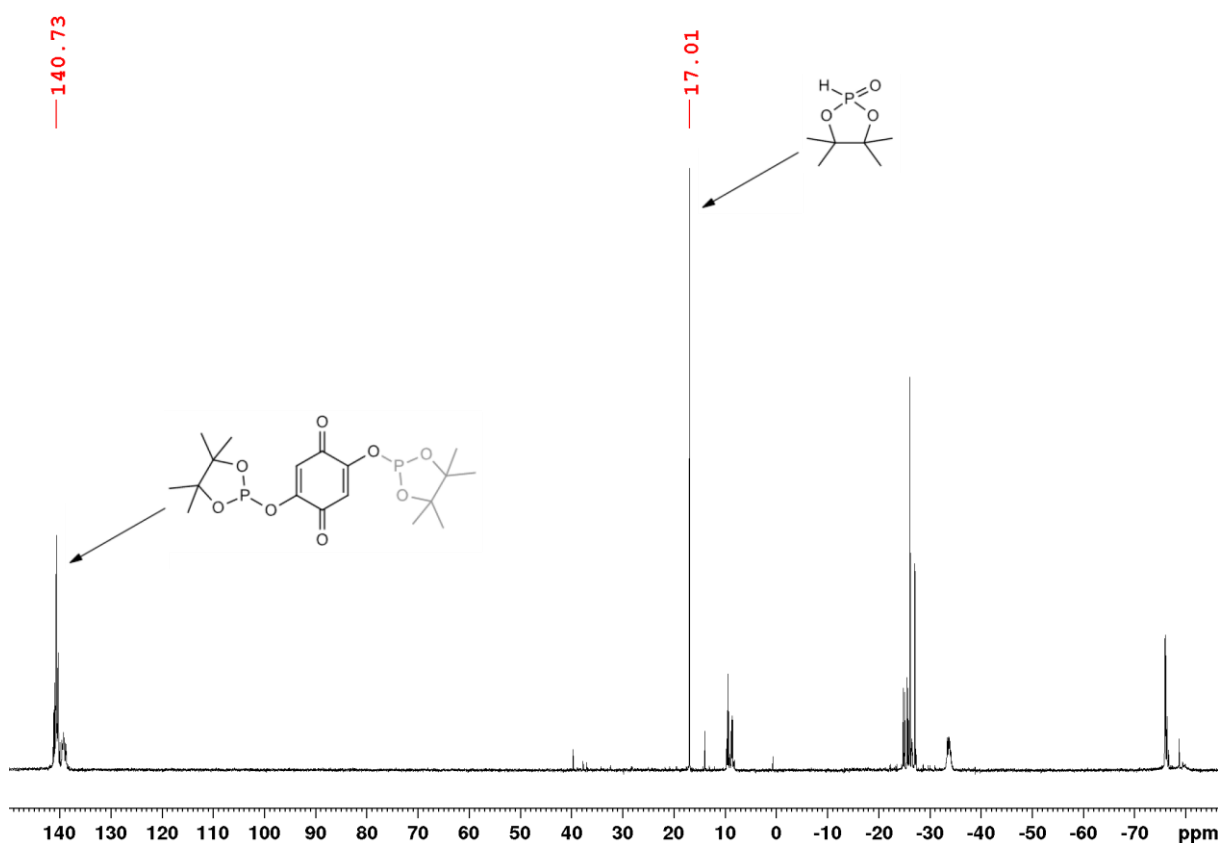


Figure 31: Proton-decoupled ^{31}P -NMR spectrum resulting from the phosphorylation of DHBQ **12** with phospholane (TMDP) in deuterated pyridine and the correspondingly presumably* phosphorylated derivative formed at 140.73 ppm. Oxidized TMDP **24** appeared as a product in this reaction at 17.01 ppm. NMR-solvent: C_5D_5N . *... "presumably" since the structure could not be fully elucidated by NMR spectroscopy.

By phosphorylation of DHBQ **12**, a plethora of components was formed resulting in severe signal overlap in the NMR spectra. Therefore, the precise evaluation of the NMR spectra and the exact assignment of the resulting peaks was unfortunately not possible.

Two peaks are marked in the ^{31}P spectrum (Figure 31) with the resonance at 140.73 ppm corresponding to the phosphitylated DHBQ. Although the structure could not be fully assigned despite combinatorial evaluation of ^1H -, ^{13}C - and ^{31}P -NMR spectra, it is nevertheless evident from the $^1\text{H}/^{31}\text{P}$ -HMBC experiment (Figure 32) that the peak at 140.73 ppm couples to the aromatic protons of DHBQ as well as to the protons of the methyl groups from TMDP (peaks circled in red in the spectrum in Figure 32), indicating the addition of phospholane to DHBQ. Because DHBQ is highly reactive the NMR spectra suggest that polymerization may also have occurred.

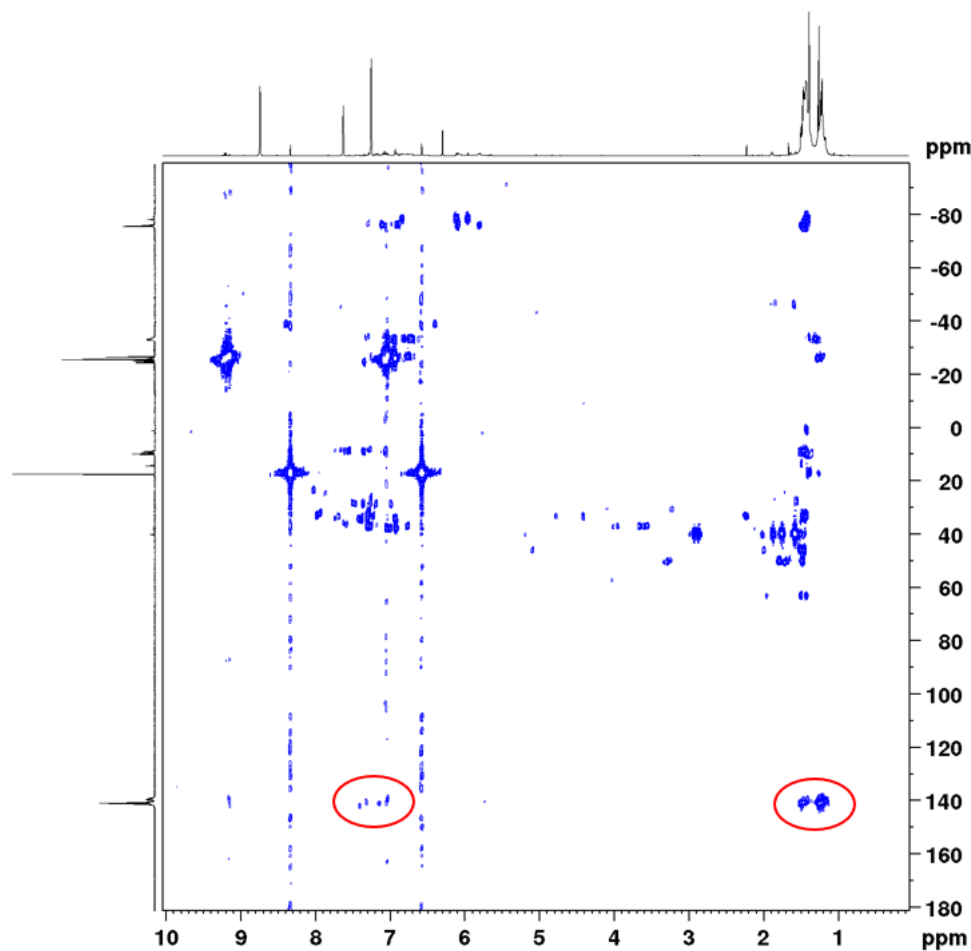


Figure 32: $^1\text{H}/^{31}\text{P}$ -HMBC spectrum resulting from the phosphitylation reaction of DHBQ **12** with TMDP. The $^{31}\text{P}/^1\text{H}$ cross-peaks circled in red prove successful phosphitylation of DHBQ. The ^1H -spectrum is plotted on the x-axis and the ^{31}P -spectrum on the y-axis. NMR-solvent: $\text{C}_5\text{D}_5\text{N}$

For illustration purposes, the structure of phosphitylated DHBQ was drawn as shown in Figure 31 (left structure). However, due to possible hydrogen bonding in this molecule, given in Figure 33 below, it cannot be determined with certainty where exactly the phosphitylation took place and whether the mono- or di-phosphitylated derivative was formed (thus one phospholane group is presented in gray in the structure).

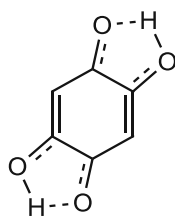


Figure 33: Potential hydrogen bonding in DHBQ.

The peak at 17.00 ppm can be assigned to the oxidized form of the phosphitylation reagent TMDP. This structure is discussed in more detail in chapter 3.5.2.10.

Unfortunately, the remaining peaks, which can be seen in Figure 31 and Figure 32, could not be assigned using $^1\text{H}/^{31}\text{P}$ -HMBC. According to conjecture, the signals in the high field probably represent oxidation products formed during the reaction.

3.5.2.2 5,8-Dihydroxy-1,4-naphthoquinone

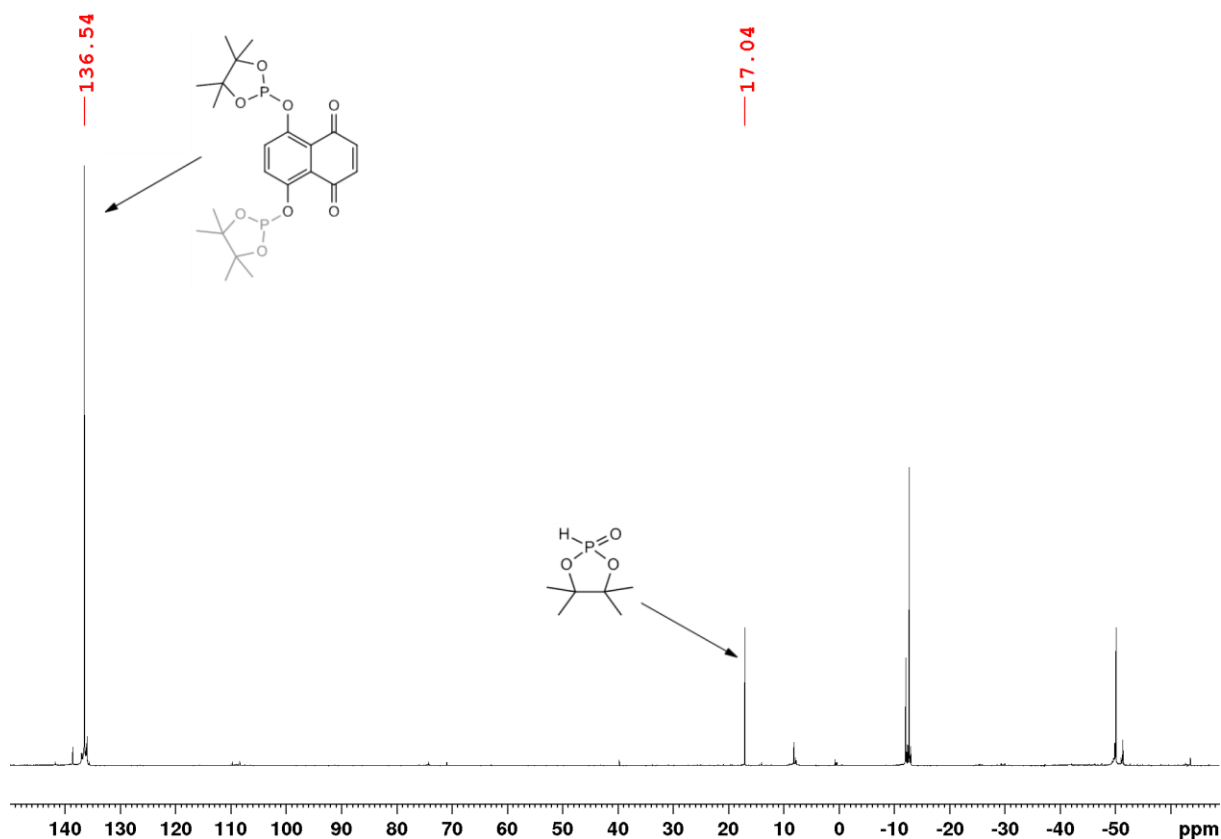


Figure 34: Proton-decoupled ^{31}P -NMR spectrum resulting from the phosphitylation of DHNQ **13** with phospholane (TMDP) in deuterated pyridine and the correspondingly “presumably” phosphitylated derivative with a chemical shift at 136.54 ppm. Oxidized TMDP **24** appeared at 17.04 ppm in this reaction. NMR-solvent: $\text{C}_5\text{D}_5\text{N}$. *... “presumably” since the structure could not be fully elucidated by NMR spectroscopy.

The phosphitylation reaction of DHNQ **13** with TMDP also yielded many products and, unfortunately, the complete evaluation of the resulting components could not be performed. The peak at 136.54 ppm in the proton-decoupled ^{31}P -spectrum, shown in Figure 34, indicates the presence of phosphitylated DHNQ proved by long-range cross-peaks to aromatic protons and also to the methyl group protons from TMDP in the $^1\text{H}/^{31}\text{P}$ HMBC experiment, illustrated by the cross-peaks circled in red in Figure 36. As discussed in the previous chapter 3.5.2.1 for DHBQ, in the case of DHNQ it was also not possible to determine with certainty whether the derivative is mono- or disubstituted owing to possible intramolecular hydrogen bonding (Figure 35).

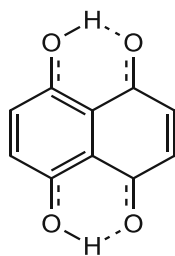


Figure 35: Potential hydrogen bonding in DHNQ.

Unfortunately, a precise assignment and determination of the chemical shifts could not be carried out for these components, since the spectra originating from the phosphitylation reaction provided many overlapping signals. The peak at 17.04 ppm again originates from the oxidation product of TMDP and is designated as component **24**, which will be discussed in more detail in chapter 3.5.2.10.

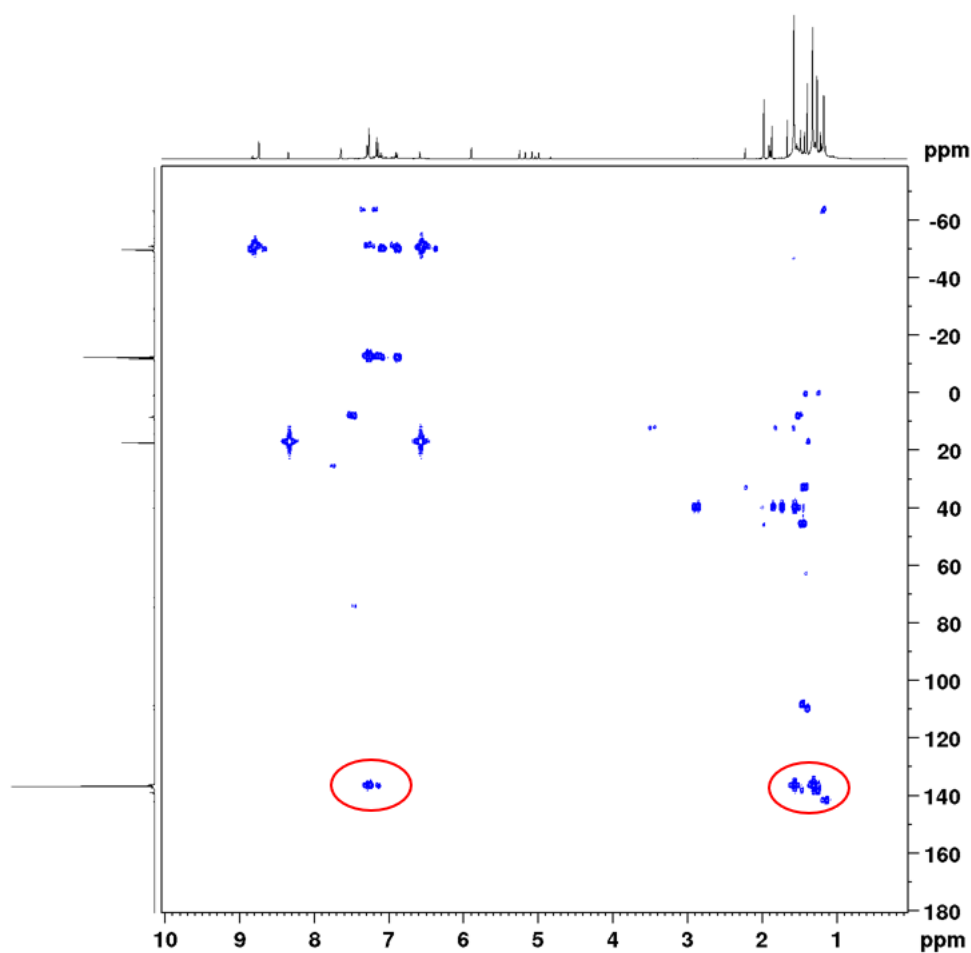
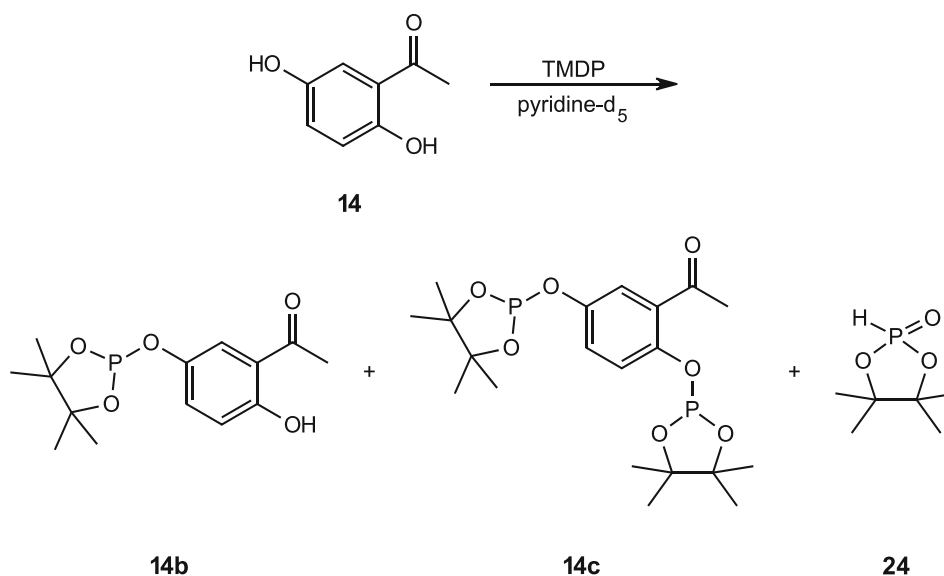


Figure 36: $^1\text{H}/^{31}\text{P}$ -HMBC spectrum resulting from the phosphitylation reaction of DHNQ **13** with TMDP. The $^1\text{H}/^{31}\text{P}$ cross-peaks circled in red prove successful phosphitylation of DHNQ. The ^1H -spectrum is plotted on the x-axis and the ^{31}P -spectrum on the y-axis. NMR-solvent: $\text{C}_5\text{D}_5\text{N}$

3.5.2.3 2,5-Dihydroxyacetophenone

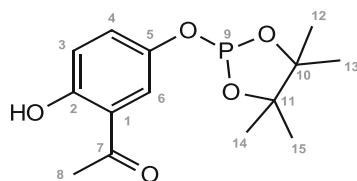
The evaluation of the corresponding spectra and the assignment of the resulting products was more straightforward for this reaction (2,5-DHAP + TMDP) therefore a more detailed analysis is given here.



Scheme 29: Reaction of 2,5-DHAP **14** with TMDP in deuterated pyridine and the corresponding formed phosphitylated products **14b** and **14c**. The oxidized phosphitylation reagent **24** also resulted from this reaction.

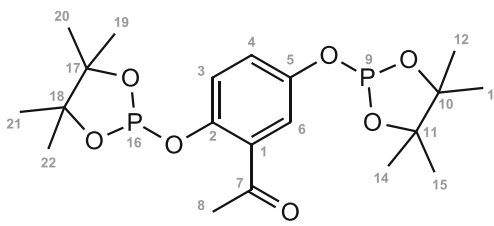
Table 47 and Table 48 provide the respective ^1H -, ^{13}C - and ^{31}P - chemical shifts of the phosphitylated products **14b** and **14c**. The corresponding proton-decoupled ^{31}P -spectrum is shown in Figure 37.

Table 47: ^1H -, ^{13}C - and ^{31}P -shifts of the meta-phosphitylated component **14b** resulting from the reaction of 2,5-dihydroxyacetophenone **14** and TMDP in $\text{C}_5\text{D}_5\text{N}$. (NMR-solvent: $\text{C}_5\text{D}_5\text{N}$).

**14b**

Atom number	^1H		^{13}C		^{31}P
	δ (ppm)	J^{HH} (Hz)	δ (ppm)	J^{CP} (Hz)	δ (ppm)
1			121.51		
2			159.29		
3	7.13 (d)	8.9	120.17		
4	7.35 (dd)	8.9; 2.8	130.43 (d)	7.7	
5			144.64 (d)	8.0	
6	7.63 (d)	2.8	123.05 (d)	7.7	
7			204.65		
8	2.55 (s)		27.97		
9					140.64
10, 11			86.66 (d)	7.8	
12, 14	1.49 (s)		25.62		
13, 15	1.27 (s)		26.01		

Table 48: ^1H -, ^{13}C - and ^{31}P -shifts of the di-phosphitylated component **14c** resulting from the reaction of 2,5-dihydroxyacetophenone **14** and TMDP in $\text{C}_5\text{D}_5\text{N}$. (NMR-solvent: $\text{C}_5\text{D}_5\text{N}$).



14c

Atom number	^1H		^{13}C		^{31}P δ (ppm)
	δ (ppm)	J^{HH} (Hz)	δ (ppm)	J^{CP} (Hz)	
1			133.23 (d)	1.5	
2			148.40 (d)	8.1	
3	7.24 (d)		123.73 (d)		
4	7.32 (dd)	8.7; 2.9	126.50 (d)	7.7	
5			149.06 (d)	8.1	
6	7.75 (d)	2.9	122.60 (d)	8.8	
7			198.45		
8	2.69 (s)		32.49		
9					140.09*
10, 11			86.99 ^a		
12, 14	1.43		25.56		
13, 15	1.25		25.96		
16					140.01*
17, 18			86.76 ^b		
19, 21	1.43		25.56		
20, 22	1.25		25.96		

*, a, b... exchangeable

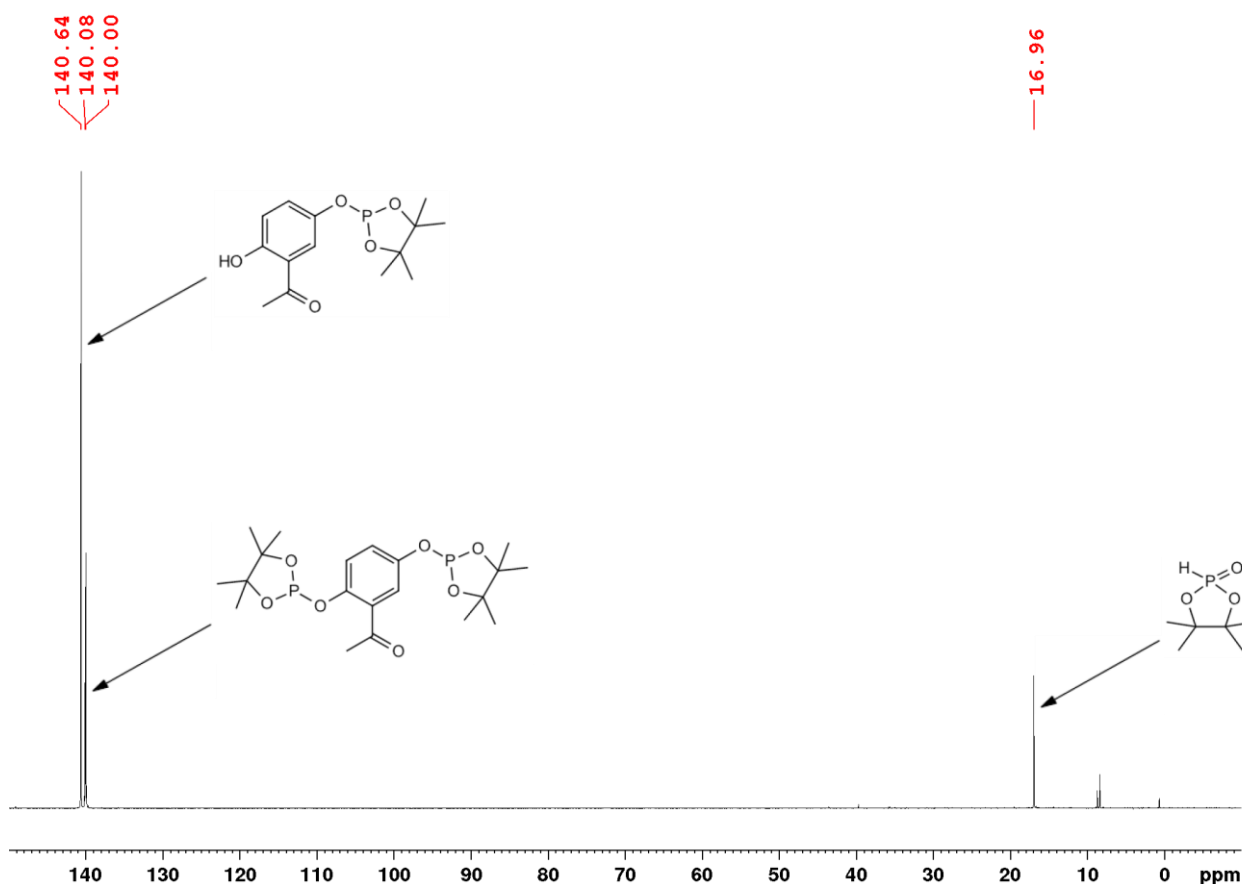


Figure 37: Proton-decoupled ^{31}P -NMR spectrum resulting from the phosphitylation of 2,5-DHAP **14** with phospholane (TMDP) in deuterated pyridine and the correspondingly phosphitylated derivatives at approx. 140 ppm. Oxidized TMDP **24** at 16.96 ppm also appeared as a product in this reaction. NMR-solvent: $\text{C}_5\text{D}_5\text{N}$.

In Figure 37 three peaks are evident at about 140 ppm. The left peak (140.64 ppm) could be assigned to the meta-phosphitylated 2,5-DHAP **14b**. For the other two peaks (140.08 and 140.00 ppm), it is not entirely certain whether they are two components or whether the peaks belong together and are split by $^{13}\text{C}/^{31}\text{P}$ coupling. However, the fact that the peak at 140.64 ppm also does not show any coupling splitting indicates that it is more likely that two different peaks are involved. Based on the $^1\text{H}/^{31}\text{P}$ -HMBC experiment, however, only one of the two peaks could be assigned to a component, resulting in the di-phosphitylated 2,5-DHAP **14c**. Since the peaks are very close to each other, the acquisition of spectra with higher resolution will be required to distinguish them. In the $^1\text{H}/^{31}\text{P}$ -HMBC spectrum in Figure 38, the cross-peaks indicative for phosphitylated 2,5-DHAP are circled in red.

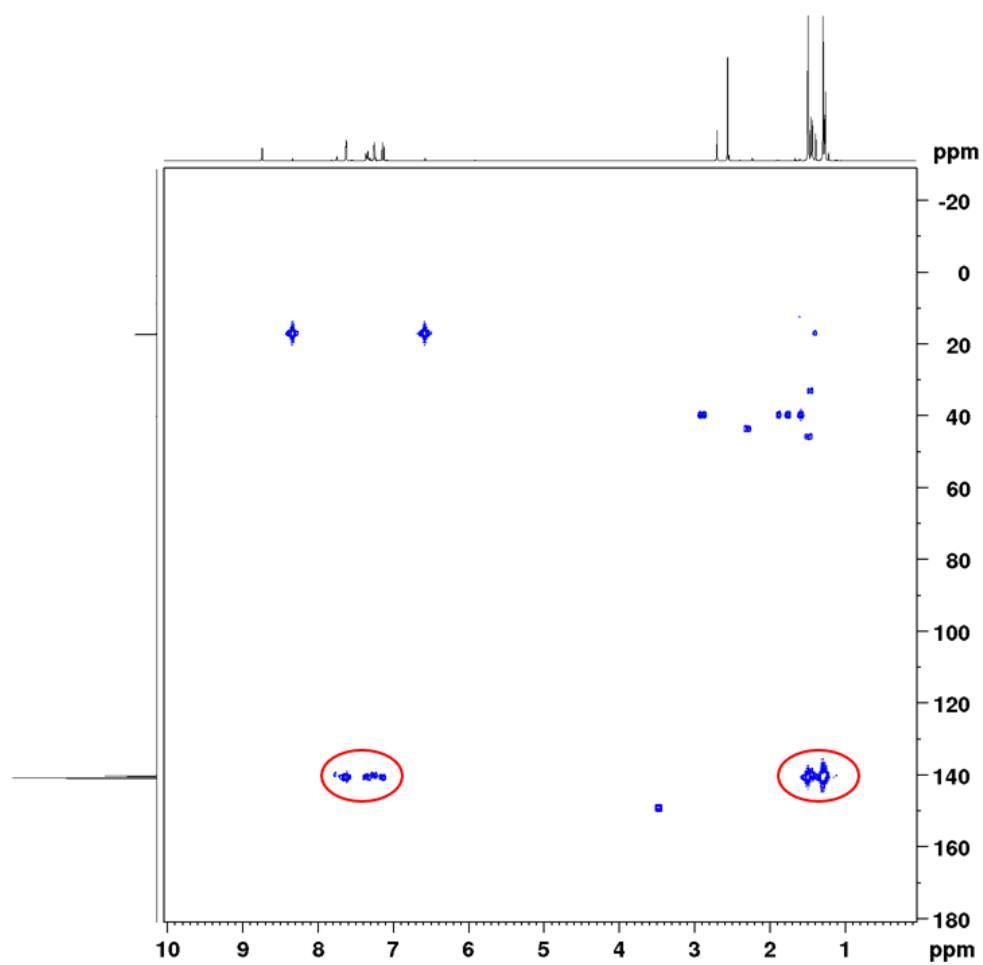
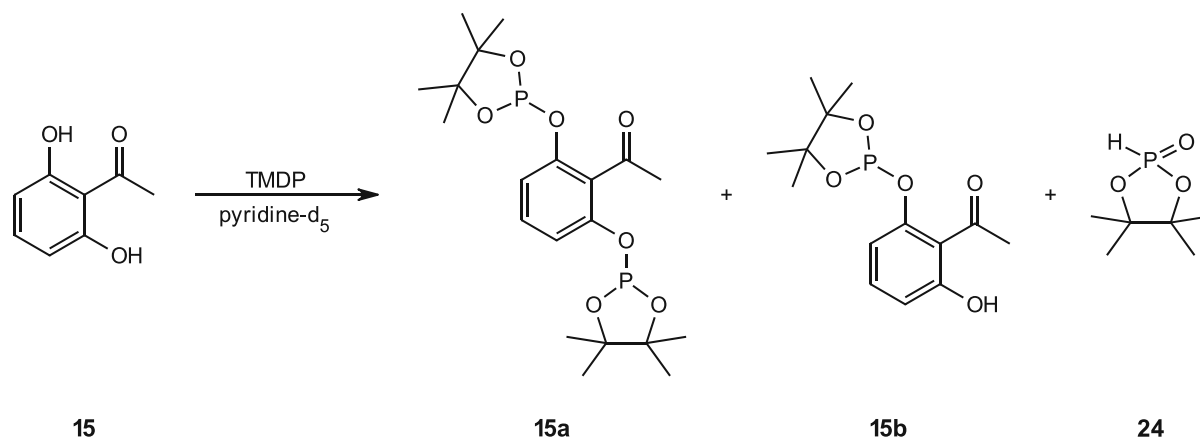


Figure 38: $^1\text{H}/^{31}\text{P}$ -HMBC spectrum resulting from the phosphorylation reaction of 2,5-DHAP **14** with TMDP. The $^1\text{H}/^{31}\text{P}$ cross-peaks circled in red indicate successful phosphorylation of 2,5-DHAP. The ^1H -spectrum is plotted on the x-axis and the ^{31}P -spectrum on the y-axis. NMR-solvent: $\text{C}_5\text{D}_5\text{N}$.

3.5.2.4 2,6-Dihydroxyacetophenone

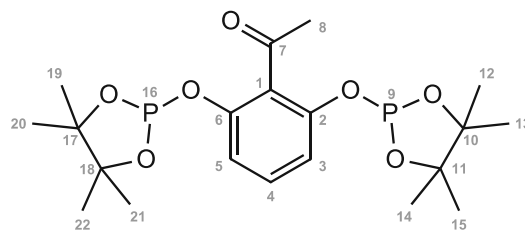
The evaluation of the spectra and the assignment of the resulting products also caused no problems for this reaction (2,6-DHAP + TMDP) as well.



Scheme 30: Reaction of 2,6-DHAP **15** with TMDP in deuterated pyridine and the corresponding formed phosphitylated products **15a** and **15b**. The oxidized phosphitylation reagent **24** also resulted from this reaction.

Table 49 and Table 50 present the corresponding ¹H-, ¹³C- and ³¹P- chemical shifts of the phosphitylated products **15a** and **15b**. The corresponding proton-decoupled ³¹P spectrum is shown in Figure 39.

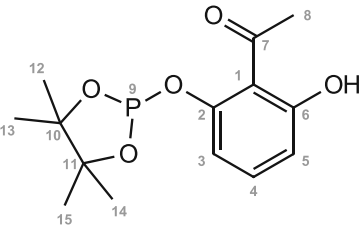
Table 49: ^1H -, ^{13}C - and ^{31}P -shifts of the di-phosphitylated component **15a** resulting from the reaction of 2,6-dihydroxyacetophenone **15** and TMDP in $\text{C}_5\text{D}_5\text{N}$. (NMR-solvent: $\text{C}_5\text{D}_5\text{N}$).



15a

Atom number	^1H		^{13}C		^{31}P
	δ (ppm)	J^{HH} (Hz)	δ (ppm)	J^{CP} (Hz)	δ (ppm)
1			129.17 (t)	2.0	
2, 6			164.44		
3, 5	7.05 (d)	8.2	116.93 (d)	14.2	
4	7.30 (t)	8.2	131.47		
7			200.76		
8	2.59 (s)		33.49		
9, 16					139.73
10, 17			86.93 (d)	7.4	
11, 18			86.93 (d)	7.4	
12, 19	1.23 (s)		25.96		
13, 20	1.41 (s)		25.45		
14, 21	1.23 (s)		25.96		
15, 22	1.41 (s)		25.45		

Table 50: ^1H -, ^{13}C - and ^{31}P -shifts of the mono-phosphitylated component **15b** resulting from the reaction of 2,6-dihydroxyacetophenone **15** and TMDP in $\text{C}_5\text{D}_5\text{N}$. (NMR-solvent: $\text{C}_5\text{D}_5\text{N}$).



15b

Atom number	^1H		^{13}C		^{31}P
	δ (ppm)	J^{HH} (Hz)	δ (ppm)	J^{CP} (Hz)	δ (ppm)
1			117.64		
2			162.80		
3	7.03		114.07		
4	7.34 (t)	8.1	134.81		
5	6.76 (dd)	8.1	111.75		
6			153.25		
7			204.55		
8	2.72 (s)		34.10		
9					138.51
10, 11			86.95 (d)	7.4	
12, 14	1.27 (s)		25.92		
13, 15	1.43 (s)		25.45		

The evaluation of the mono-substituted component **15b** was more challenging since the signal of H3 (7.03 ppm) was not directly observed in the ^1H -spectrum. However, a correlation to the other two aromatic protons H4 (7.34 ppm) and H5 (6.76 ppm) could be detected by cross-peaks in the COSY spectrum. In addition, also the $^1\text{H}/^{31}\text{P}$ -HMBC displayed a cross-peak, indicating the coupling of H3 to the ^{31}P -resonance at 138.51 ppm. A possible explanation for the varying appearance of the signals in the spectra might be an unfinished reaction during the first measurements and, given the time offset of the NMR measurements, 2,6-DHAP may have continued to react.

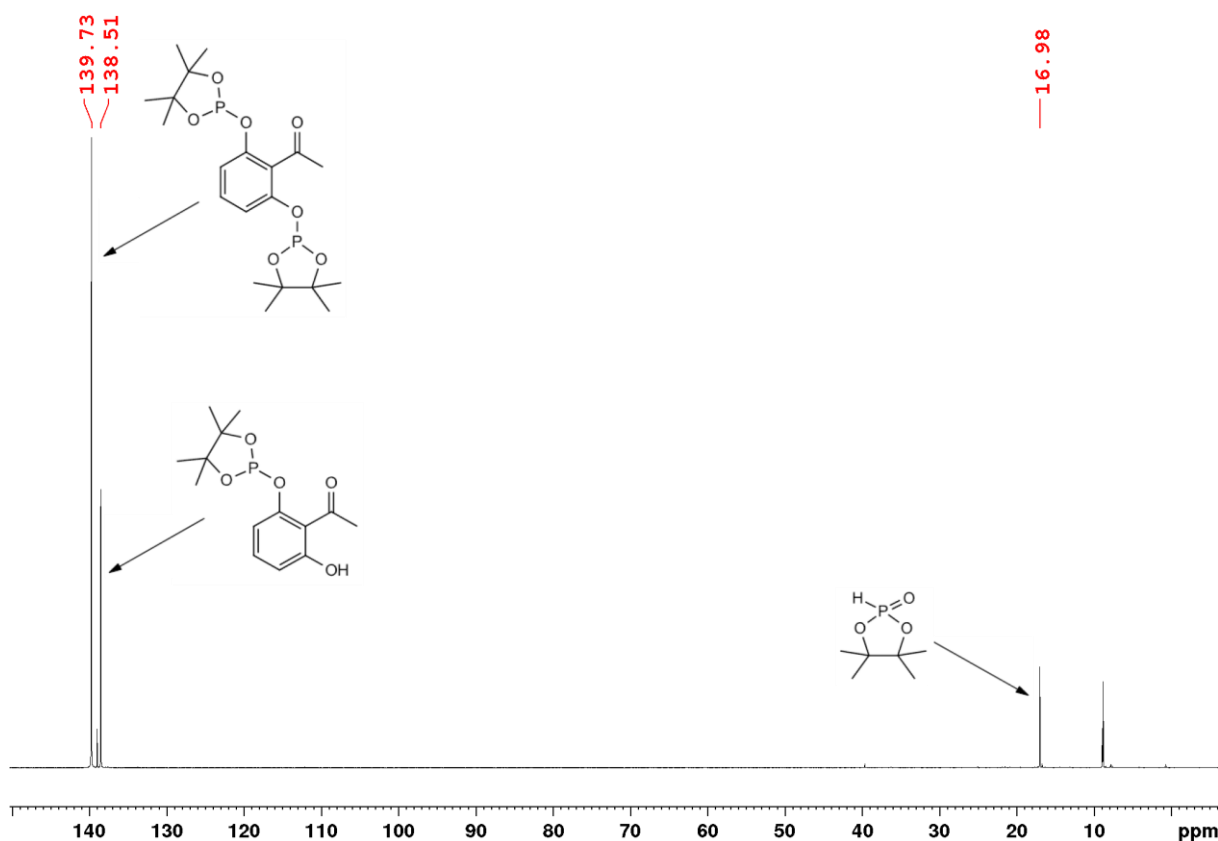


Figure 39: Proton-decoupled ^{31}P -NMR spectrum resulting from the phosphitylation of 2,6-DHAP **15** with phospholane (TMDP) in deuterated pyridine and the correspondingly phosphitylated derivatives at approx. 139 ppm. Oxidized TMDP **24** at 16.98 ppm also appeared as a product in this reaction. NMR-solvent: $\text{C}_5\text{D}_5\text{N}$.

Owing to magnetic equivalence the resonance in Figure 39 at 139.73 ppm can be assigned to di-phosphitylated 2,6-DHAP **15a**, while the one at 138.51 ppm corresponds to mono-phosphitylated 2,6-DHAP **15b** due to the presence of three different aromatic protons. Compound **24**, 4,4,5,5-tetramethyl-1,3,2 λ^5 -dioxaphospholan-2-one, the oxidized phosphitylation reagent, emerges at 16.98 ppm (*c.f.* chapter 3.5.2.10).

At approximately 9 ppm, another peak-group is detected, which, however, could not be assigned. The fact that these peaks are in the high field region and observed long-range couplings to aromatic protons leads to the assumption that oxidation products of the phosphitylated products **15a** and **15b** might be involved. However, due to the numerous overlapping peaks, an exact evaluation was not possible, thus no firm conclusions can be drawn, and this consideration remains an assumption. Figure 40 shows the corresponding $^1\text{H}/^{31}\text{P}$ -HMBC spectrum, where the cross-peaks circled in red derive from the phosphitylated products.

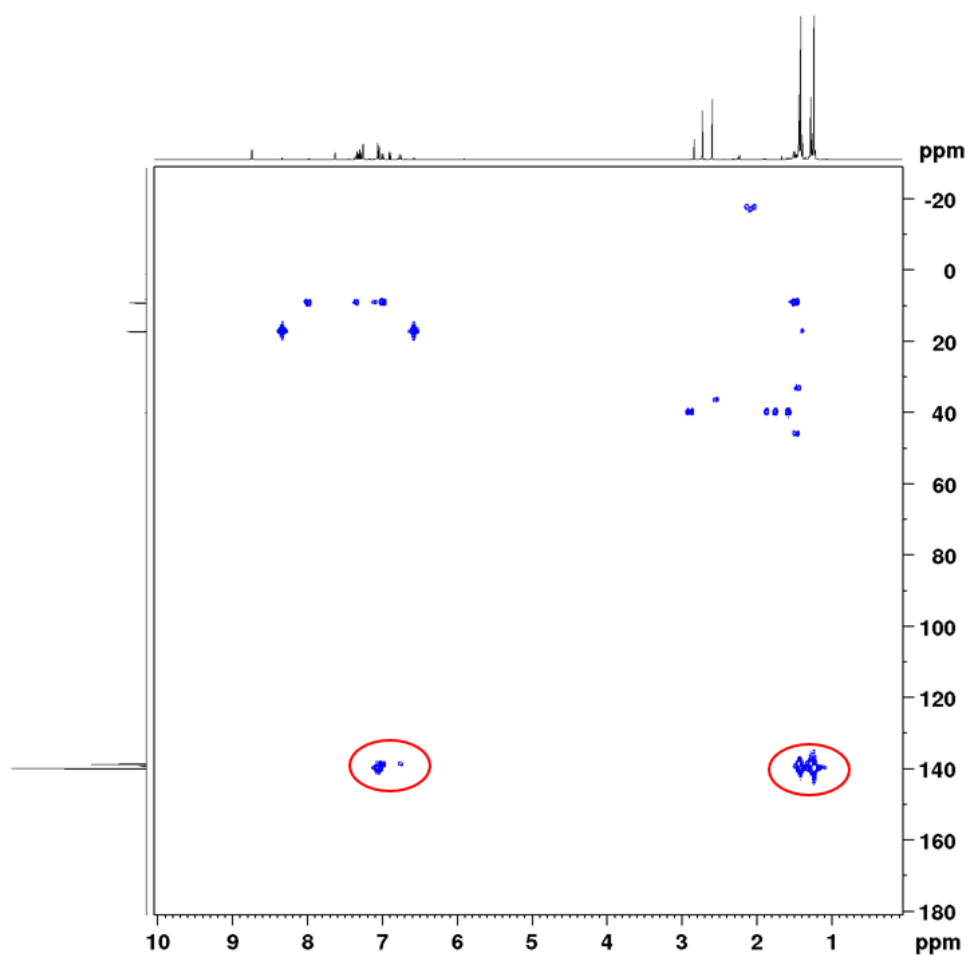


Figure 40: $^1\text{H}/^{31}\text{P}$ -HMBC spectrum resulting from the phosphitylation reaction of 2,6-DHAP **15** with TMDP. The $^1\text{H}/^{31}\text{P}$ cross-peaks circled in red indicate successful phosphitylation of 2,6-DHAP. The ^1H -spectrum is plotted on the x-axis and the ^{31}P -spectrum on the y-axis. NMR-solvent: $\text{C}_5\text{D}_5\text{N}$.

3.5.2.5 Imidazole

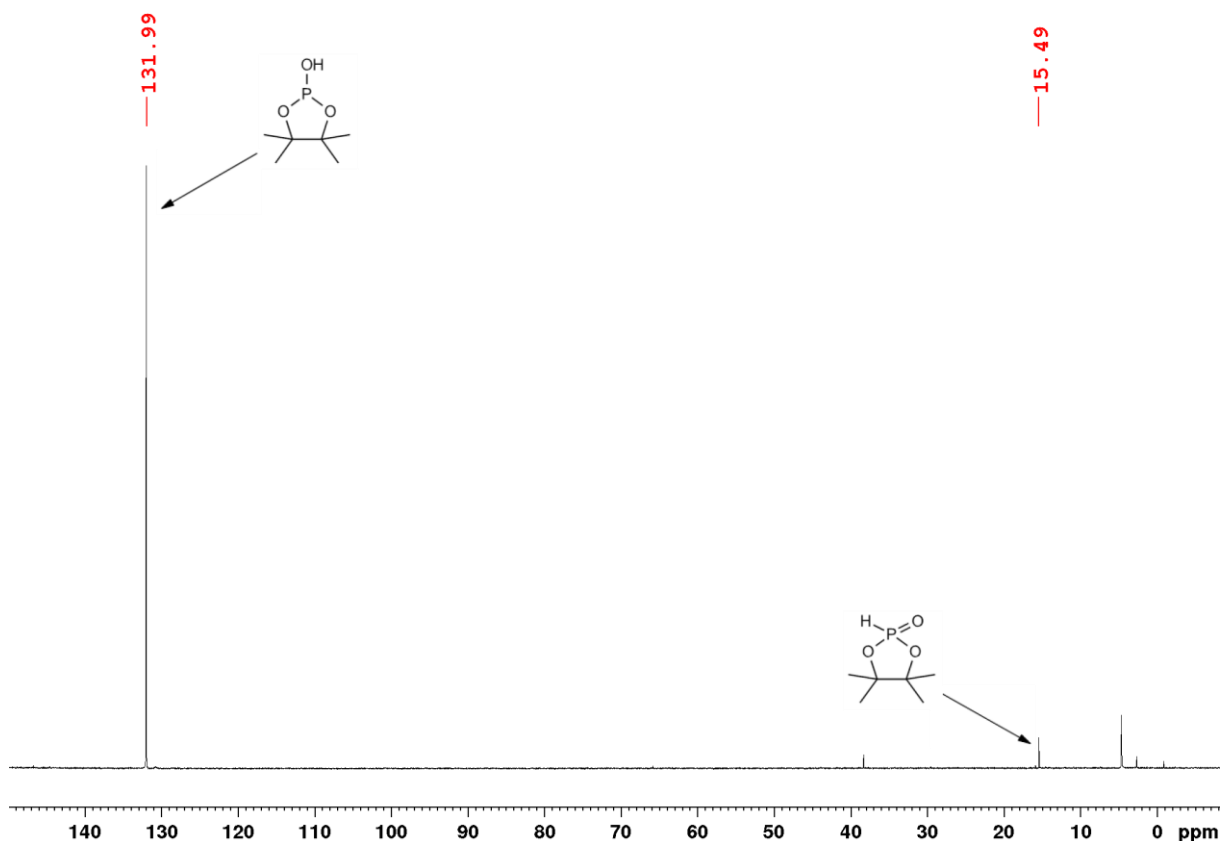


Figure 41: Proton-decoupled ^{31}P -NMR spectrum resulting from the phosphitylation of imidazole **16** with phospholane (TMDP) in deuterated pyridine and the correspondingly formed components. Oxidized TMDP **24** emerges at 15.49 ppm and TMPD + H₂O at 131.99 ppm. NMR-solvent: C₅D₅N.

As can be seen in Figure 41, the phosphitylation reaction with imidazole **16** was not successful as no imidazole-phosphitylated products were formed. This is unexpected since given the structure of imidazole (c.f. Figure 2) the so-called "labile proton" (N-H) at which phosphitylation could take place is present. In this case, it can be assumed that the starting material may have been moist, and thus the phosphitylation reagent TMDP reacted with water. The derivatization reagent is very sensitive to moisture and can react with water almost instantly. The peak at 131.99 ppm is assigned to this product [22]. Within the $^1\text{H}/^{31}\text{P}$ -HMBC spectrum, shown in Figure 42, this ^{31}P -peak shows couplings to the TMDP-derived methyl groups only (cross-peak circled in red). The oxidized form of TMDP **24** is detected at 15.49 ppm and will be discussed in more detail in chapter 3.5.2.10.

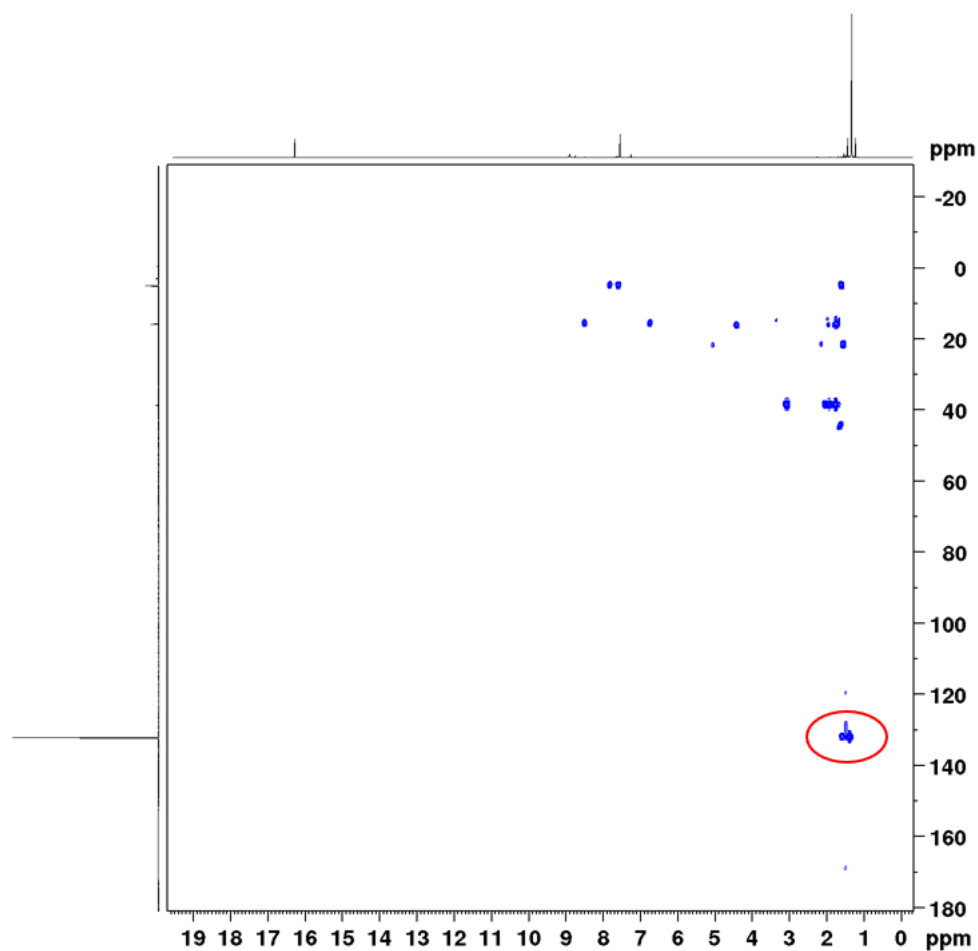
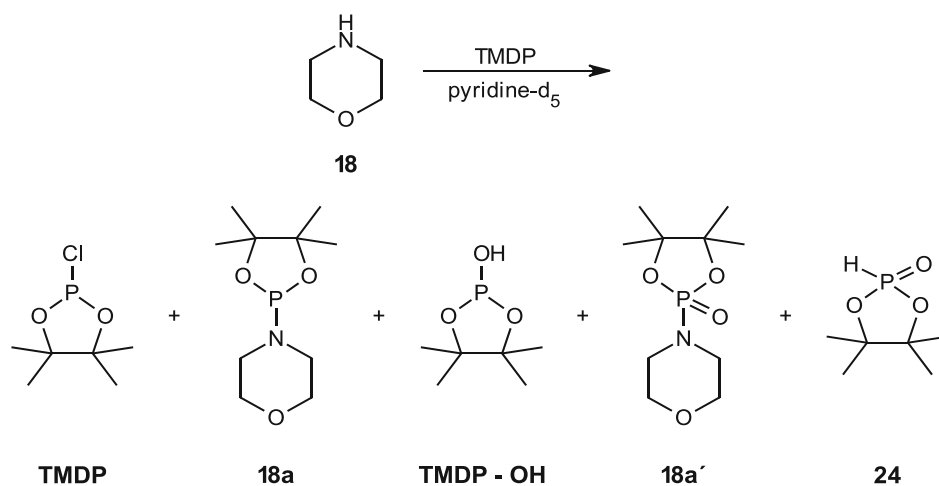


Figure 42: $^1\text{H}/^{31}\text{P}$ -HMBC spectrum resulting from the phosphitylation reaction of imidazole **16** with TMDP. The $^1\text{H}/^{31}\text{P}$ cross-peak circled in red represents the product formed from the reaction of TMDP and water. The ^1H -spectrum is plotted on the x-axis and the ^{31}P -spectrum on the y-axis. NMR-solvent: $\text{C}_5\text{D}_5\text{N}$.

3.5.2.6 Morpholine

The analysis of the phosphitylated derivative of morpholine could be performed more accurately and the assignment of chemical shifts in the NMR spectra was more feasible.



Scheme 31: Reaction of morpholine **18** with TMDP in deuterated pyridine and the corresponding formed phosphitylated product **18a**. Other products of the reaction were the phosphitylation reagent TMDP which was still present and its oxidized component **24**, as well as the oxidized form of phosphitylated morpholine **18a'** and the product derived from the reaction of TMDP with H_2O .

Table 51 contains the respective 1H -, ^{13}C - and ^{31}P - chemical shifts of the phosphitylated derivative **18a** and Table 52 those of **18a'** while the corresponding ^{31}P spectrum is given in Figure 43.

Table 51: ^1H -, ^{13}C - and ^{31}P -shifts of the phosphitylated morpholine **18a** resulting from the reaction of morpholine **18** and TMDP in $\text{C}_5\text{D}_5\text{N}$. (NMR-solvent: $\text{C}_5\text{D}_5\text{N}$).

18a

Atom number	^1H		^{13}C		^{31}P
	δ (ppm)	J^{HH} (Hz)	δ (ppm)	J^{CP} (Hz)	δ (ppm)
1, 4	3.21 (m)		44.72 (d)	18.0	
2, 3	3.57 (m)		68.78 (d)	4.8	
5					139.37
6, 7			81.87 (d)	5.1	
8, 10	1.28 (s)		25.68		
9, 11	1.28 (s)		25.68		

Table 52: ^1H -, ^{13}C - and ^{31}P -shifts of the oxidized phosphitylated morpholine **18a'** resulting from the reaction of morpholine **18** and TMDP in $\text{C}_5\text{D}_5\text{N}$. (NMR-solvent: $\text{C}_5\text{D}_5\text{N}$).

18a'

Atom number	^1H		^{13}C		^{31}P
	δ (ppm)	J^{HH} (Hz)	δ (ppm)	J^{CP} (Hz)	δ (ppm)
1, 4	3.31 (m)		45.79 (d)	2.0	
2, 3	3.62 (m)		67.71 (d)	5.2	
5					18.48
6, 7			87.12		
8, 10	1.32 (s)		25.30		
9, 11	1.32 (s)		25.30		

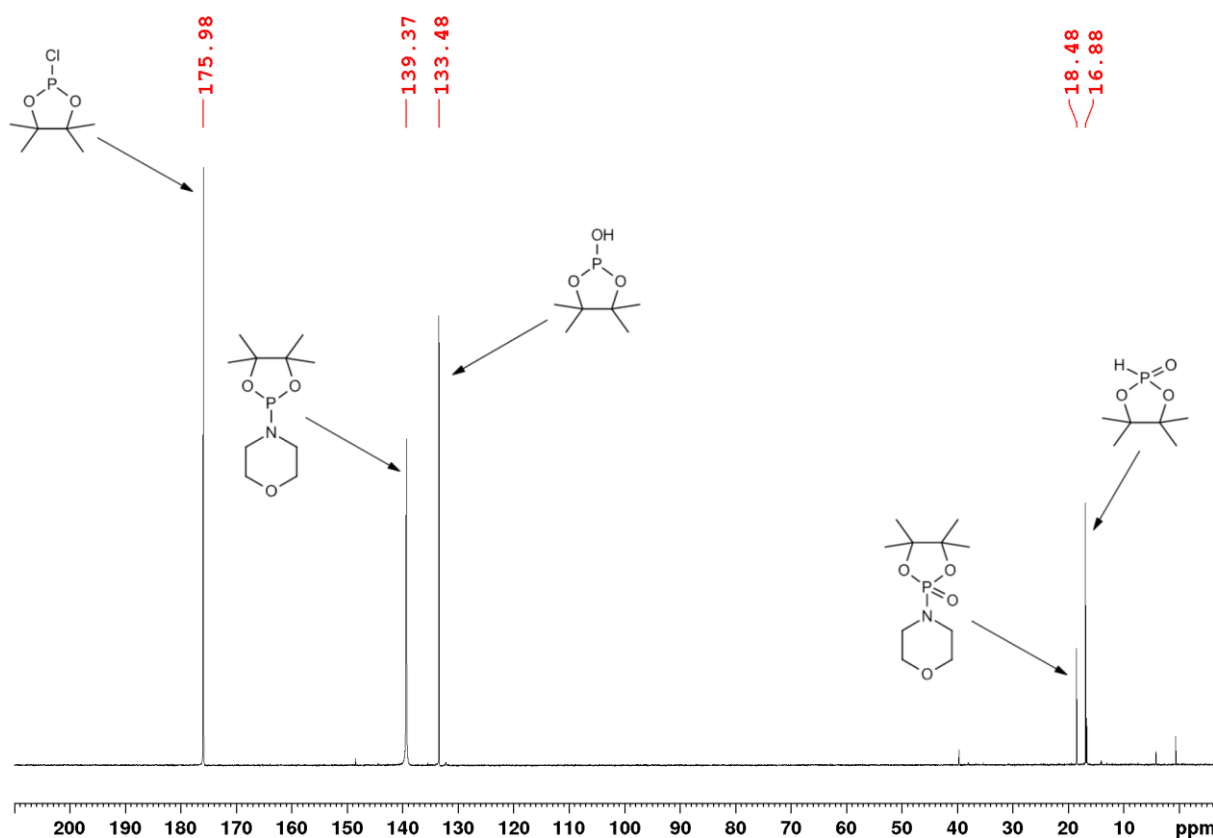


Figure 43: Proton-decoupled ^{31}P -NMR spectrum resulting from the phosphitylation of morpholine **18** with phospholane (TMDP) in deuterated pyridine and the correspondingly formed components. The phosphitylated product **18a** is indicated by the peak at 139.37 ppm and its oxidation product **18a'** appears at 18.48 ppm. Still available starting material (TMDP) is represented by the peak at 175.98 ppm. Further, oxidized TMDP **24** at 16.88 ppm and TMDP-OH at 133.48 ppm arise during the reaction. NMR-solvent: $\text{C}_5\text{D}_5\text{N}$.

According to the literature [21], the peak at 175.98 ppm corresponds to that of the phosphitylation reagent TMDP, which was obviously not completely converted in this reaction. The signal at 139.37 ppm can be assigned to the phosphitylated morpholine **18a**, while the ^{31}P -resonance at 18.48 ppm corresponds to the oxidized derivative **18a'**. Based on the peak at 133.48 ppm, which corresponds to the product of TMDP and water, it is suspected that some water content (possibly moist starting materials) was also present in this reaction. As in the other reactions, the oxidized TMDP **24** appears in the high field at 16.88 ppm, in detail described in chapter 3.5.2.10.

From Figure 43 it is evident that signals from other TMDP components are present in extremely low amounts as well, which made it impossible to elucidate these structures. But the high field shifts would be an indication that these peaks correspond to oxidation products formed during the reaction.

The respective $^1\text{H}/^{31}\text{P}$ -HMBC spectrum is shown in Figure 44, in which the cross-peaks, corresponding to the phosphitylated product, are circled in red.

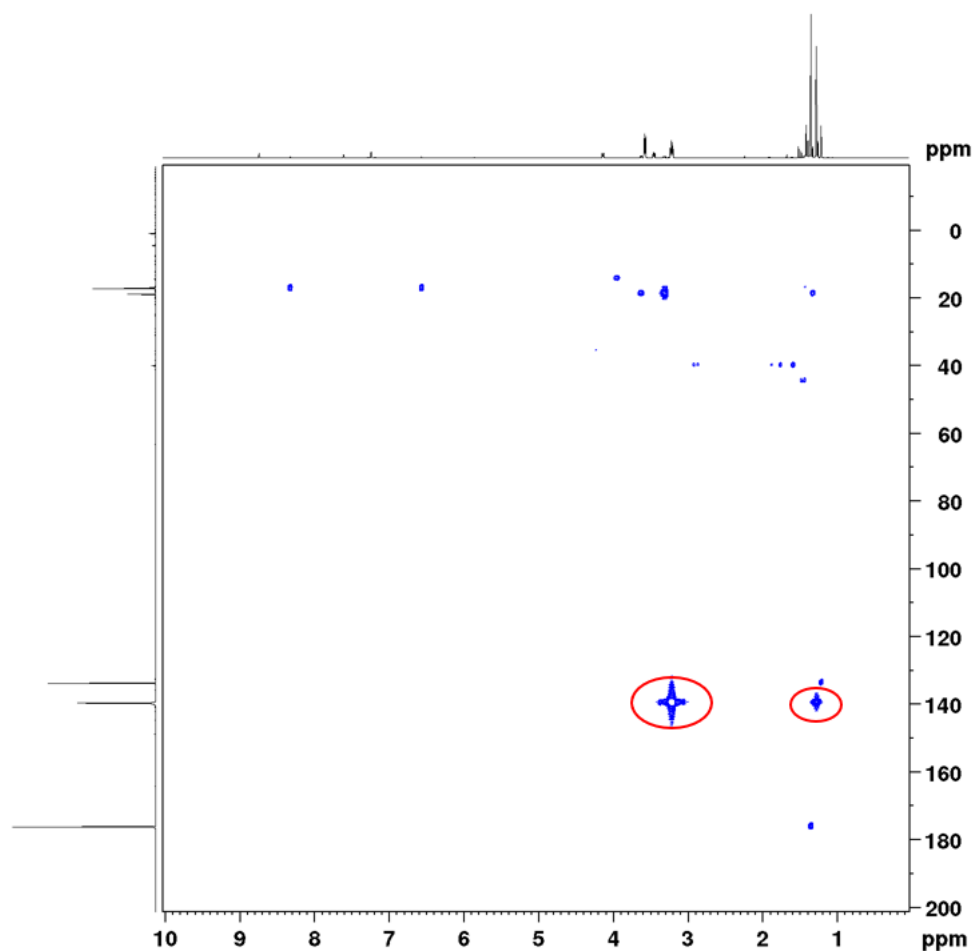


Figure 44: $^1\text{H}/^{31}\text{P}$ -HMBC spectrum resulting from the phosphorylation reaction of morpholine **18** with TMDP. The $^1\text{H}/^{31}\text{P}$ cross-peaks circled in red indicate successful phosphorylation of morpholine. The ^1H -spectrum is plotted on the x-axis and the ^{31}P -spectrum on the y-axis. NMR-solvent: $\text{C}_5\text{D}_5\text{N}$.

3.5.2.7 Ellagic acid

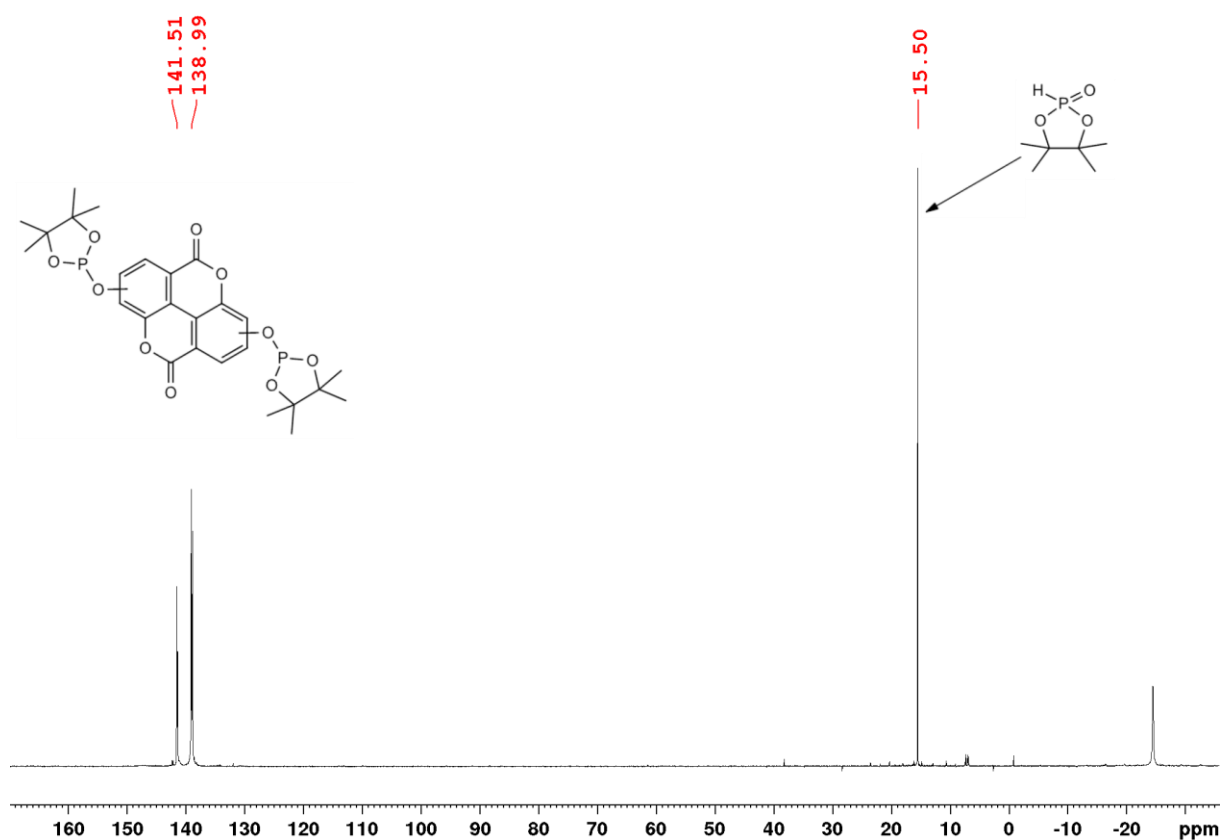


Figure 45: Proton-decoupled ^{31}P -NMR spectrum resulting from the phosphitylation of ellagic acid **20** with phospholane (TMDP) in deuterated pyridine and the correspondingly formed components. The two peaks at 141.51 and 138.99 ppm belong to phosphitylated derivatives of ellagic acid, while the peak at 15.50 ppm corresponds to component **24**, the oxidation product of TMDP. Unfortunately, it has not been confirmed where exactly in the molecule phosphitylation occurred and therefore, the structure has been presented in a more general form. NMR-solvent: $\text{C}_5\text{D}_5\text{N}$.

From the $^1\text{H}/^{31}\text{P}$ -HMBC experiment, shown in Figure 46, it is evident that the ^{31}P -resonances at 141.51 and 138.99 ppm originate from phosphitylated ellagic acid. The coupling of the ^{31}P -resonances to the aromatic proton (≈ 8.14 ppm) of ellagic acid in the ^1H -spectrum could be detected as well as the couplings to the protons of methyl groups of the attached TMDP (refer to the cross-peaks circled in red in Figure 46). However, when analyzing these two phosphitylated products, it was difficult to determine with certainty which hydroxy group was phosphitylated, and whether mono-, di-, tri-, or tetra- phosphitylated components were formed. The multiplicity of both ^{31}P -signals reveals a doublet of doublets. This observation could indicate the P-P-coupling in the molecule, leading to the conjecture that both derivatives are multi-substituted.

The oxidized TMDP **24** appears in the high field at 15.50 ppm is explained in more detail in chapter 3.5.2.10. The emerging peak at about -25 ppm shows hardly any coupling in the $^1\text{H}/^{31}\text{P}$ -HMBC and could therefore not be evaluated. Considering the ^{31}P -shift and the structure of ellagic acid, this peak

could possibly correspond to an attached tetraoxaphosphaspiro[9.9]nonane-group (c.f. chapters 3.5.2.8 and 3.5.2.9).

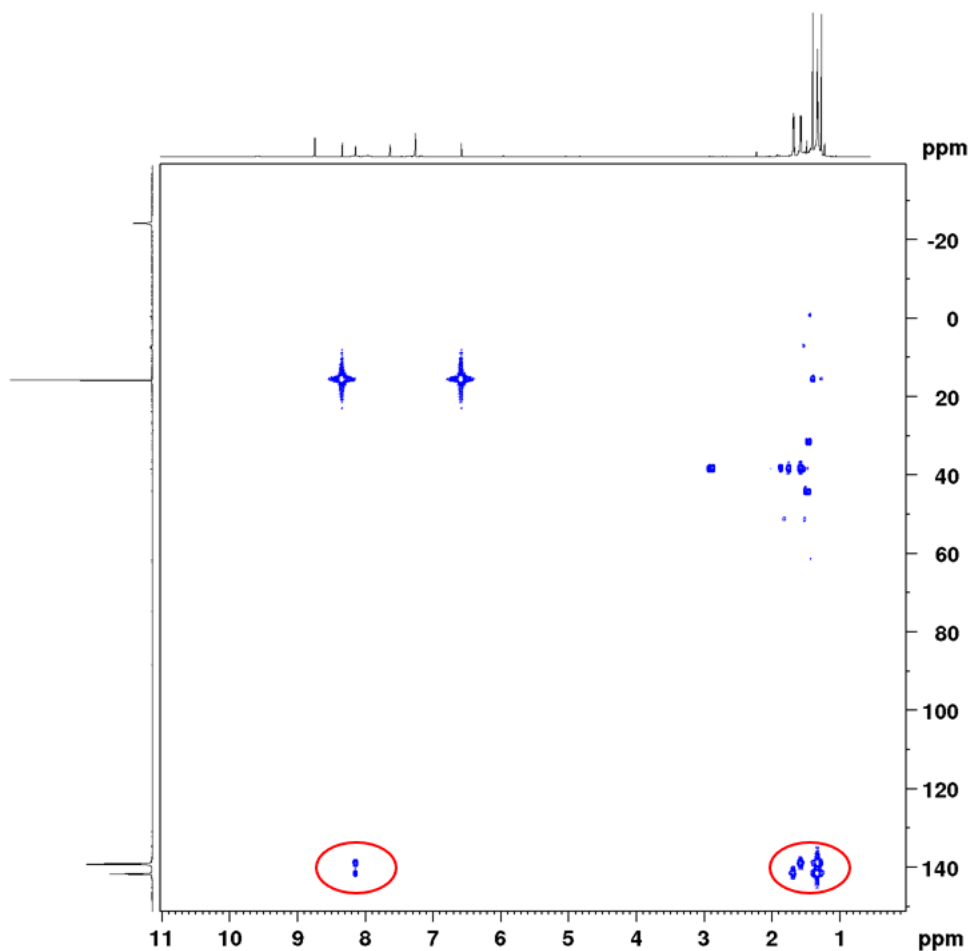
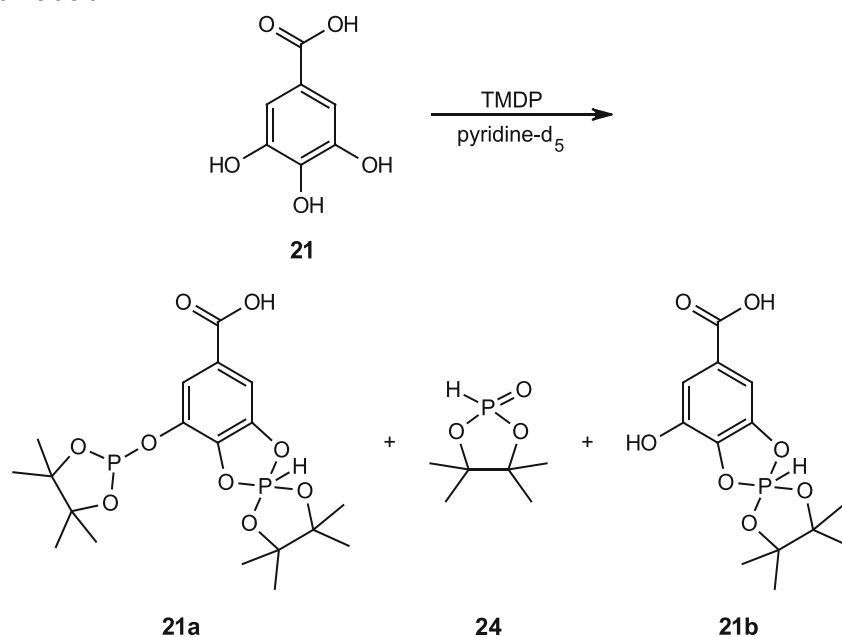


Figure 46: $^1\text{H}/^{31}\text{P}$ -HMBC spectrum resulting from the phosphitylation reaction of ellagic acid **20** with TMDP. The $^1\text{H}/^{31}\text{P}$ cross-peaks circled in red prove successful phosphitylation of ellagic acid. The ^1H -spectrum is plotted on the x-axis and the ^{31}P -spectrum on the y-axis. NMR-solvent: $\text{C}_5\text{D}_5\text{N}$.

3.5.2.8 Gallic acid



Scheme 32: Reaction of gallic acid **21** with TMDP in deuterated pyridine and the corresponding formed phosphitylated derivative **21a**, which is additionally substituted by an oxidized phosphorus group. The oxidized TMDP **24** occurred in this reaction as well as another gallic acid derivative **21b** including an oxidized phosphorus-group.

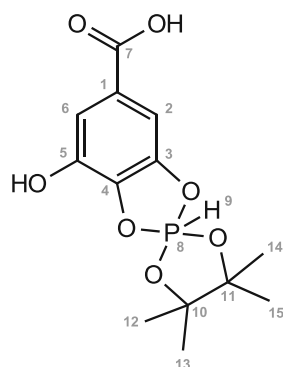
Table 53 shows the respective ^1H -, ^{13}C - and ^{31}P - chemical shifts of the phosphitylated derivative of gallic acid **21a**, which is additionally substituted with a tetraoxaphosphaspiro[9.9]nonane-group. Table 54 contains the respective ^1H -, ^{13}C - and ^{31}P - chemical shifts of the tetraoxaphosphaspiro[9.9]nonane-derivative of gallic acid **21b**, while the corresponding proton-decoupled ^{31}P spectrum is given below in Figure 47.

Table 53: ^1H -, ^{13}C - and ^{31}P -shifts of the phosphitylated and additionally oxidized-phosphorus-substituted gallic acid **21a** resulting from the reaction of gallic acid **21** and TMDP in $\text{C}_5\text{D}_5\text{N}$. (NMR-solvent: $\text{C}_5\text{D}_5\text{N}$).

21a

Atom number	^1H		^{13}C		^{31}P	
	δ (ppm)	J^{HH} (Hz)	δ (ppm)	J^{CP} (Hz)	δ (ppm)	J^{HP} (Hz)
1			125.00			
2	8.08 (m)		119.32 (d)	9.7		
3			136.90 (d)	4.2		
4			142.67 (d)			
5			145.53			
6	7.91 (br. s)		109.20 (d)	13.5		
7			168.90			
8					141.17	
9, 10			86.92 (t)	7.2		
11, 13	1.24 (s)		24.37			
12, 14	1.47 (s)		25.66 (d)	6.9		
15					-24.70	874
16	9.31/7.13 (d)					874
17, 18			81.74			
19, 21	1.24		24.37			
20, 22	1.24		24.37			

Table 54: ^1H -, ^{13}C - and ^{31}P -shifts of the oxidized phosphorus derivative of gallic acid **21b** resulting from the reaction of gallic acid **21** and TMDP in $\text{C}_5\text{D}_5\text{N}$. (NMR-solvent: $\text{C}_5\text{D}_5\text{N}$).



21b

Atom number	^1H		^{13}C		^{31}P	
	δ (ppm)	J^{HH} (Hz)	δ (ppm)	J^{CP} (Hz)	δ (ppm)	J^{HP} (Hz)
1			125.78			
2	7.78 (m)		104.93 (d)	13.0		
3			145.98 (d)	1.5		
4			138.33 (d)	2.2		
5			143.82 (d)	12.4		
6	8.14 (d)	1.6	114.98			
7			169.59			
8					-25.85 (d)	862
9	9.29/7.14 (d)					862
10, 11			82.02			
12, 14	1.23 (m)		24.35			
13, 15	1.23 (m)		24.35			

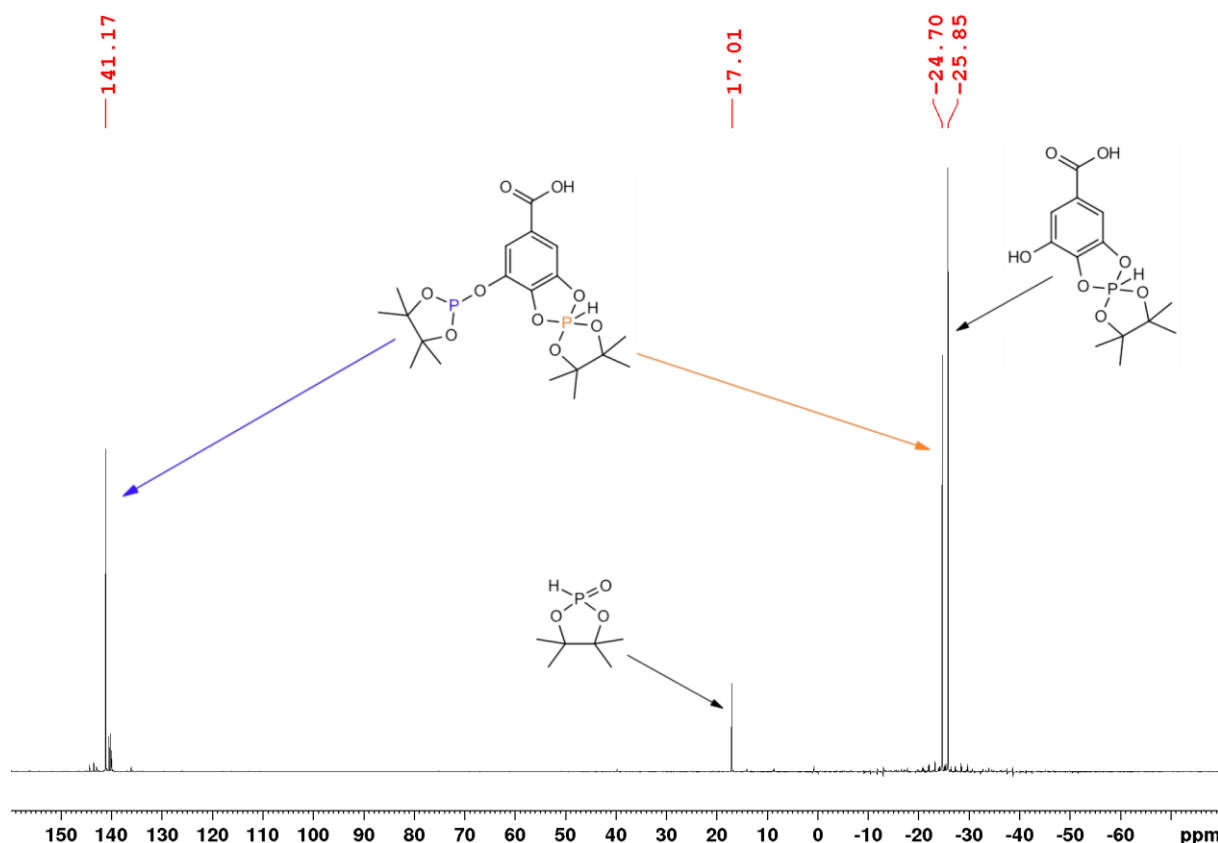


Figure 47: Proton-decoupled ^{31}P -NMR spectrum resulting from the phosphitylation of gallic acid **21** with phospholane (TMDP) in deuterated pyridine and the correspondingly formed components. The phosphitylated product **21a** is indicated by the peak at 141.17 ppm and the peak at -24.70 ppm, which represents an attached tetraoxaphosphaspiroonane-group, belongs to the same product. Oxidized TMDP **24** appears at 17.01 ppm and another oxidized phosphorus derivative of gallic acid **21b** is represented by the resonance at -25.85 ppm. NMR-solvent: $\text{C}_5\text{D}_5\text{N}$.

As shown in Figure 47, the reaction of gallic acid with TMDP resulted in a product involving two phosphorus atoms, appearing at entirely different ^{31}P -chemical shifts (141.17 and -24.70 ppm). Gallic acid is provided with three hydroxy groups and obviously, successful phosphitylation took place at one of the three groups. A reaction of the other two hydroxy groups with oxidized TMDP was apparently responsible for the formation of a tetraoxaphosphaspiroonane-group under ring closure. In addition, an oxidized derivative of gallic acid at -25.85 ppm was formed with the reaction of oxidized TMDP. In this reaction, two hydroxy groups were involved, resulting again in a ring closure and the formation of a tetraoxaphosphaspiroonane-group. The arrangement of the hydroxy groups obviously favors this type of reaction with oxidized TMDP.

The cross-peaks of the ^{31}P -resonance at 141.17 ppm (circled in red) in the $^1\text{H}/^{31}\text{P}$ -HMBC spectrum (Figure 48) prove the formation of a phosphitylated derivative.

In the $^1\text{H}/^{31}\text{P}$ -HMBC spectrum, it is evident that the two different ^{31}P -atoms (141.17 and -24.70 ppm) display couplings to the same aromatic protons (red circled cross-peaks in the aromatic ppm-range). This observation led to the conclusion that only one compound with different ^{31}P -atoms is included.

The occurrence of a ring closure with the two hydroxy groups and the formation of the tetraoxaphosphaspiroonane-group could be determined based on the H-P coupling constant. Strong cross-peaks from the ^{31}P -atom in the high field (-24.70 ppm) to proton signals at δ_{H} 9.29 + 7.14 were detected, indicated by the orange arrowed cross-peaks. In the ^1H spectrum, the corresponding resonances were separated by 874 Hz and the respective ^{31}P -atom at -24.70 ppm also showed the same signal splitting of 874 Hz in the proton-coupled ^{31}P -spectrum. This revealed the presence of a proton directly bound to a phosphorous atom with a coupling constant of $^1J(\text{CP}) = 874$ Hz. According to the literature [26], this coupling constant corresponds approximately to the characteristic H-P coupling in a tetraoxaphosphaspiroonane-group.

The other ^{31}P -atom (-25.85 ppm) from the oxidized phosphorus gallic acid derivative, appearing as a doublet in the proton-coupled ^{31}P -spectrum, also shows cross-peaks to a ^1H -doublet, both featuring a H-P coupling constant of 862 Hz. Thus, the reaction with oxidized TMDP was also concluded here. The visible cross-peaks of the two ^{31}P -resonances (-24.70 and -25.85 ppm) to the protons of the methyl groups were decisive for the conclusion that the tetraoxaphosphaspiroonane-group is tetramethylated and originates from the reaction with TMDP.

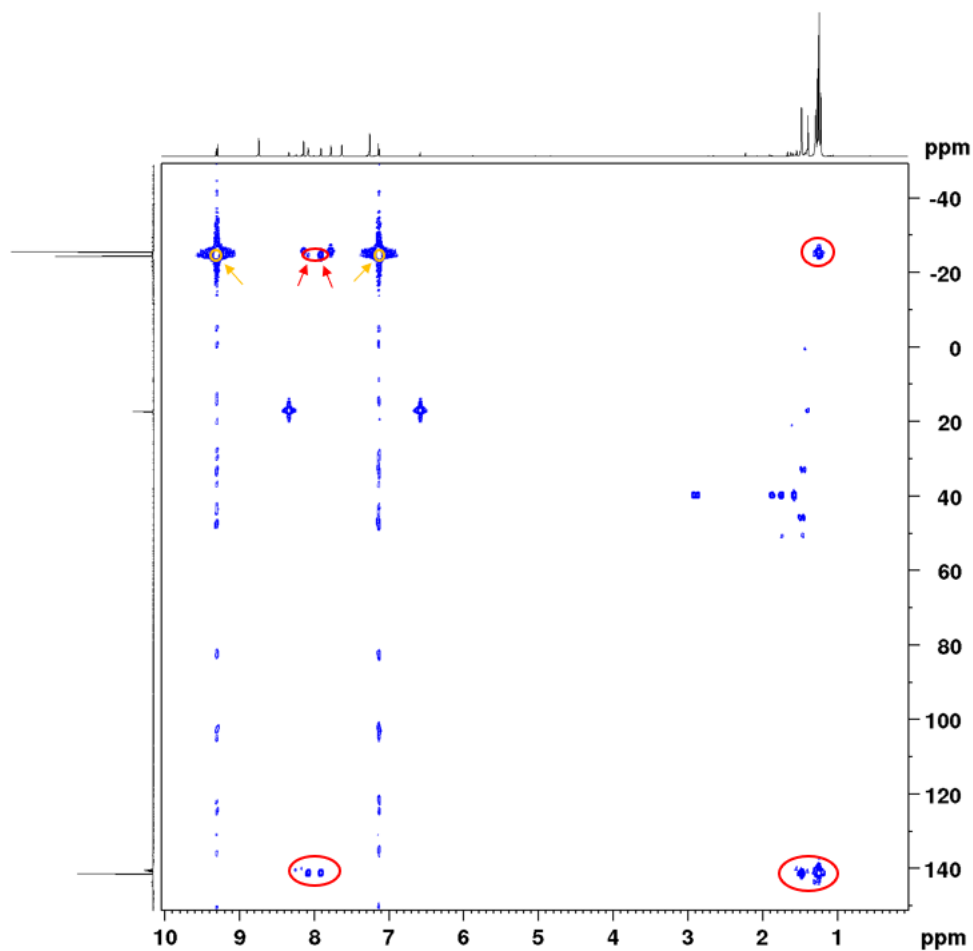
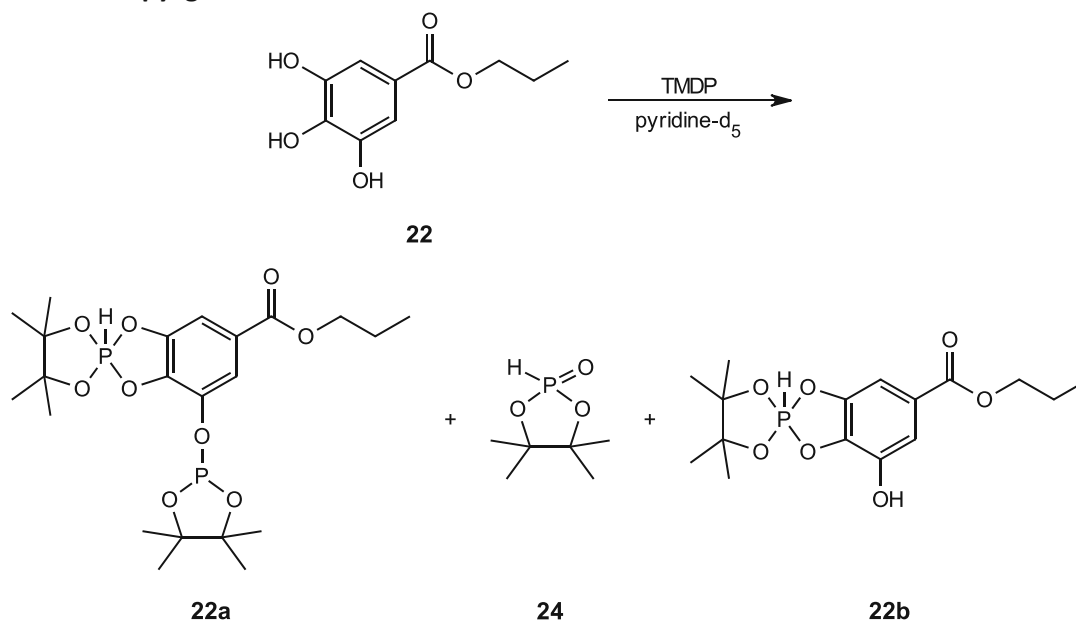


Figure 48: $^1\text{H}/^{31}\text{P}$ -HMBC spectrum resulting from the phosphitylation reaction of gallic acid **21** with TMDP. The $^1\text{H}/^{31}\text{P}$ cross-peaks circled in red indicate successful phosphitylation of gallic acid. The orange circled cross-peaks indicate the H-P-coupling in the attached oxidized phosphorus group. The ^1H -spectrum is plotted on the x-axis and the ^{31}P -spectrum on the y-axis. NMR-solvent: $\text{C}_5\text{D}_5\text{N}$.

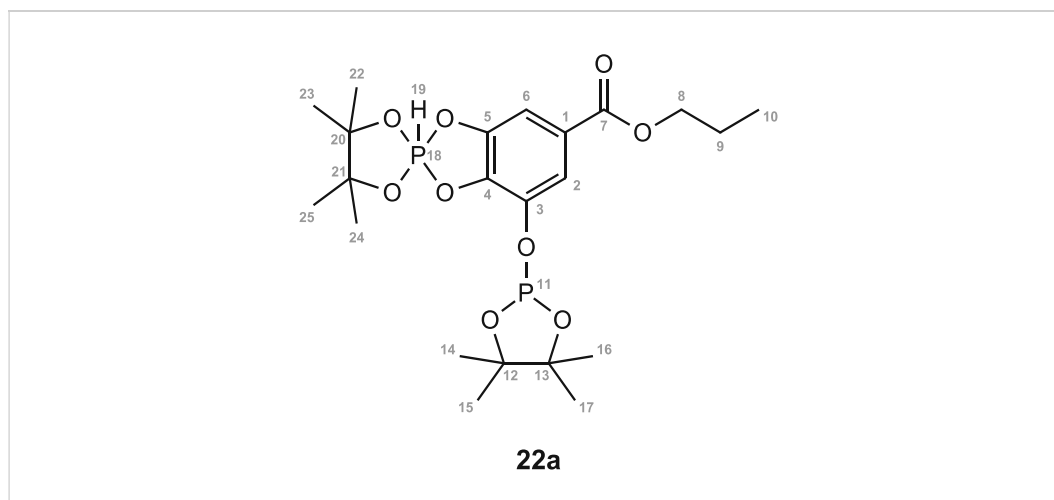
3.5.2.9 Propyl gallate



Scheme 33: Reaction of propyl gallate **22** with TMDP in deuterated pyridine and the corresponding formed phosphitylated derivative **22a**, which is additionally substituted by an oxidized phosphorus group. The oxidized TMDP **24** occurred in this reaction as well as another propyl gallate derivative **22b** including an oxidized phosphorus-group.

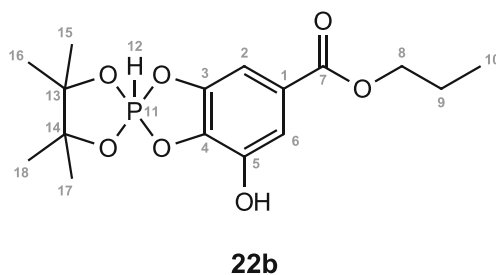
Table 55 shows the respective ^1H -, ^{13}C - and ^{31}P - chemical shifts of the phosphitylated derivative of propyl gallate **22a**, which is additionally substituted with a tetraoxaphosphaspiro[9.9]nonane-group. Table 56 contains the respective ^1H -, ^{13}C - and ^{31}P - chemical shifts of the oxidized derivative of propyl gallate **22b**, while the corresponding ^{31}P spectrum is given in Figure 49.

Table 55: ^1H -, ^{13}C - and ^{31}P -shifts of the phosphitylated and additionally oxidized-phosphorus-substituted propyl gallate **22a** resulting from the reaction of propyl gallate **22** and TMDP in $\text{C}_5\text{D}_5\text{N}$. (NMR-solvent: $\text{C}_5\text{D}_5\text{N}$).



Atom number	^1H		^{13}C		^{31}P	
	δ (ppm)	J^{HH} (Hz)	δ (ppm)	J^{CP} (Hz)	δ (ppm)	J^{HP} (Hz)
1			123.11			
2	7.87 (d)	1.6	119.08 (d)	9.5		
3			145.41 (d)			
4			143.12 (d)			
5			136.91 (m)			
6	7.68 (br. s)		108.78 (d)	13.6		
7			166.38			
8	4.23 (m)		67.21			
9	1.62 (m)		22.95			
10	0.86 (m)		11.13			
11					139.89	
12, 13			86.89			
14, 16	1.47 (br. s)		25.58 (d)	6.6		
15, 17	1.23 (m)		25.94			
18					-25.95 (d)	876
19	9.32/7.13 (d)					876
20, 21			81.71			
22, 24	1.25 (m)		25.94			
23, 25	1.25 (m)		25.94			

Table 56: ^1H -, ^{13}C - and ^{31}P -shifts of the oxidized phosphorus derivative of propyl gallate **22b** resulting from the reaction of propyl gallate **22** and TMDP in $\text{C}_5\text{D}_5\text{N}$. (NMR-solvent: $\text{C}_5\text{D}_5\text{N}$).



Atom number	^1H		^{13}C		^{31}P	
	δ (ppm)	J^{HH} (Hz)	δ (ppm)	J^{CP} (Hz)	δ (ppm)	J^{HP} (Hz)
1			124.02			
2	7.56 (m)		104.51			
3			145.82 (d)	2.2		
4			138.74 (d)	2.2		
5			143.87			
6	7.92 (d)	1.7	114.71			
7			167.08			
8	4.23 (m)		66.96			
9	1.62 (m)		22.98			
10	0.86 (m)		11.19			
11					-27.16 (d)	864
12	9.27/7.14 (d)					864
13, 14			83.30			
15, 17	1.24		24.20			
16, 18	1.24		24.20			

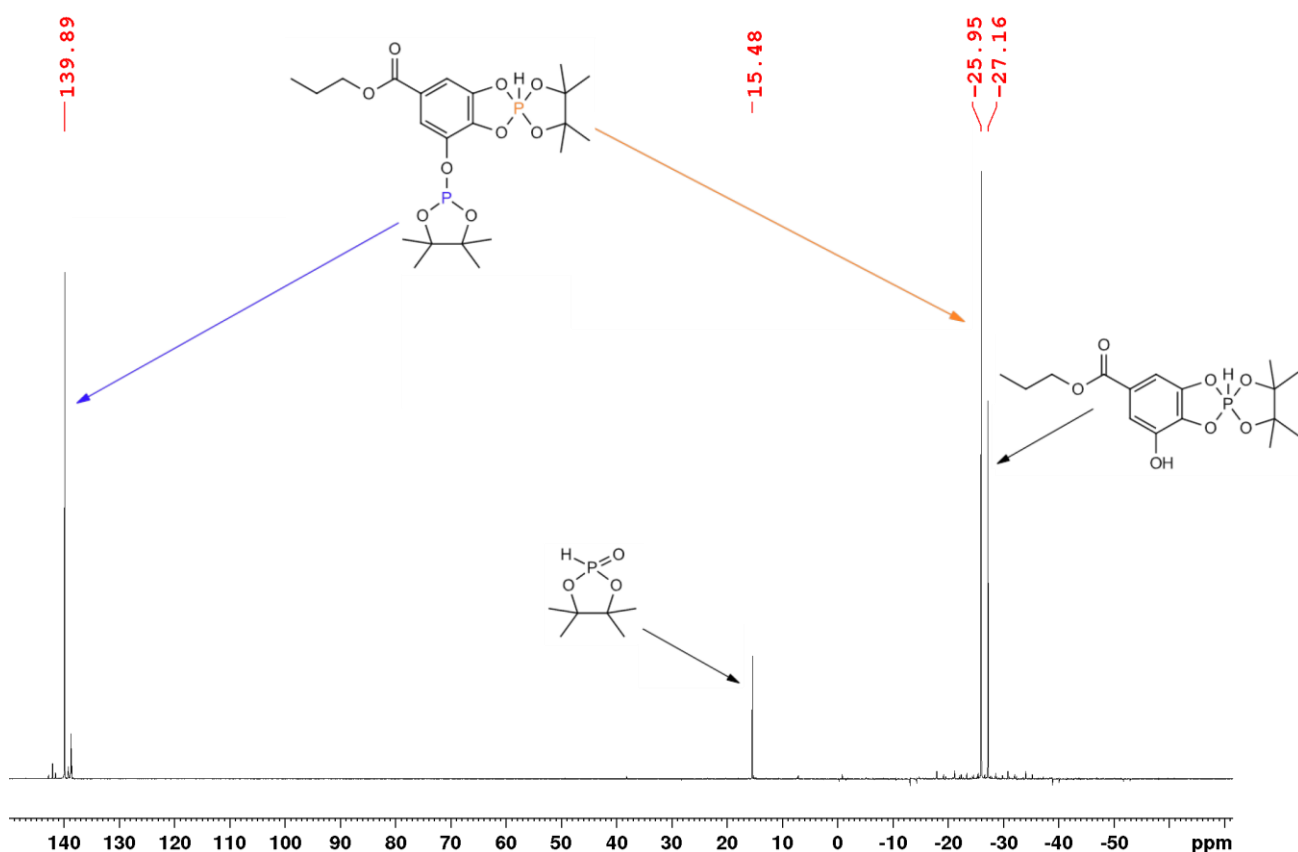


Figure 49: Proton-decoupled ^{31}P -NMR spectrum resulting from the phosphitylation of propyl gallate **22** with phospholane (TMDP) in deuterated pyridine and the correspondingly formed components. The phosphitylated product **22a** is indicated by the peak at 139.89 ppm and the peak at -25.95 ppm, which represents an attached tetraoxaphosphaspiro[9.9]nonane-group, belongs to the same product. Oxidized TMDP **24** appears at 15.48 ppm and another oxidized phosphorus derivative of propyl gallate **22b** is represented by the resonance at -27.16 ppm. NMR-solvent: $\text{C}_5\text{D}_5\text{N}$.

The reaction of propyl gallate with TMDP can be regarded as analogous to the reaction of gallic acid with TMDP, therefore reference can be made to chapter 3.5.2.8 for a more detailed description.

In the $^1\text{H}/^{31}\text{P}$ -HMBC spectrum shown in Figure 50, the key cross-peaks confirming successful phosphitylation of propyl gallate are marked with red circles. It can be observed in the spectrum that both ^{31}P -signals at 139.89 ppm and at the high field at -25.95 ppm couple with the same aromatic protons, decisive for the conclusion that it involves a single component with two different ^{31}P -atoms. The cross-peaks marked in orange indicate the characteristic H-P-coupling ($^1J(\text{HP}) = 864 \text{ Hz}$) in the tetraoxaphosphaspiro[9.9]nonane-group.

Apparently, the three adjacent hydroxy groups in both model compounds gallic acid **21** and propyl gallate **22** initiate this unusual reaction with oxidized TMDP.

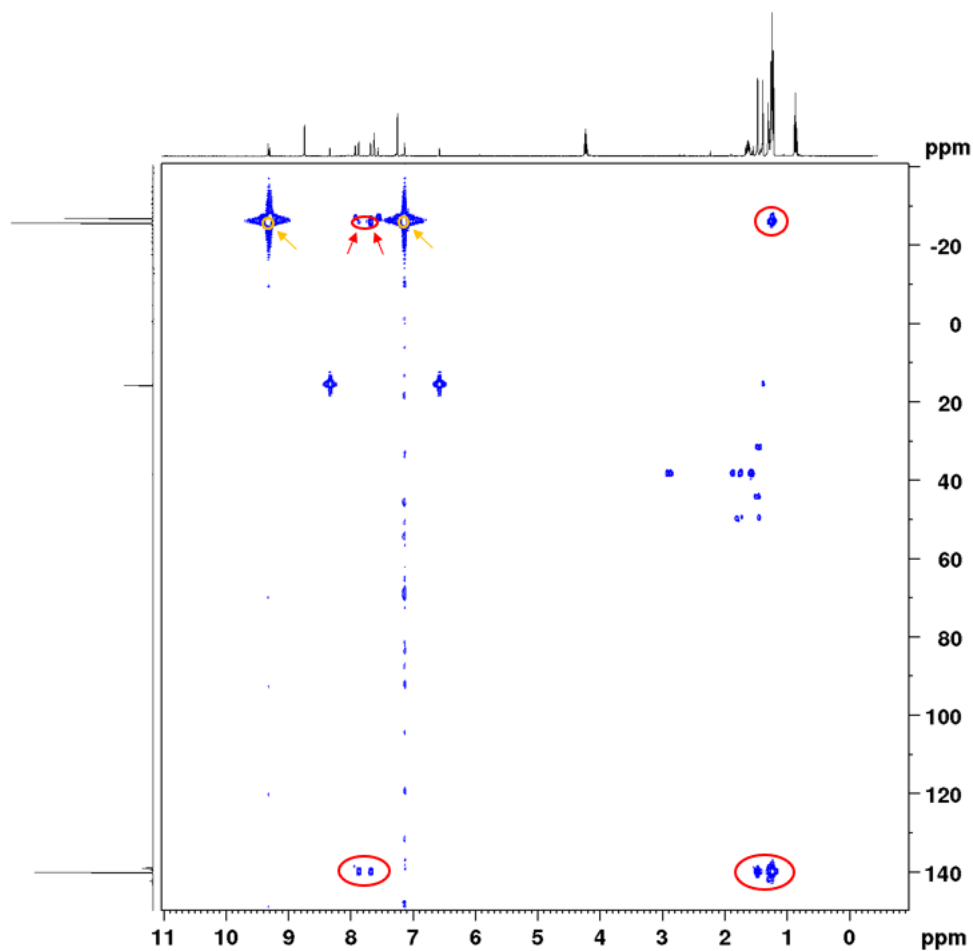


Figure 50: $^1\text{H}/^{31}\text{P}$ -HMBC spectrum resulting from the phosphitylation reaction of propyl gallate **22** with TMDP. The $^1\text{H}/^{31}\text{P}$ cross-peaks circled in red indicate successful phosphitylation of propyl gallate. The orange circled cross-peaks indicate the H-P-coupling in the attached oxidized phosphorus group. The ^1H -spectrum is plotted on the x-axis and the ^{31}P -spectrum on the y-axis. NMR-solvent: $\text{C}_5\text{D}_5\text{N}$.

3.5.2.10 4,4,5,5-Tetramethyl-1,3,2λ⁵-dioxaphospholan-2-one

As shown in the previous chapters, each phosphorylation reaction resulted in the oxidation product of TMDP, 4,4,5,5-Tetramethyl-1,3,2λ⁵-dioxaphospholan-2-one **24**, which appears at a ³¹P chemical shift of approximately 15-17 ppm. Since this component is present in every reaction, the coupling between the NMR active atoms ¹H and ³¹P is explained in more detail based on the ¹H/³¹P-HMBC spectrum. Figure 52 illustrates the coupling between the H atom (orange) and the P-atom (blue) of 4,4,5,5-tetramethyl-1,3,2λ⁵-dioxaphospholan-2-one (Figure 51), with a characteristic coupling constant of ¹J = 704 Hz. In the non-proton-decoupled ³¹P-spectrum, this ³¹P-peak also represents a doublet with the same coupling constant of 704 Hz.

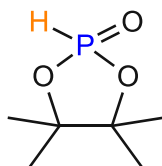


Figure 51: Structure of 4,4,5,5-Tetramethyl-1,3,2λ⁵-dioxaphospholan-2-one **24**.

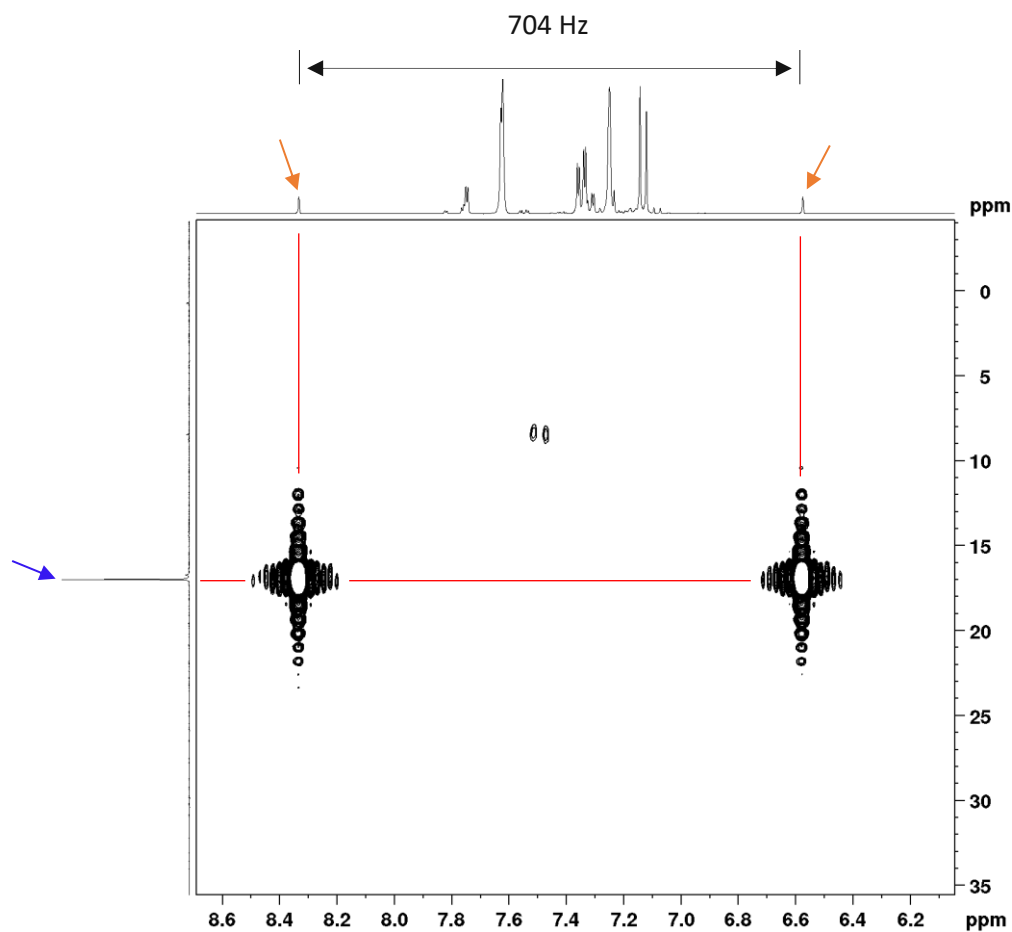


Figure 52: Cross-peaks in the $^1\text{H}/^{31}\text{P}$ -HMBC-spectrum, which confirms the coupling between the H-atom and the P-atom in component **24**. On the x-axis, the ^1H -NMR, and on the y-axis, the proton-decoupled ^{31}P -NMR is plotted. The orange arrows indicate the ^1H peaks (doublet with a coupling of 704 Hz) and the blue arrow points to the ^{31}P resonance. This spectrum originates from the phosphitylation of 2,5-DHAP but is intended only as an example to illustrate since compound **24** also occurs in all other reactions.

Table 57 lists the corresponding ^1H -, ^{13}C - and ^{31}P - chemical shifts of component **24**.

Table 57: ^1H -, ^{13}C - and ^{31}P -shifts of the oxidation product of TMDP, 4,4,5,5-Tetramethyl-1,3,2 λ^5 -dioxaphospholan-2-one **24** resulting from the phosphorylation reaction of 2,5-DHAP in $\text{C}_5\text{D}_5\text{N}$. (NMR-solvent: $\text{C}_5\text{D}_5\text{N}$).

24

Atom number	^1H		^{13}C	^{31}P	
	δ (ppm)	J^{HP} (Hz)	δ (ppm)	δ (ppm)	J^{HP} (Hz)
1				17.00 (d)	704
2, 3			89.50		
4, 6	1.38		25.20		
5, 7	1.25		24.31		
8	8.33/6.57 (d)	704			

3.6 NMR-Measurements - Phosphitylation

The NMR shifts of the resulting derivatives from phosphitylation are listed below. Only those chemical shifts that were unequivocally assigned in the spectra are included in the NMR data. The number of C-atoms was only explicitly stated in the NMR code if more than one C-atom was involved.

3.6.1 2,5-Dihydroxyacetophenone

14b

¹H-NMR (400 MHz, C₅D₅N): δ [ppm] 1.27 (s, 3H), 1.49 (s, 3H), 2.55 (s, 3H), 7.13 (d, *J* = 8.9 Hz, 1H), 7.35 (dd, *J* = 8.9, 2.8 Hz, 1H), 7.63 (d, *J* = 2.8 Hz, 1H).

¹³C-NMR (101 MHz, C₅D₅N): δ [ppm] 26.01 (q), 25.62 (q), 27.97 (q), 86.66 (s) (d, *J*_{CP} = 7.8 Hz), 120.17 (d), 121.51 (s), 123.05 (d) (d, *J*_{CP} = 7.7 Hz), 130.43 (d) (d, *J*_{CP} = 7.7 Hz), 144.64 (s) (d, *J*_{CP} = 8.0 Hz), 159.29 (s), 204.65 (s).

³¹P-NMR (162 MHz, C₅D₅N) δ [ppm] 140.64.

14c

¹H-NMR (400 MHz, C₅D₅N): δ [ppm] 1.25 (12H), 1.43 (12H), 2.69 (s, 3H), 7.24 (d, 1H), 7.32 (dd, *J* = 8.7, 2.9 Hz, 1H), 7.75 (d, *J* = 2.9 Hz, 1H).

¹³C-NMR (101 MHz, C₅D₅N): δ [ppm] 25.56 (q, 4C), 25.96 (q, 4C), 32.49 (q), 86.76^a (s), 86.99^a (s), 122.60 (d) (d, *J*_{CP} = 8.8 Hz), 123.73 (d) (d), 126.50 (d) (d, *J*_{CP} = 7.7 Hz), 133.23 (s) (d, *J*_{CP} = 1.5 Hz), 148.40 (s) (d, *J*_{CP} = 8.1 Hz), 149.06 (s) (d, *J*_{CP} = 8.1 Hz), 198.45 (s).
^a... exchangeable

³¹P-NMR (162 MHz, C₅D₅N) δ [ppm] 140.01*, 140.09*.
*... exchangeable

3.6.2 2,6-Dihydroxyacetophenone

15a

¹H-NMR (400 MHz, C₅D₅N):	δ [ppm] 1.23 (s, 12H), 1.41 (s, 12H), 2.59 (s, 3H), 7.05 (d, <i>J</i> = 8.2 Hz, 2H), 7.30 (t, <i>J</i> = 8.2 Hz, 1H).
¹³C-NMR (101 MHz, C₅D₅N):	δ [ppm] 25.45 (q, 4C), 25.96 (q, 4C), 33.49 (q), 86.93 (s, 2C) (d, <i>J</i> _{CP} = 7.4 Hz), 116.93 (d, 2C) (d, <i>J</i> _{CP} = 14.2 Hz), 129.17 (s) (t, <i>J</i> _{CP} = 2.0 Hz), 131.47 (d), 164.44 (s, 2C), 200.76 (s).
³¹P-NMR (162 MHz, C₅D₅N)	δ [ppm] 139.73.

15b

¹H-NMR (400 MHz, C₅D₅N):	δ [ppm] 1.27 (s, 6H), 1.43 (s, 6H), 2.72 (s, 3H), 6.76 (dd, <i>J</i> = 8.1 Hz, 1H), 7.03 (1H), 7.34 (t, <i>J</i> = 8.1 Hz, 1H).
¹³C-NMR (101 MHz, C₅D₅N):	δ [ppm] 25.45 (q, 2C), 25.92 (q, 2C), 34.10 (q), 86.95 (s, 2C) (d, <i>J</i> _{CP} = 7.4 Hz), 111.75 (d), 114.07 (d), 117.64 (s), 134.81 (d), 153.25 (s), 162.80 (s), 204.55 (s).
³¹P-NMR (162 MHz, C₅D₅N)	δ [ppm] 138.51.

3.6.3 Morpholine

18a

¹H-NMR (400 MHz, C₅D₅N): δ [ppm] 1.28 (s, 12H), 3.21 (m, 4H), 3.57 (m, 4H).

¹³C-NMR (101 MHz, C₅D₅N): δ [ppm] 25.68 (q, 4C), 44.72 (t, 2C) (d, J_{CP} = 18.0 Hz), 68.78 (t, 2C) (d, J_{CP} = 4.8 Hz), 81.87 (s, 2C) (d, J_{CP} = 5.1 Hz).

³¹P-NMR (162 MHz, C₅D₅N) δ [ppm] 139.37.

18a'

¹H-NMR (400 MHz, C₅D₅N): δ [ppm] 1.32 (s, 12H), 3.31 (m, 4H), 3.62 (m, 4H).

¹³C-NMR (101 MHz, C₅D₅N): δ [ppm] 25.30 (q, 4C), 45.79 (t, 2C) (d, J_{CP} = 2.0 Hz), 67.71 (t, 2C) (d, J_{CP} = 5.2 Hz), 87.12 (s, 2C).

³¹P-NMR (162 MHz, C₅D₅N) δ [ppm] 18.48.

3.6.4 Gallic acid

21a

¹H-NMR (400 MHz, C₅D₅N): δ [ppm] 1.24 (12H), 1.24 (s, 6H), 1.47 (s, 6H), 7.91 (br. s, 1H), 8.08 (m, 1H) 8.22 (d, J_{HP} = 874 Hz, 1H).

¹³C-NMR (101 MHz, C₅D₅N): δ [ppm] 24.37 (q, 6C), 25.66 (q, 2C) (d, J_{CP} = 6.9 Hz), 81.74 (s, 2C), 86.92 (s, 2C) (t, J_{CP} = 7.2 Hz), 109.20 (d) (d, J_{CP} = 13.5 Hz), 119.32 (d) (d, J_{CP} = 9.7 Hz), 125.00 (s), 136.90 (s) (d, J_{CP} = 4.2 Hz), 142.67 (s), 145.53 (s), 168.90 (s).

³¹P-NMR (162 MHz, C₅D₅N) δ [ppm] 141.17, -24.70 (d, J_{HP} = 874 Hz).

21b

¹H-NMR (400 MHz, C₅D₅N): δ [ppm] 1.23 (m, 12H), 7.78 (m, 1H), 8.14 (d, J = 1.6 Hz, 1H), 8.23 (d, J_{HP} = 862 Hz, 1H).

¹³C-NMR (101 MHz, C₅D₅N): δ [ppm] 24.35 (q, 4C), 82.02 (s, 2C), 104.93 (d) (d, J_{CP} = 13.0 Hz), 114.98 (d), 125.78 (s), 138.33 (s) (d, J_{CP} = 2.2 Hz), 143.82 (s) (d, J_{CP} = 12.4 Hz), 145.98 (s) (d, J_{CP} = 1.5 Hz), 169.59 (s).

³¹P-NMR (162 MHz, C₅D₅N) δ [ppm] -25.85 (d, J_{HP} = 862 Hz).

3.6.5 Propyl gallate

22a

¹H-NMR (400 MHz, C₅D₅N): δ [ppm] 0.86 (m, 3H), 1.23 (m, 6H), 1.25 (m, 12H), 1.47 (br. s, 6H), 1.62 (m, 2H), 4.23 (m, 2H), 7.68 (br. s, 1H), 7.87 (d, *J* = 1.6 Hz, 1H), 8.23 (d, *J*_{HP} = 876 Hz, 1H).

¹³C-NMR (101 MHz, C₅D₅N): δ [ppm] 11.13 (q), 22.95 (t), 25.58 (q) (d, *J*_{CP} = 6.6 Hz, 2C), 25.94 (q, 6C), 67.21 (t), 81.71 (s, 2C), 86.89 (s, 2C), 108.78 (d) (d, *J*_{CP} = 13.6 Hz), 119.08 (d) (d, *J*_{CP} = 9.5 Hz), 123.11 (s), 136.91 (s), 143.12 (s), 145.41 (s), 166.38 (s).

³¹P-NMR (162 MHz, C₅D₅N) δ [ppm] -25.95 (d, *J*_{HP} = 876 Hz).

22b

¹H-NMR (400 MHz, C₅D₅N): δ [ppm] 0.86 (m, 3H), 1.24 (12H), 1.62 (m, 2H), 4.23 (m, 2H), 7.56 (m, 1H), 7.92 (d, *J* = 1.7 Hz, 1H), 8.21 (d, *J*_{HP} = 864 Hz, 1H).

¹³C-NMR (101 MHz, C₅D₅N): δ [ppm] 11.19 (q), 22.98 (t), 24.20 (q, 4C), 66.96 (t), 83.30 (s, 2C), 104.51 (d), 114.71 (d), 124.02 (s), 138.74 (s) (d, *J*_{CP} = 2.2 Hz), 143.87 (s), 145.82 (s) (d, *J*_{CP} = 2.2 Hz), 167.08 (s).

³¹P-NMR (162 MHz, C₅D₅N) δ [ppm] -27.16 (d, *J*_{HP} = 864 Hz).

3.6.6 4,4,5,5-Tetramethyl-1,3,2λ⁵-dioxaphospholan-2-one**24**

¹H-NMR (400 MHz, C₅D₅N): δ [ppm] 1.25 (6H), 1.38 (6H), 7.45 (d, *J*_{HP} = 704 Hz, 1H).

¹³C-NMR (101 MHz, C₅D₅N): δ [ppm] 24.31 (q, 2C), 25.20 (q, 2C), 89.50 (s, 2C).

³¹P-NMR (162 MHz, C₅D₅N) δ [ppm] 17.00 (d, *J*_{HP} = 704 Hz).

4 CONCLUSION AND OUTLOOK

4.1 Derivatization Method I – Iodination

Within this thesis, derivatization reactions with an iodination reagent (PyI₂) were carried out with 14 different model compounds (*c.f.* Figure 1). According to the protocol [20], all those compounds possessing a hydroxylated aromatic structure should undergo iodination at the *ortho*-position (if unsubstituted, otherwise also at the *para*-position).

Table 58 lists the fourteen model compounds selected for iodination and the corresponding result of whether iodination at the *ortho*-position was successful (+) or not (-).

Table 58: Model compounds selected for iodination and the associated result whether iodination has occurred (+) in the *ortho*-position or has not (-).

	Model compound	Hydroxylated	<i>Ortho</i> -iodination
1	Methyl isoeugenol	-	-
2	Isoeugenol	+	+
3	Vanillin	+	+
4	Vanillyl alcohol	+	+
5	Veratraldehyde	-	-
6	Veratryl alcohol	-	-
7	Veratric acid	-	-
8	<i>p</i> -cresol	+	+
9	Coniferyl alcohol	+	+
10	Veratrylglycerol- β -guaiacyl ether	-	-
11	Guaiacylglycerol- β -guaiacyl ether	+	-
12	2,5-Dihydroxy-1,4-benzoquinone	+	-
13	5,8-Dihydroxy-1,4-naphthoquinone	+	-
14	2,5-Dihydroxyacetophenone	+	-

As shown in Table 58, five of the investigated model compounds (isoeugenol **2**, vanillin **3**, vanillyl alcohol **4**, *p*-cresol **8**, coniferyl alcohol **9**) have undergone a successful iodination reaction within the derivatization reaction with PyI₂, resulting in an *ortho*-iodinated product, depicted in Figure 53.

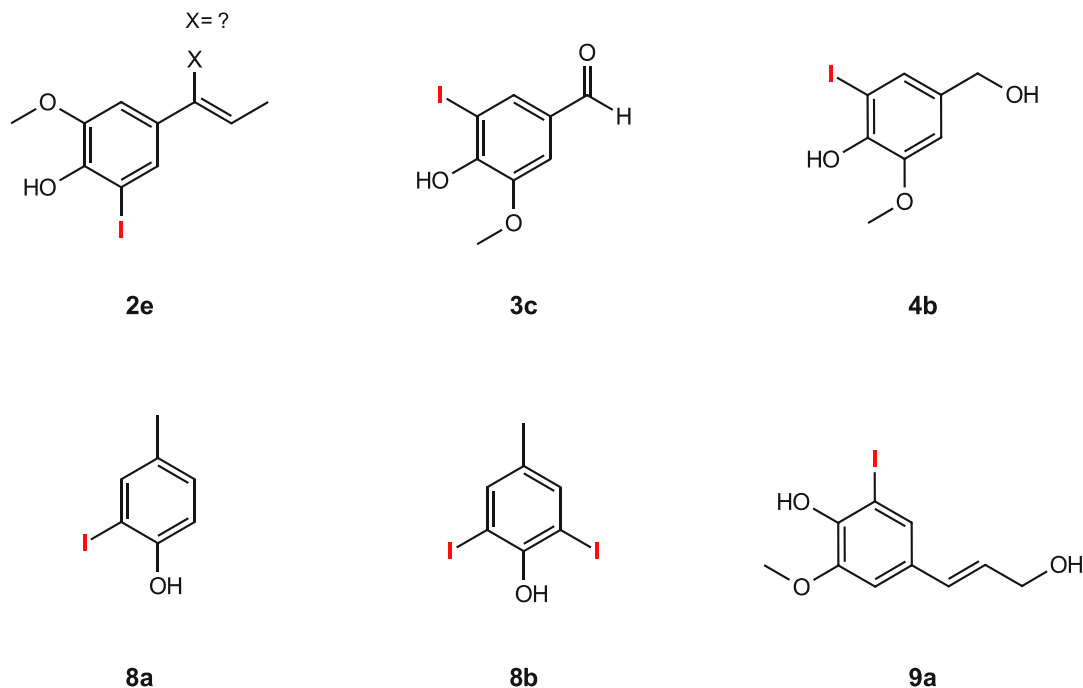


Figure 53: Iodinated derivatives resulting from the iodination reaction with PyI₂. **2e**: iodinated derivative of isoeugenol; **3c**: iodinated derivative of vanillin; **4b**: iodinated derivative of vanillyl alcohol; **8a**: single iodinated derivative of *p*-cresol; **8b**: double iodinated derivative of *p*-cresol; **9a**: iodinated derivative of coniferyl alcohol.

Noticeable features observed in the derivatization reactions include the reactive behavior of the double bond of the model compounds methyl isoeugenol **1** and isoeugenol **2**. Side reactions at the double bond were detected in almost all reactions carried out with the two compounds. Attempts were made (*c.f.* chapter 3) to establish potential reaction mechanisms, but the determination of some substituents was inconclusive.

Another observation made within the derivatization reactions was the formation of by-products when methanol (protonated or deuterated) was used as the solvent.

A plausible explanation for unsuccessful derivatization reactions could not be found for all compounds. For this purpose, the reactions need to be analyzed in more detail.

Iodination at the *ortho*-position with PyI₂ was not successful for all model compounds, despite the presence of a hydroxylated aromatic structure. However, for those components not carrying a hydroxy group in their structure, the derivatization reaction with PyI₂ was unsuccessful, which was to be

expected according to the protocol. These findings represent important information concerning the evaluation of the methodology.

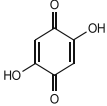
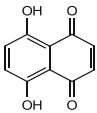
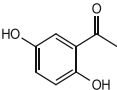
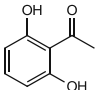
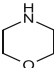
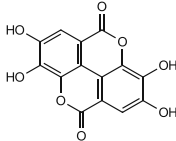
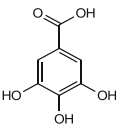
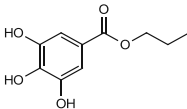
To determine the effectiveness of this derivatization method, several other suitable model compounds would have to be investigated. Enabling the establishment of the method and its subsequent application, e.g. for lignin analysis, further investigations concerning both the behavior of the model compounds as well as the mechanism of the derivatization reactions would still be required.

4.2 Derivatization Method II – Phosphitylation

Phosphitylation reactions with TMDP were performed with twelve selected model substances (*c.f.* Figure 2). The ^{31}P -chemical shifts of the successfully phosphitylated derivatives were determined to avoid misinterpretation of the peaks that might occur during lignin analysis. Eight of the twelve model compounds investigated have undergone a successful phosphitylation reaction.

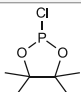
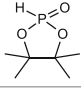
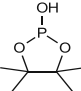
Table 59 shows the resulting ^{31}P -chemical shifts of the successfully phosphitylated model compounds. Table 60 additionally lists the ^{31}P -chemical shifts of frequently occurring components during the phosphitylation reactions.

Table 59: ^{31}P -NMR chemical shifts δ (ppm) of the model compounds phosphitylated with TMDP.

Compound	Structure	^{31}P -shift (ppm)	
		OH	NH
2,5-Dihydroxy-1,4-benzoquinone		140.73	-
5,8-Dihydroxy-1,4-naphthoquinone		136.54	-
2,5-Dihydroxyacetophenone		140.64 (<i>m</i>) 140.05 (<i>di</i>)	-
2,6-Dihydroxyacetophenone		139.73 (<i>di</i>) 138.51 (<i>mono</i>)	-
Morpholine		-	139.37
Ellagic acid		141.51 138.99	-
Gallic acid		141.17	-
Propyl gallate		139.89	-

m, meta-substituted; *di*, di-substituted; *mono*, mono-substituted;

Table 60: ^{31}P -NMR chemical shifts δ (ppm) of the frequently occurring compounds during phosphorylation reactions with TMDP.

Compound	Structure	^{31}P -shift (ppm)
TMDP		≈ 175.98
4,4,5,5-Tetramethyl-1,3,2 λ^5 -dioxaphospholan-2-one		$\approx 15-17$
TMDP-OH		$\approx 131-133$

Since the model compounds are biomass-related components that may still appear as traces in lignin, the results also contribute to qualitative analysis of lignin. To expand the database, a wide range of model compounds that can potentially occur in isolated lignin would still need to be investigated applying this method. The more chemical shifts are identified and can be assigned, the more analysis of lignin will be improved.

5 BIBLIOGRAPHY

1. Galkin, M.V. and J.S. Samec, *Lignin Valorization through Catalytic Lignocellulose Fractionation: A Fundamental Platform for the Future Biorefinery*. ChemSusChem, **2016**. 9(13): p. 1544-58.
2. Rinaldi, R., et al., *Paving the Way for Lignin Valorisation: Recent Advances in Bioengineering, Biorefining and Catalysis*. Angew Chem Int Ed Engl, **2016**. 55(29): p. 8164-215.
3. Li, M., et al., *³¹P NMR Chemical Shifts of Solvents and Products Impurities in Biomass Pretreatments*. ACS Sustainable Chemistry & Engineering, **2017**. 6(1): p. 1265-1270.
4. Lin, S.Y., *Methods in Lignin Chemistry*. Springer Series in Wood Science, (Ed.: C. W. Dence), Springer, Berlin, **1992**.
5. Crawford, R.L., *Lignin Biodegradation and Transformation*. Wiley, New York, **1980**.
6. Whetten, R. and R. Sederoff, *Lignin Biosynthesis*. The plant cell, **1995**. 7: p. 1001-1013.
7. Calvo-Flores, F.G. and J.A. Dobado, *Lignin as Renewable Raw Material*. ChemSusChem, **2010**. 3(11): p. 1227-1235.
8. Calvo-Flores, F.G., J.A. Dobado, and J. Isac-Garcia, *Lignin and Lignans as Renewable Raw Materials*. John Wiley & Sons, Ltd, **2015**: p. 3-20.
9. Whetten, R.W., J.J. MacKay, and R.R. Sederoff, *Recent advances in understanding lignin biosynthesis*. Annu. Rev. Plant Physiol. Plant Mol Biol., **1998**. 49: p. 585-609.
10. Patil, N.D., N.R. Tanguy, and N. Yan, *Lignin Interunit Linkages and Model Compounds, in Lignin in Polymer Composites*. 2016. p. 27-47.
11. Sannigrahi, P., Y. Pu, and A. Ragauskas, *Cellulosic biorefineries—unleashing lignin opportunities*. Current Opinion in Environmental Sustainability, **2010**. 2(5-6): p. 383-393.
12. Ralph, J., G. Brunow, and W. Boerjan, *Lignins*, in *eLS*. 2007.
13. Ando, D. and J. Ralph, *Method to Regioselectively Iodine-Tag Free-Phenolic Aromatic End-Groups in Lignin for ¹H–¹³C-HSQC NMR Analysis*. ACS Sustainable Chemistry & Engineering, **2019**. 7(22): p. 18624-18629.
14. Berlin, A. and M. Balakshin, *Industrial Lignins*, in *Bioenergy Research: Advances and Applications*. 2014. p. 315-336.
15. Thielemans, W., et al., *Novel applications of lignin in composite materials*. Journal of Applied Polymer Science, **2002**. 83(2): p. 323-331.
16. Balakshin, M.Y., et al., *New Opportunities in the Valorization of Technical Lignins*. ChemSusChem, **2021**. 14(4): p. 1016-1036.
17. Balakshin, M.Y., et al., *Elucidation of the Structures of Residual and Dissolved Pine Kraft Lignins Using an HMQC NMR Technique*. Agricultural and Food Chemistry, **2003**. 51 (21): p. 6116-6127.
18. Demuner, I.F., et al., *Biorefinery Review: Wide-Reaching Products Through Kraft Lignin*. BioResources, **2019**. 14 (3): p. 7543-7581.

19. Holladay, J.E., et al., *Top Value-Added Chemicals from Biomass*. Pacific Northwest National Laboratory, **2007**. 2: p. 1-79.
20. Khansole, S.V., et al., *Pyridinium Iodochloride: An Efficient Reagent for Iodination of Hydroxylated Aromatic Ketones and Aldehydes*. Journal of the Chinese Chemical Society, **2008**. 55: p. 871-874.
21. Granata, A. and D.S. Argyropoulos, *2-Chloro-4,4,5,5-tetramethyl-1,3,2-dioxaphospholane, a Reagent for the Accurate Determination of the Uncondensed and Condensed Phenolic Moieties in Lignins*. J. Agric. Food Chem., **1995**. 43 (6): p. 1538-1544.
22. Meng, X., et al., *Determination of hydroxyl groups in biorefinery resources via quantitative ³¹P NMR spectroscopy*. Nature Protocols, **2019**. 14(9): p. 2627-2647.
23. Argyropoulos, D., *Quantitative Phosphorus-31 NMR Analysis of Six Soluble Lignins*. Journal of Wood Chemistry and Technology, **1994**. 14(1): p. 65-82.
24. Argyropoulos, D.S., *³¹P NMR in wood chemistry: A review of recent progress*. Res. Chem. Intermed., **1995**. 21: p. 373-395.
25. Friebolin, H., *Ein- und zweidimensionale NMR-Spektroskopie - Eine Einführung*. 5. ed. **2013**: Wiley-VCH. 452.
26. Berger, S., S. Braun, and H.-O. Kalinowski, *NMR Spectroscopy of the Non-Metallic Elements*. **1997**: John Wiley & Sons.
27. Tobimatsu, Y., et al., *Solution-state Multidimensional NMR of Lignins: Approaches and Applications*. Nova Science Publishers, **2019**.
28. Inkrod, C., et al., *Characteristics of Lignin Extracted from Different Lignocellulosic Materials via Organosolv Fractionation*. BioEnergy Research, **2018**. 11(2): p. 277-290.
29. Nandanwar, R.A., A.R. Chaudhari, and E.J. D., *Nitrobenzene Oxidation for Isolation of Value Added Products from Industrial Waste Lignin*. Journal of Chemical, Biological and Physical Sciences, **2016**. 6 (3): p. 501-513.
30. Kaur, B. and D. Chakraborty, *Biotechnological and molecular approaches for vanillin production: a review*. Appl Biochem Biotechnol, **2013**. 169(4): p. 1353-72.
31. Posoknistakul, P., et al., *Predominant formation of aromatic aldehyde and acid from a dimeric β -O-4-type lignin model compound under hydrogen peroxide bleaching conditions with high pH levels*. Journal of Wood Science, **2017**. 63(2): p. 173-182.
32. Recabarren, R., I. Fuenzalida-Valdivia, and J. Alzate-Morales, *Studying the binding mechanisms of veratryl alcohol to *P. chrysosporium* lignin peroxidase: insights from theoretical approaches*. Theoretical Chemistry Accounts, **2016**. 135(3).
33. Hishiyama, S., et al., *Convenient synthesis of chiral lignin model compounds via optical resolution: four stereoisomers of guaiacylglycerol- β -guaiacyl ether and both enantiomers of 3-hydroxy-1-(4-hydroxy-3-methoxyphenyl)-2-(2-methoxyphenoxy)-propan-1-one (erone)*. Tetrahedron Letters, **2012**. 53(7): p. 842-845.

34. Zwirchmayr, N.S., et al., *Degradation of the Cellulosic Key Chromophore 5,8-Dihydroxy-[1,4]-naphthoquinone by Hydrogen Peroxide under Alkaline Conditions*. J Org Chem, **2017**. 82(21): p. 11558-11565.
35. Rosenau, T., et al., *Isolation and Identification of Residual Chromophores in Cellulosic Materials*. Macromolecular Symposia, **2005**. 223(1): p. 239-252.
36. Rosenau, T., et al., *Isolation and identification of residual chromophores in cellulosic materials*. Polymer, **2004**. 45(19): p. 6437-6443.
37. LENZING, A., *Verfahren zum Abtrennen von Wasser aus einer verdünnten, wässrigen Lösung von N-Methylmorpholin-N-Oxid, N-Methylmorpholin und/oder Morpholin*, in *Europäisches Patentamt*. 1990: Austria.
38. Hettegger, H., et al., *Reaction of 2,5-dihydroxy-[1,4]-benzoquinone with nucleophiles - ipso-substitution vs. addition/elimination*. Chem Commun (Camb), **2020**. 56(84): p. 12845-12848.
39. Rosenau, T., et al., *Autocatalytic Decomposition of N-Methylmorpholine N-Oxide Induced by Mannich Intermediates*. J. Org. Chem, **1999**. 64 (7): p. 2166-2167.
40. Liebner, F., et al., *Thermal aging of 1-alkyl-3-methylimidazolium ionic liquids and its effect on dissolved cellulose*. Holzforschung, **2010**. 64(2).
41. Guggenberger, M., et al., *Degradation of the cellulosic key chromophore 2,5-dihydroxy-[1,4]-benzoquinone (DHBQ) under conditions of chlorine dioxide pulp bleaching: formation of rhodizone as secondary chromophore—a combined experimental and theoretical study*. Cellulose, **2020**. 27(7): p. 3623-3649.
42. Fu, B., et al., *One-Pot Bioconversion of Lignin-Derived Substrates into Gallic Acid*. J Agric Food Chem, **2021**. 69(38): p. 11336-11341.
43. Bianco, M.-A., A. Handaji, and H. Savolainen, *Quantitative analysis of ellagic acid in hardwood samples*. The Science of the Total Environment, **1998**. 222: p. 123-126.
44. Nguyen, V.H., et al., *Propyl Gallate*. Molbank, **2021**. 2021(2).
45. Goriparti, S., M.N.K. Harish, and S. Sampath, *Ellagic acid – A Novel Organic Electrode Material for High Capacity Lithium Ion Batteries*. The Royal Society of Chemistry **2013**.
46. Robien, W. *CSEARCH / NMRPREDICT-Server*. Available from: <https://nmrpredict.orc.univie.ac.at/>.
47. Vi Cha, J., et al., *Relativistic Heavy-Neighbor-Atom Effects on NMR Shifts: Concepts and Trends Across the Periodic Table*. Chem Rev, **2020**. 120 (15): p. 7065-7103.
48. Neto, A.C., et al., *Heavy Halogen Atom Effect on ¹³C NMR Chemical Shifts in Monohalo Derivatives of Cyclohexane and Pyran. Experimental and Theoretical Study*. J. Chem. Theory Comput., **2009**. 5: p. 2222–2228.
49. Hettegger, H., et al., *Pitfalls in the chemistry of cellulosic key chromophores*. Cellulose, **2018**. 26(1): p. 185-204.

6 APPENDIX

Table 61: Summary of the NMR measurements of the model compounds used for iodination including file names and performed NMR experiments with respective NMR solvents and additional information of the resulting products in the respective measurement. In case of measurement of the pure component, the number of the model compound is given, and an empty column indicates that no relevant product was formed. Otherwise, the designation of the respective derivatives is shown.

Model compound	File-name	NMR-Solvent	NMR-Experiments	Product
1	<i>jozi-methyl-isoeugenol</i>	CD ₃ OD	¹ H, ¹³ C, COSY, HSCQ, HMBC	1
	<i>jozi-methyl-isoeugenol-Pyr-ICl-extr</i>	CD ₃ OD	¹ H, ¹³ C, COSY, HSCQ, HMBC	1a, 1b
	<i>jozi-methyl-isoeugenol-Pyr-ICl-MeOH-extr.</i>	CDCl ₃	¹ H, ¹³ C, COSY, HSCQ, HMBC	1c
	<i>jozi-methyl-isoeugenol-Pyr-ICl-CHCl3-extr.</i>	CDCl ₃	¹ H, ¹³ C, COSY, HSCQ, HMBC	1d, 1e
	<i>maba-methyl-isoeugenol, 10.5 mg</i>	C ₅ D ₅ N	¹ H, ¹³ C, COSY, HSCQ, HMBC	1
	<i>maba-methyl-isoeugenol-Pyr-ICl. 10.5 + 28.4 mg</i>	C ₅ D ₅ N	¹ H, ¹³ C, COSY, HSCQ, HMBC	1d
2	<i>jozi-isoeugenol. MeOD</i>	CD ₃ OD	¹ H, ¹³ C, COSY, HSCQ, HMBC	2
	<i>jozi-isoeugenol-Pyr-ICl-extr</i>	CD ₃ OD	¹ H, ¹³ C, COSY, HSCQ, HMBC	2a, 2b, 2c
	<i>maba-isoeugenol, 17.6 mg</i>	C ₅ D ₅ N	¹ H, ¹³ C, COSY, HSCQ, HMBC	2
	<i>maba-isoeugenol-Pyr-ICl</i>	C ₅ D ₅ N	¹ H, ¹³ C, COSY, HSCQ, HMBC	2d, 2e, 2f
3	<i>jozi-vanillin</i>	CD ₃ OD	¹ H, ¹³ C, COSY, HSCQ, HMBC	3
	<i>jozi-vanillin-Pyr-ICl-extr</i>	CD ₃ OD	¹ H, ¹³ C, COSY, HSCQ, HMBC	3a, 3b, 3c
	<i>jozi-vanillin-Pyr-ICl-MeOH-extr.</i>	CDCl ₃ +DMSO-d ₆	¹ H, ¹³ C, COSY, HSCQ, HMBC	3c
	<i>jozi-vanillin-Pyr-ICl-CHCl3-extr.</i>	CDCl ₃ +DMSO-d ₆	¹ H, ¹³ C, COSY, HSCQ, HMBC	3c
	<i>jozi-Vanillin-Pyr</i>	C ₅ D ₅ N	¹ H, ¹³ C, COSY, HSCQ, HMBC	3
	<i>jozi-Vanillin-Pyr-ICl</i>	C ₅ D ₅ N	¹ H, ¹³ C, COSY, HSCQ, HMBC	3c
4	<i>jozi-vanillyl alcohol. neu</i>	CD ₃ OD	¹ H, ¹³ C, COSY, HSCQ, HMBC	4
	<i>jozi-vanillyl alcohol-Pyr-ICl-2</i>	CD ₃ OD	¹ H, ¹³ C, COSY, HSCQ, HMBC	4a
	<i>jozi-Vanillyl-Alcohol-Pyr</i>	C ₅ D ₅ N	¹ H, ¹³ C, COSY, HSCQ, HMBC	4
	<i>jozi-Vanillyl-Alcohol-Pyr-ICl</i>	C ₅ D ₅ N	¹ H, ¹³ C, COSY, HSCQ, HMBC	4b
5	<i>jozi-veratraldehyde</i>	CD ₃ OD	¹ H, ¹³ C, COSY, HSCQ, HMBC	5
	<i>jozi-veratryl-aldehyd-Pyr-ICl-extr.</i>	CD ₃ OD	¹ H, ¹³ C, COSY, HSCQ, HMBC	5a

6	<i>jozi-veratryl alcohol</i>	CD ₃ OD	¹ H, ¹³ C, COSY, HSCQ, HMBC	6
	<i>jozi-Veratryl-Alcohol-Pyr</i>	C ₅ D ₅ N	¹ H, ¹³ C, COSY, HSCQ, HMBC	
7	<i>jozi-veratric acid</i>	CD ₃ OD	¹ H, ¹³ C, COSY, HSCQ, HMBC	7
	<i>jozi-Veratric-Acid-Pyr</i>	C ₅ D ₅ N	¹ H, ¹³ C, COSY, HSCQ, HMBC	
8	<i>jozi-p-cresol</i>	CDCl ₃	¹ H, ¹³ C, COSY, HSCQ, HMBC	8
	<i>jozi-p-cresol-PyrICl</i>	CDCl ₃	¹ H, ¹³ C, COSY, HSCQ, HMBC	8a, 8b
9	<i>jozi-coniferyl-alcohol</i>	CDCl ₃	¹ H, ¹³ C, COSY, HSCQ, HMBC	9
	<i>jozi-coniferyl-alcohol-Pyr-ICl</i>	CDCl ₃	¹ H, ¹³ C, COSY, HSCQ, HMBC	9a
10	<i>jozi-veratrylglycerol-dimer</i>	CDCl ₃	¹ H, ¹³ C, COSY, HSCQ, HMBC	10
	<i>jozi-veratrylglycerol-dimer-Pyr-ICl</i>	CDCl ₃	¹ H	
11	<i>jozi-guaiacyl-dimer</i>	CDCl ₃	¹ H, ¹³ C, COSY, HSCQ, HMBC	11
	<i>jozi-guaiacyl-dimer-Pyr-ICl</i>	CDCl ₃	¹ H, ¹³ C, COSY, HSCQ, HMBC	
12	<i>jozi-dhbq</i>	C ₅ D ₅ N	¹ H, ¹³ C, HSCQ, HMBC	12
	<i>jjozi-dhbq-pyr-ICl</i>	C ₅ D ₅ N	¹ H, HSCQ	
13	<i>jozi-dhnq</i>	C ₅ D ₅ N	¹ H, ¹³ C, COSY, HSCQ, HMBC	13
	<i>jozi-dhnq-pyr-ICl</i>	C ₅ D ₅ N	¹ H, ¹³ C, HSCQ	
14	<i>jozi-2-5-dhap</i>	C ₅ D ₅ N	¹ H, ¹³ C, COSY, HSCQ, HMBC	14
	<i>jozi-2-5-dhap-pyr-ICl</i>	C ₅ D ₅ N	¹ H, ¹³ C, COSY, HSCQ, HMBC	14a
Spruce	<i>jozi-spruce</i>	DMSO-d ₆	¹ H, HSCQ	spruce
	<i>jozi-spruce-PyrICl</i>	DMSO-d ₆	¹ H, COSY, HSCQ, HMBC	
Beech	<i>jozi-beech</i>	DMSO-d ₆	¹ H, HSCQ	beech
	<i>jozi-beech-PyrICl</i>	DMSO-d ₆	¹ H, COSY, HSCQ, HMBC	

Table 62: Summary of the NMR measurements of the model compounds used for phosphitylation including file names and performed NMR experiments with respective NMR solvents and additional information of the resulting products in the respective measurement. In the case of measurement of the pure compound, the number of the model compound is given, and an empty column indicates that no relevant product was formed. Otherwise, the designation of the respective derivatives is shown and "phosp." implies that a phosphitylated product of the model compounds was formed, but no precise structures could be elucidated.

Model compound	File-name	NMR-Solvent	NMR-Experiments	Product
12	jozi-dhbq	C ₅ D ₅ N	¹ H, ¹³ C, HSCQ, HMBC	12
	jozi-dhbq-cdcl3	CDCl ₃	¹ H, ¹³ C, COSY, HSCQ, HMBC, ³¹ P_zg30, ³¹ P_zgdc	phosp. 12
	jozi-dhbq-cdcl3-pyr	CDCl ₃	¹ H, COSY, HSCQ, HMBC, ³¹ P_zg30, ³¹ P_zgdc	phosp. 12
	jozi-dhbq-pyr	C ₅ D ₅ N	¹ H, ¹³ C, COSY, HSCQ, HMBC, ³¹ P_zg30, ³¹ P_zgdc, ¹ H/ ³¹ P-HMBC	phosp. 12
13	jozi-dhnq	C ₅ D ₅ N	¹ H, ¹³ C, HSCQ, HMBC	13
	jozi-dhnq-cdcl3	CDCl ₃	¹ H, ¹³ C, COSY, HSCQ, HMBC, ³¹ P_zg30, ³¹ P_zgdc	phosp. 13
	jozi-dhnq-cdcl3-pyr-31p	CDCl ₃	¹ H, ¹³ C, COSY, HSCQ, HMBC, ³¹ P_zg30, ³¹ P_zgdc	phosp. 13
	jozi-dhnq-pyr	C ₅ D ₅ N	¹ H, ¹³ C, COSY, HSCQ, HMBC, ³¹ P_zg30, ³¹ P_zgdc, ¹ H/ ³¹ P-HMBC	phosp. 13
14	jozi-2-5-dhap	C ₅ D ₅ N	¹ H, ¹³ C, COSY, HSCQ, HMBC	14
	jozi-2,5-dhap-cdcl3	CDCl ₃	¹ H, ¹³ C, COSY, HSCQ, HMBC	14b, 14c
	jozi-2-5-dhap-cdcl3-pyr	CDCl ₃	¹ H, COSY, HSCQ, HMBC, ³¹ P_zg30, ³¹ P_zgdc	14b, 14c
	jozi-2-5-dhap-pyr	C ₅ D ₅ N	¹ H, ¹³ C, COSY, HSCQ, HMBC, ³¹ P_zg30, ³¹ P_zgdc, ¹ H/ ³¹ P-HMBC	14b, 14c
15	jozi-2-6-dhap	CDCl ₃	¹ H, ¹³ C, COSY, HSCQ, HMBC	15
	jozi-2,6-dhap-cdcl3	CDCl ₃	¹ H, ¹³ C, COSY, HSCQ, HMBC, ³¹ P_zg30, ³¹ P_zgdc	15a, 15b
	jozi-2-6-dhap-cdcl3-pyr	CDCl ₃	¹ H, ¹³ C, COSY, HSCQ, HMBC, ³¹ P_zg30, ³¹ P_zgdc	15a, 15b
	jozi-2-6-dhap-pyr	C ₅ D ₅ N	¹ H, ¹³ C, COSY, HSCQ, HMBC, ³¹ P_zg30, ³¹ P_zgdc, ¹ H/ ³¹ P-HMBC	15a, 15b
16	jozi-imidazol	CDCl ₃	¹ H, ¹³ C, COSY, HSCQ, HMBC	16
	jozi-imidazol-cdcl3	CDCl ₃	¹ H, ¹³ C, COSY, HSCQ, HMBC, ³¹ P_zg30, ³¹ P_zgdc	
	jozi-imidazol-cdcl3-pyr	CDCl ₃	¹ H, ¹³ C, COSY, HSCQ, HMBC, ³¹ P_zg30, ³¹ P_zgdc	
	jozi-imidazol-pyr	C ₅ D ₅ N	¹ H, ¹³ C, COSY, HSCQ, HMBC, ³¹ P_zg30, ³¹ P_zgdc, ¹ H/ ³¹ P-HMBC	

17	jozi-methyl-imidazol	CDCl ₃	¹ H, ¹³ C, COSY, HSCQ, HMBC	17
	jozi-methyl-imidazol-cdcl3	CDCl ₃	¹ H, ¹³ C, COSY, HSCQ, HMBC, ³¹ P_zg30, ³¹ P_zgdc	
	jozi-methyl-imidazol-cdcl3-pyr	CDCl ₃	¹ H, COSY, HSCQ, HMBC, ³¹ P_zg30, ³¹ P_zgdc	
18	jozi-morpholine	CDCl ₃	¹ H, ¹³ C, COSY, HSCQ, HMBC	18
	jozi-morpholine-cdcl3-31p	CDCl ₃	¹ H, ¹³ C, COSY, HSCQ, HMBC, ³¹ P_zg30, ³¹ P_zgdc	18a, 18'
	jozi-morpholine-cdcl3-pyr	CDCl ₃	¹ H, ¹³ C, COSY, HSCQ, HMBC, ³¹ P_zg30, ³¹ P_zgdc	18a, 18a'
	jozi-morpholine-pyr	C ₅ D ₅ N	¹ H, ¹³ C, COSY, HSCQ, HMBC, ³¹ P_zg30, ³¹ P_zgdc, ¹ H/ ³¹ P-HMBC	18a, 18a'
19	jozi-nmmo	CDCl ₃	¹ H, ¹³ C, COSY, HSCQ, HMBC	19
	jozi-nmmo-cdcl3	CDCl ₃	¹ H, ¹³ C, COSY, HSCQ, HMBC, ³¹ P_zg30, ³¹ P_zgdc	
	jozi-nmmo-cdcl3-pyr	CDCl ₃	¹ H, ¹³ C, COSY, HSCQ, HMBC, ³¹ P_zg30, ³¹ P_zgdc	
20	rosi-ellagic acid	DMSO-d ₆	¹ H, ¹³ C	20
	jozi-ellagic-acid-pyr	C ₅ D ₅ N	¹ H, ¹³ C, COSY, HSCQ, HMBC, ³¹ P_zg30, ³¹ P_zgdc, ¹ H/ ³¹ P-HMBC	phosp. 20
21	rosi-gallussaeure, 32.8 mg	DSMO-d ₆	¹ H, ¹³ C	21
	jozi-gallic-acid-pyr	C ₅ D ₅ N	¹ H, ¹³ C, COSY, HSCQ, HMBC, ³¹ P_zg30, ³¹ P_zgdc, ¹ H/ ³¹ P-HMBC	21a, 21b
22	rosi-propylgallat, 38.0 mg	DSMO-d ₆	¹ H, ¹³ C	22
	jozi-propyl-gallat-pyr	C ₅ D ₅ N	¹ H, ¹³ C, COSY, HSCQ, HMBC, ³¹ P_zg30, ³¹ P_zgdc, ¹ H/ ³¹ P-HMBC	22a, 22b
23	jozi-rhodizonic-acid-cdcl3		¹ H, ¹³ C, HSCQ, HMBC, ³¹ P_zg30, ³¹ P_zgdc	
	jozi-rhodizonic acid-cdcl3-pyr		¹ H, HSCQ, ³¹ P_zg30, ³¹ P_zgdc	

Curriculum Vitae**JOHANNA ZIEHER****PERSONAL INFO**

E-Mail zieherjohanna@gmail.com

EDUCATION

- 05/2019 - today** **Master program Technical Chemistry**
 (expected graduation 03/2022)
Vienna University of Technology (TU Wien), Vienna, Austria
 Specialization in sustainable technologies and environmental engineering
 Master thesis: Derivatization-NMR techniques in the analysis of lignocellulosics
 Supervised by: Prof. Dr. Thomas Rosenau
 Prof. Dr. Anton Friedl
- 01/2020 – 06/2020** **ERASMUS+ semester in Master program Chemistry and Chemical Engineering**
Chalmers University of Technology, Gothenburg, Sweden
 Courses in Innovative and Sustainable Chemical Engineering
- 10/2015 – 04/2019** **Bachelor program Technical Chemistry**
Vienna University of Technology (TU Wien), Vienna, Austria
 Bachelor thesis: Brønsted acid-catalyzed synthesis of coumarin derivatives
 Supervised by: Prof. Dr. Marko Mihovilovic
 Dr. Sebastian Hecko
- 2006 - 2014** **Bundesgymnasium Vöcklabruck**
Vöcklabruck, Austria

WORK EXPERIENCE

- 10/2019 – 12/2019** **Tutor**
 at Process Engineering Laboratory Course of Bachelor program Technical Chemistry
TU Wien, Vienna, Austria
- 07/2019** **Lenzing AG**
Lenzing, Austria
 Infrastructure R&D
- 08/2018** **Lenzing AG**
Lenzing, Austria
 Infrastructure R&D

07/2017	Lenzing AG <i>Lenzing, Austria</i> Infrastructure R&D
07/2016	Lenzing AG <i>Lenzing, Austria</i> Infrastructure R&D
04/2015 – 07/2015	Lenzing AG <i>Lenzing, Austria</i> Pulp laboratory

ADDITIONAL SKILLS

Fond computer Skills	MS-Office Word, Excel, Powerpoint Chemistry related software ChemDraw, ChemDoodle TopSpin, MestreNova
Language Skills	German native English advanced high Spanish basic

FURTHER INFORMATION

10/2014 – 04/2015	New Zealand trip between graduation and start of university
Hobbies	Travelling, ski sport, hiking, cooking & baking